HIV-1 capsid engages nucleoporin NUP153 to promote viral nuclear entry

HIV-1 capsid engages nucleoporin NUP153 to promote viral nuclear entry

A dissertation presented

by

Kenneth Anzai Matreyek

to

The Division of Medical Sciences

In partial fulfillment of the requirements

for the degree of

Doctor of Philosophy

in the subject of

Virology

Harvard University

Cambridge, Massachusetts

October, 2013

Dissertation Advisor: Dr. Alan Engelman Kenneth Anzai Matreyek

HIV-1 capsid engages nucleoporin NUP153 to promote viral nuclear entry

Abstract

Lentiviruses can infect non-dividing cells, and various cellular nuclear transport proteins provide crucial functions for lentiviral nuclear entry and integration. Genome-wide small interfering RNA screens previously identified nuclear pore complex component nucleoporin 153 (NUP153) as being important for infection by human immunodeficiency virus type 1 (HIV-1). We found that HIV-1 infection of NUP153 depleted cells resulted in normal levels of reverse transcription, a moderate reduction of 2-long terminal repeat circles, and a relatively large reduction in integrated proviruses, consistent with a role for NUP153 during nuclear entry of the HIV-1 pre-integration complex. We ascertained the capsid (CA) to be the major viral determinant for NUP153 dependence during infection, and accordingly observed a direct interaction between the CA N-terminal domain and the phenylalanine-glycine (FG)-repeat enriched NUP153 C-terminal domain ($NUP153_C$). $NUP153_C$ fused to the effector domains of the rhesus Trim5α restriction factor (Trim-$NUP153_C$) potently restricted HIV-1, providing an intracellular readout for the $NUP153_C$-CA interaction during retroviral infection. Primate lentiviruses and equine infectious anemia virus (EIAV) bound $NUP153_C$ under these conditions, results that correlated with direct binding between purified recombinant proteins in vitro. These binding phenotypes moreover correlated with the requirement for endogenous NUP153 function during infection. Mutagenesis experiments identified

$NUP153_C$ and CA residues important for binding, and different FG motifs within $NUP153_C$ mediated binding to HIV-1 versus EIAV CA proteins. HIV-1 CA binding mapped to residues that line a common alpha helix 3/4 hydrophobic pocket that also mediates binding to the small molecule PF-3450074 (PF74) inhibitor and cleavage and polyadenylation specific factor 6 (CPSF6) protein, with Asn57 (Asp58 in EIAV) playing a particularly important role. PF74 and CPSF6 each competed with $NUP153_C$ for binding to HIV-1 CA, and significantly higher concentrations of PF74 were needed to inhibit HIV-1 infection in the face of Trim-$NUP153_C$ expression or NUP153 knockdown. Correlation between CA mutant viral cell cycle and NUP153 dependencies moreover indicated that the $NUP153_C$-CA interaction underlies the ability of HIV-1 to infect non-dividing cells. We propose that HIV-1 CA binds NUP153 FG motifs to affect viral nuclear import, serving as a novel example of viral hijacking of a fundamental cellular process.

Acknowledgements

Foremost, I thank Professor Alan Engelman. Alan was an excellent mentor during my doctoral studies, and provided the right combination of advising – sometimes direct, sometimes hands-off – for me to grow as a research scientist. I hope to emulate his critical eye for details in my future work. I also thank the professors who oversaw the various stages of my dissertation work: Drs. Joseph Sodroski, Dana Gabuzda, and Karl Munger for serving on my dissertation advisory committee; Drs. Todd Allen, Welkin Johnson, and Jeremy Luban for serving as dissertation examiners. I would like to acknowledge Joe in particular, not only for serving as the chair of my advisory and examination committees, but also for his insightful comments throughout my studies.

I wish to thank my cohorts from the Harvard Virology Program: while we may have finished at different times, I still feel that we all went through the journey of graduate school together. I acknowledge Anna Bruchez in particular: besides being a fantastic partner in life, I cherish our mutual love of science. I look forward to our future, both in and out of the scientific realm.

Lastly, I would like to thank the individuals who were instrumental in my academic development leading up to my graduate studies. I dedicate this dissertation to my parents, Walter and Mineko Matreyek: not only are they great parents, but their innate interests in science were likely largely responsible for sparking my own appreciation of biology. I also thank Dr. Hector Aguilar-Carreno, who served as a fantastic mentor when I initially began scientific research, and Dr. Benhur Lee, whose lab provided a great environment to start virology research as an undergraduate.

Table of Contents

Table of Figures

Chapter 1

Introduction

The pre-integrative steps of HIV-1 infection, and the significance of the nuclear pore for viral nuclear import

Kenneth A. Matreyek and Alan Engelman

Department of Cancer Immunology and AIDS, Dana-Farber Cancer Institute, and Department of Medicine, Harvard Medical School, Boston, Massachusetts 02215

* This chapter is adapted from a review article submitted to the journal Viruses for publication.

Contributions: Alan Engelman and I both wrote the manuscript.

The HIV-1 replication cycle

Human immunodeficiency virus type 1 (HIV-1) is the causative agent of acquired immunodeficiency syndrome (AIDS) [1-3]. HIV/AIDS remains a global pandemic with ~ 34 million individuals infected as of 2010, and the virus was estimated to have caused ~ 1.8 million deaths in that same year [4]. There are currently no effective prophylactic or therapeutic vaccines for HIV-1 infection. Although the development of combined anti-retroviral therapy regimens have curtailed AIDS progression in HIV infected individuals in developed nations, these treatments are not widely available in either Sub-Saharan Africa or South and Southeast Asia, which are experiencing the greatest disease burden.

Aside from its epidemiological relevance, HIV-1 is the prototypical lentivirus, and provides a common model to understand the molecular processes undertaken by viruses of the family *Retroviridae*. Like all viruses, HIV-1 must initiate its replication cycle by first gaining entry into the target cell (**Figure 1-1**). HIV-1 initiates viral entry by binding the cell surface protein CD4 [5], which is expressed to high levels on a number of immune cells, including CD4 positive subsets of T-lymphocytes, macrophages, and dendritic cells. This binding event triggers conformational changes in the viral envelope protein, revealing its site for co-receptor binding. Binding to an HIV-1 co-receptor, most commonly proteins CCR5 [6-10] or CXCR4 [11-13], triggers a cascade of events resulting in the fusion of the viral and cellular membranes, releasing the viral core into the cell cytoplasm.

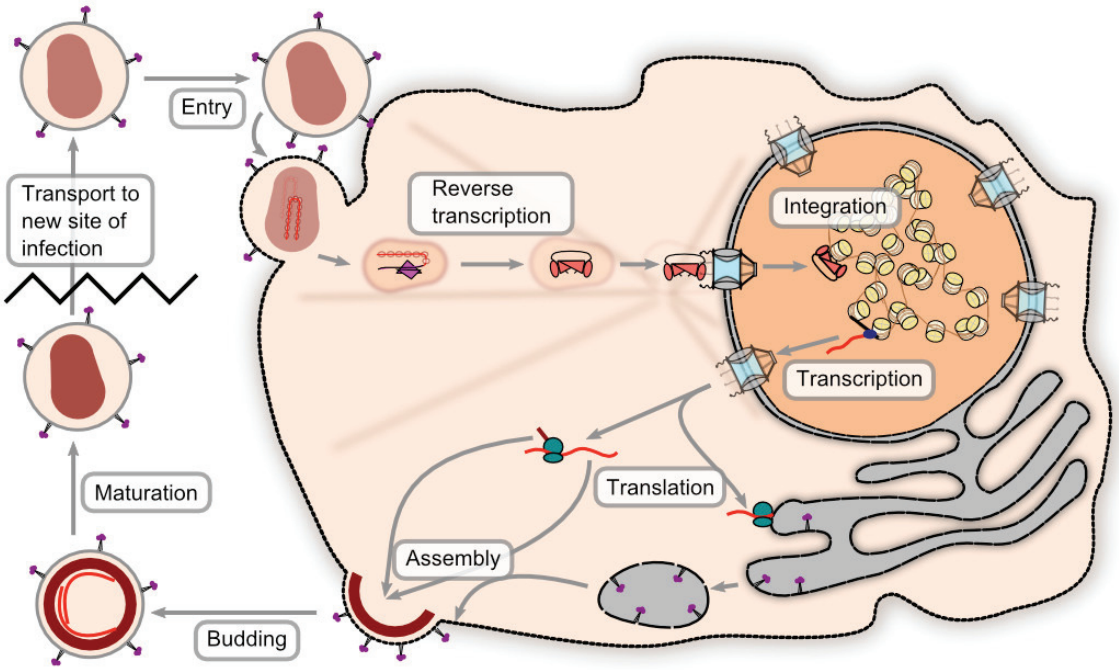

Figure 1-1. Schematic of the HIV-1 replication cycle. HIV-1 infection is initiated when the virion binds to receptor molecules on the target cell, which triggers fusion between the viral and cellular membranes (Entry). Reverse transcriptase (RT) housed within the capsid core then creates a double stranded DNA templated by the viral RNA genome (Reverse transcription). Upon trafficking into the nucleus, the viral DNA is integrated into a host chromosome by the viral integrase (IN) protein (Integration). This completes the first half of the HIV-1 replication cycle. The integrated provirus is next transcribed by host RNA polymerases to yielded viral transcripts (Transcription), which are alternatively spliced and later translated to create the various viral protein products (Translation). Unspliced genomic RNA, along with the viral structural proteins, traffick to sites of virion assembly at the plasma membrane (Assembly). Here, the developing virion buds from host membrane and releases (Budding). Lastly, the nascent HIV-1 particle must undergo a maturation step to form a fully infectious virion (Maturation). The viral particle is now ready to find its next target cell to begin a new round of its replication cycle.

While in the cytoplasm, HIV-1 reverse transcribes its genome, creating a double-stranded DNA templated by the RNA genomes packaged within its core [14]. Retroviruses such as HIV-1 differ from other animal viruses by requiring integration into host chromosomes as an obligate step of their life cycles. Accordingly, upon trafficking into the nucleus, the double stranded viral DNA is inserted into a host chromosome by the viral IN protein [15-17]. Once integrated, the virus is transcribed by host RNA polymerase II. The resulting RNA molecules are either left intact or alternatively spliced to yield blueprints for the full complement HIV-1 viral proteins [18]. Once translated, the resulting protein products assemble with the unspliced viral genomic RNA at the plasma membrane [19]. The viral particle buds from the plasma membrane until it completes its assembly process and releases [20]. After release, the HIV-1 protease (PR) cleaves the intravirion components of the immature virion, in a process termed maturation . The mature virion, now exhibiting the classical conical core morphology associated with HIV, is now fully infectious and ready to embark on another round of infection.

General retroviral strategies for nuclear entry

Although many of the molecular mechanisms that govern the steps of the replication cycle are now well characterized, the molecular processes HIV-1 undertakes to gain access to the host chromosomes are not well understood. Aside from the periods of time when animal cells are actively dividing, cell chromosomes and the associated nucleoplasm are separated from the cytoplasm by two sets of adjoining membranes, together referred to as the nuclear envelope. Seven retroviral genera, including α through ε, lenti-, and spuma-, comprise *Retroviridae*. The γ-retrovirus Moloney murine leukemia

virus (MLV) and lentivirus HIV-1 are historic model systems for the study of retroviral nuclear import due to their contrasting dependencies on the cycling state of the cells that they infect. MLV is highly dependent on cellular mitosis, and accordingly requires the dissolution of the nuclear envelope to gain access to host chromosomes [21]. Contrastingly, HIV-1 productively infects post-mitotic cell types [22], and accordingly possesses a mechanism to bypass an intact nuclear envelope to gain access to host chromosomes.

The classical mechanism of protein import through the nuclear pore

HIV-1 nucleoprotein complexes are believed to enter the nucleoplasm by passing through nuclear pore complexes (NPCs), which stably perforate the nuclear envelope during interphase and gate-keep the trafficking of molecules between the cell nucleus and cytoplasm (**Figure 1-2**). Each NPC is composed of ~ 30 different protein constituents called nucleoporins (NUPs) [23,24], which are found in various multiples of 8 to yield the ~ 120 MDa tubular structures found in animal cells [25]. Transport through the NPC is highly selective; molecules less than ~ 9 nm in diameter are able to passively diffuse through the channel, while those up to ~ 39 nm must be actively transported by interacting with specific carrier proteins [26]. Protein cargos are most often imported by members of the karyopherin (KPN) β superfamily [27]. These proteins pass through the pore by interacting with phenylalanine-glycine (FG) motifs that are found in highly flexible domains present in about one-third of the NUPs and line the inner channel of the NPC structure. Though the precise biophysical mechanism of nuclear transport is not

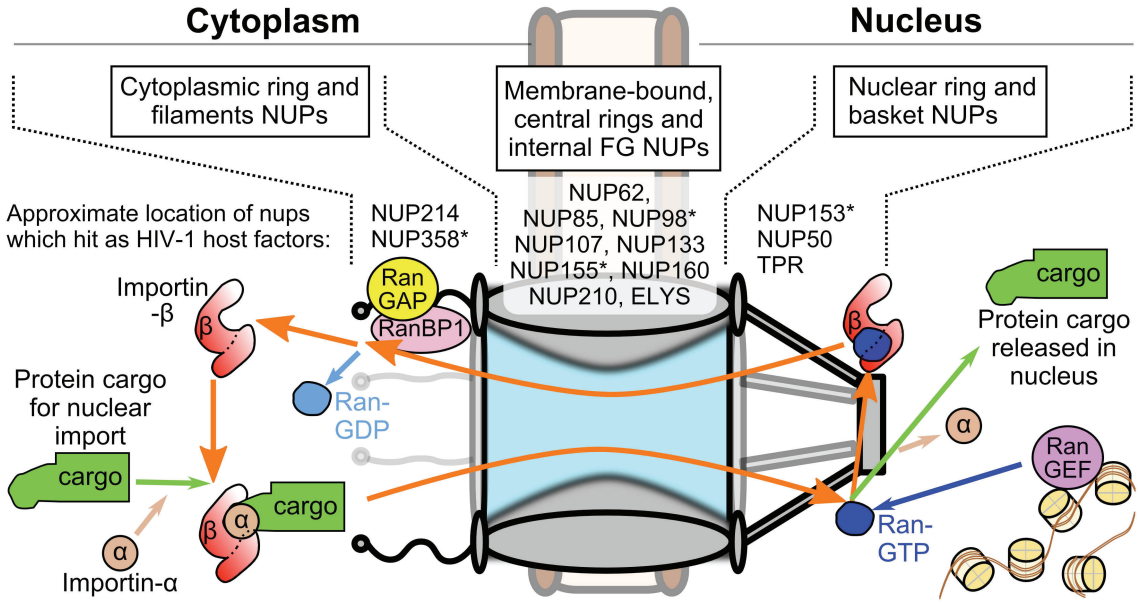

Figure 1-2. Schematic of the NPC and classical nuclear import pathway. (top) General NPC substructures and locations of NUPs that scored as potential HIV-1 co-factors in genome-wide RNA interference (RNAi) screens [28-31]. Asterisks denote NUPs that scored in more than one screen. (bottom) The Ran-based nuclear import cycle. Import protein cargo binds to a KPN β protein, oftentimes bridged by a member of the KPN α protein family (KPN β1, which is also referred to as importin β1, and KPN α2 or importin α1, depicted, are canonical members of each protein family). KPN β1 ferries the complex through the NPC channel. The engagement of KPN β1 by Ran-GTP concentrated at the nuclear basket releases the KPN α-cargo complex into the nucleus. KPN β1 becomes free to bind additional import cargo after Ran dissociates from it upon RanBP1 binding and Ran-GTP hydrolysis, stimulated by RanGAP concentrated at the cytoplasmic filaments.

completely understood, it is clear that transport is largely dictated by the properties exerted by these FG-containing domains [32].

Directionality of nuclear translocation is governed by the gradient of the small Ras-related nuclear (Ran) GTPase protein, which is established through the asymmetric distribution of two Ran co-factors on opposite sides of the nuclear envelope (**Figure 1-2**). Regulator of chromosome condensation (RCC) 1, which is also referred to as Ran guanine nucleotide exchange factor (RanGEF), achieves nuclear compartmentalization through its association with nucleosomes [33], while Ran GTPase activating protein (RanGAP) is found associated with NUP358 filaments emanating from the cytoplasmic face of the NPC [34]. The classical mechanism of protein nuclear import is governed by two features: Ran binds KPN β proteins when it is complexed with guanosine triphosphate (GTP) rather than guanosine diphosphate (GDP), and protein cargos undergoing nuclear import preferentially bind Ran-free KPN β proteins. Due to the Ran gradient, KPN β proteins bind their import cargos within the cytoplasm, and ferry their cargos through the nuclear pore by interacting with the FG barrier [35]. Once in the nucleus, abundantly present RanGTP binds the KPN β protein, freeing the protein cargo within the nucleus. RanGTP-bound KPN β proteins are able to transit back into the cytoplasm, where Ran binding protein (RanBP) 1 and RanGAP stimulate the conversion of RanGTP to RanGDP [36] and dissociate Ran from the KPN β protein, completing the import cycle. Protein nuclear export cargos differ by preferentially binding RanGTP-bound carrier proteins, such as exportin (XPO) 1, to form ternary complexes that are released into the cytoplasm when Ran is freed upon binding with RanBP1/2 [37,38].

The HIV-1 substrate for nucleocytoplasmic transport

Mature HIV-1 virions harbor a relatively full complement of viral proteins, including *gag*- (matrix, MA; capsid, CA; nucleocapsid, NC; p6) and *pol*- (PR; RT; IN) encoded proteins, as well as a handful of accessory proteins (Vif, Vpr, and Nef). CA is composed of two independently folded protein domains, the N-terminal domain (NTD) and C-terminal domain (CTD), which are separated by a flexible linker [39]. During particle maturation, approximately one-half of the complement of CA protein condenses into a conical shell that is predominantly comprised of hexameric CA rings; twelve pentameric rings afford shape declinations necessary to enclose retroviral CA shells [40-43]. The mature core shell encases the viral components that are necessary to complete the early steps of retroviral infection, which includes the two copies of the viral RNA in complex with NC, RT, and IN. The viral core undergoes its first step in a series of conformational and compositional changes that occur following its entry into the cytoplasm, when the virus begins to reverse transcribe its genome in the context of a subviral complex commonly referred to as the reverse transcription complex (RTC) (**Figure 1-3**) [44]. DNA synthesis likely triggers CA shell disassembly, as prevention of reverse transcription can delay the steps of core uncoating [45]. As the CA core begins to disassemble, some viral proteins diffuse away from the now permeable CA shell [46]. The combination of CA core disassembly and additional host-protein recruitment increases the size of the RTC to an estimated ~ 100-250 nm in diameter [47-49]. The number of complete, or near-complete reverse transcribed genomes in a population of infected cells can be readily measured by quantitative PCR, most commonly with a primer pair that generates an amplicon spanning from the upstream long terminal repeat

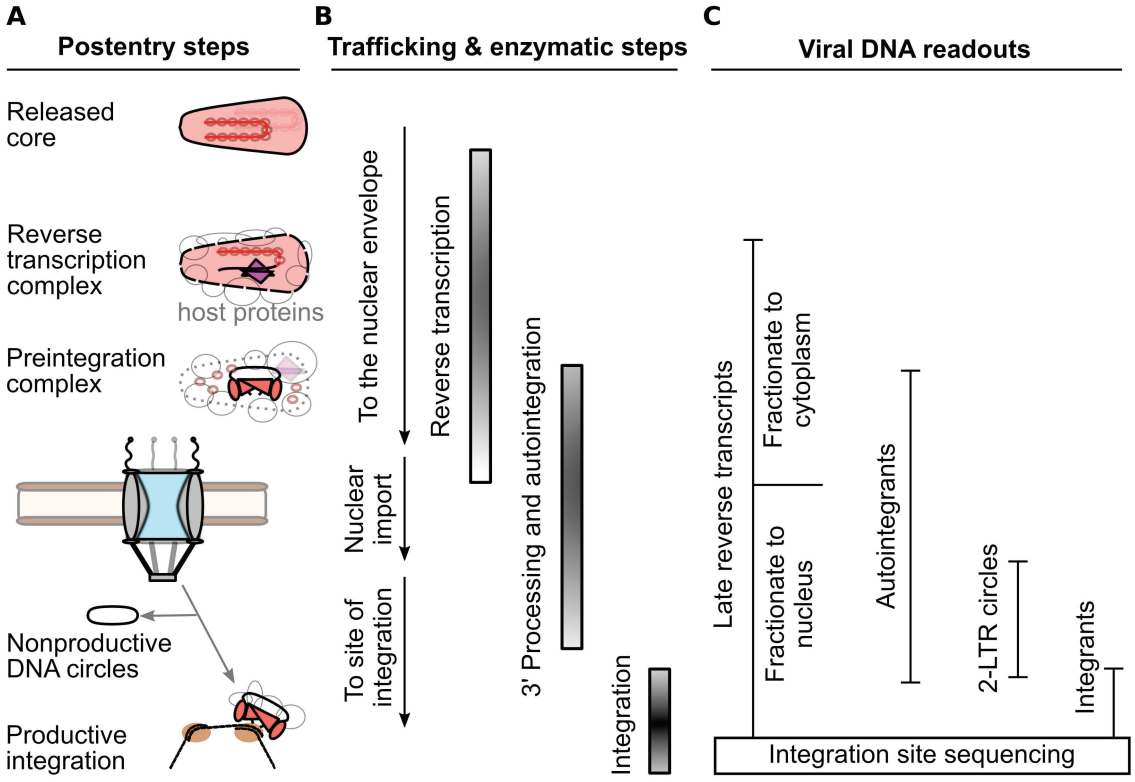

Figure 1-3. PCR-based methods for detection of post-entry to viral DNA integration steps of HIV-1 infection. (**A**) Generalized replication intermediates and byproducts leading up to integration. (**B**) Order of viral trafficking and RT and IN enzymatic steps. (**C**) Summary of viral DNA species that serve as markers for the various infection intermediates and byproducts.

(LTR) to a sequence past the primer binding site, such as a sequence in the upstream region of the *gag* gene; the viral DNAs detected by such reactions are commonly referred to as late reverse transcription (LRT) products because they depend on the second template switch of reverse transcription for their formation [50,51]. Once reverse transcription is completed, IN hydrolyzes the extremities of the linear viral DNA adjacent to conserved cytosine-adenine dinucleotides located within the viral LTRs to generate reactive CA_{OH}-3' ends [52,53]; the resulting 3'-hydroxyl groups are subsequently used by IN to cut target DNA to effect viral DNA joining [54]. By convention, the integration-competent nucleoprotein complex formed by IN 3' processing activity is referred to as the preintegration complex (PIC). These preceding steps are believed to largely occur within the cytoplasm, as the virus traffics to the nuclear periphery along microtubules [49].

Techniques for measurement of HIV-1 nuclear import

The majority of HIV-1 particles are noninfectious [55], and it is accordingly challenging to observe HIV-1 PIC nuclear transport directly with certainty. Nuclear transport is routinely inferred through comparison of steady-state levels of readily detectable markers of the bulk infection (**Figure 1-3**). Arguably, the most direct method is quantitative assessment of LRT DNA in cytoplasmic versus nuclear fractions. Importantly, this requires careful validation of the fidelity of fractionation, using control protein or nucleic acid markers appropriate to represent the separate compartments [56,57]. While many fractionation procedures likely separate soluble cytoplasmic components adequately, protocols likely differ in their abilities to distinguish

nucleoplasmic viral DNA from PICs associated with the NPC, or strongly associated with the cytoskeleton. Before successfully integrating into a host chromosome, a subset of PICs [58] are instead diverted to form non-productive DNA products through the action of host cell-mediated DNA repair pathways: 1-LTR circles can be produced by homologous recombination [59] or from aberrant reverse transcription [60,61], while 2-LTR circles are formed through non-homologous end joining of the viral DNA [62]. PCR primers that amplify products that span the LTR-LTR circle junction provide a convenient, albeit indirect measurement for assessing the competence of the virus to reach the nuclear interior [61]. Due to the generation of reactive CA_{OH} ends by IN 3' processing activity, a fraction of PICs aberrantly integrate their LTR ends back into an internal region of the viral DNA in a process referred to as autointegration [63-66]. Importantly, autointegrants formed by the insertion of one LTR end in the vicinity of the second viral DNA end can score as positive in assays quantitating 2-LTR circles, confounding the use of 2-LTR circle measures as readouts for nuclear viral DNA [66]. Specific aspects of PCR design, which take into account the DNA sequence at the LTR-LTR circle junction, can accordingly help to mitigate this complication [66]. Absolute and relative levels of integration can be measured through PCR reactions specific for integrated proviral DNA [51,67], while the distribution of integration sites along chromosomes are assessed by identifying sequences of viral-cellular DNA junctions within the infected cell population [68,69]. Although continuous advancement of various microscopy-based approaches provides an important additional avenue to assess HIV-1 nuclear import and integration [48,70,71], high-throughput, live-cell approaches capable of kinetically witnessing individual nuclear import events are not yet available.

Various biochemical approaches have yielded insight into the viral proteins that remain as part of the viral nucleoprotein substrate for nuclear import. The RTC/PIC observed in the cytoplasm exceeds the diameter of the pore [48,49], so only a fraction of the viral and cellular proteins that associate with the PIC in the cytoplasm likely enter the nucleus [48]. The double-stranded reverse-transcribed viral DNA and a tetramer of IN protein form the heart of the PIC, as they comprise the intasome nucleoprotein complex that drives integration [72,73]. Keeping in mind that only one functional PIC is formed per infectious event, the identities of other PIC-associated viral proteins have been difficult to identify precisely. MA, RT, and Vpr were repeatedly found to be components of viral nucleoprotein complexes isolated from nuclear fractions [56,74-77]. A handful of studies found NC and PR as well [75,76,78], while CA was noticeably absent from many of these same studies [56,74-78]. In fact, CA was either observed to be absent [44,77], or found in only scant amounts [79] within viral complexes extracted from whole-cell or cytoplasmic extracts, prompting initial belief that the HIV-1 core uncoats completely prior to PIC formation. Subsequent microscopy studies have more readily observed CA in association with cytoplasmic nucleoprotein complexes [48,49,80], though the duration of this association remains largely unknown. While some studies have detected CA in the nuclear fraction following HIV-1 infection [81,82], it is not entirely clear how much of this signal represents intranuclear CA rather than CA protein associated with the nuclear envelope. It would therefore be instructive to determine how much of this signal co-fractionates with nuclear PICs.

Viral and cellular elements implicated in HIV-1 PIC nuclear import

Many of the viral elements found in association with the PIC have been proposed to be important for HIV-1 nuclear import. Nuclear localization signals (NLSs) present in MA [83,84] and IN [76,85], as well as various non-canonical karyophilic signals in Vpr [77,86-90], have each been proposed to recruit cellular nuclear transport proteins. Basic-type NLSs within IN have been proposed to recruit KPN α adaptor proteins importin α1 (Rch1) [76] and importin α3 (KPNA4) [91], which would presumably require additional binding to KPN β1 for function (**Figure 1-2**). IN can also directly interact with KPN β proteins importin 7 [92,93] and transportin 3 (TNPO3, TRN-SR2, or importin 12) [70,94], though the relevance of these interactions have been brought into question [95-97]. IN and Vpr are additionally proposed to bind NUPs directly to facilitate nuclear import without the need for adaptor KPN carrier proteins, which include interactions between IN and NUP153 [98], and Vpr with Pom121 [86] or hCG1 [99].

The reverse transcribed genome is suggested to be an important determinant of HIV-1 PIC nuclear import, primarily through a triple stranded DNA flap element generated through the action of the central polypurine tract (cPPT) and central termination signal (CTS) [100,101]. While this element is not absolutely required for either nuclear import or infection [102-104], numerous groups have confirmed that the DNA flap exerts a positive effect during infection [105-107]. DNA plus-strand extension from the cPPT primer likely decreases the overall duration of reverse transcription within the cell [106,108], which may indirectly influence viral nuclear import during instances of limiting nucleotide concentrations, for example. Such a kinetic advantage to reverse transcription conferred by the cPPT is consistent with its ability to reduce the time-frame

in which the viral single-stranded DNA is sensitive to the inhibitory activity of APOBEC3 cytosine deaminase restriction factors [109-111], and may similarly protect the RTC/PIC from other host defense proteins that could derail its trafficking.

While HIV-1 MA, IN, and Vpr NLSs can confer nuclear localization when fused to otherwise cytoplasmic proteins, some studies have refuted the importance of these signals in PIC nuclear import during infection [103,106,112-114]. Various features of HIV-1 biology can help to explain some of these discrepancies. Firstly, MA and IN in particular are not known to function as free proteins during the early phase of HIV-1 infection. Thus, studying MA or IN as recombinant proteins expressed in human cells may not uncover behaviors relevant to PIC biology. Secondly, many of the viral constituents of the PIC are multifunctional proteins, whereby mutations may result in multiple coincident defects to infection, obfuscating the targeted assessment of contributions to a particular phenotype. Lastly, there is little evidence to support that HIV-1 enters the nucleus during mitosis when its passage through the NPC is blocked [115]. Thus, the historical perspective that HIV-1 nuclear import mutants would specifically be blocked for infection of non-dividing target cell types would since appear to be largely misguided.

CA functionally determines requirements for nuclear trafficking

The field has more recently moved to view CA as the major viral protein that mediates HIV-1 nuclear import. Masahiro Yamashita and Michael Emerman demonstrated that infection by an HIV-1 chimeric virus that carried the MLV CA protein was cell cycle dependent [116], mimicking the property of parental MLV. The defect to

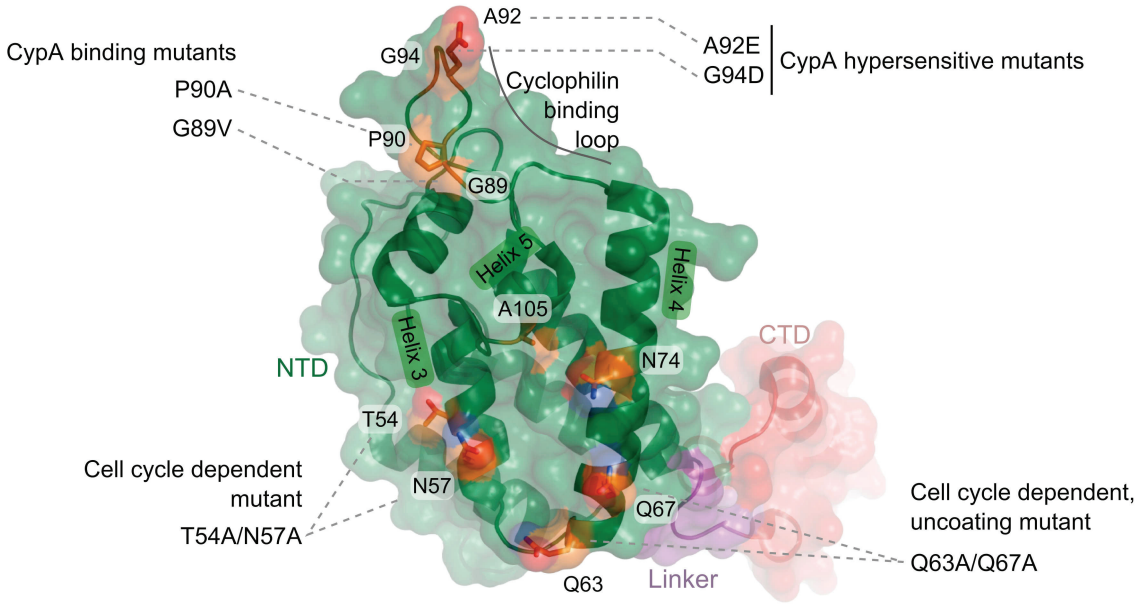

Figure 1-4. Schematic of HIV-1 CA and mutations. A single HIV-1 CA monomer (protein database code 3j34) is represented by a cartoon of the peptide backbone, as well as a semi-transparent surface: NTD, green; flexible linker, purple; CTD, red. A subset of CA residue side-chains that exhibit phenotypic differences in preintegrative steps of HIV-1 infection are shown as sticks and colored as follows: carbon, orange; nitrogen, blue; oxygen, red

infection upon cell cycle arrest was at the step of nuclear import, as a decrease in the formation of 2-LTR circle DNAs relative to wild-type (WT) HIV-1 was observed [116]. They subsequently determined that certain point mutations in HIV-1 CA, including T54A/N57A and Q63A/Q67A (**Figure 1-4**), also imparted cell cycle dependence to HIV-1 [57]. Notably, the infection defect exhibited by the T54A/N57A mutant virus upon cell cycle arrest occurred after nuclear entry but before integration [57]. While this mutant was sensitive to cell cycle arrest in all cell lines tested, the growth arrest phenotypes of A92E and G94D CA mutant viruses, which are hypersensitive to the levels of CA-interacting host protein cyclophilin A (CypA) in certain cell lines (Hela and H9 cells), were restricted to these same cells [117,118]. Cell cycle arrest also inhibited these viruses after nuclear import, as both LRT and 2-LTR circle levels remained unchanged. While the infection defects experienced by these CA mutant viruses upon cell cycle arrest occur following HIV-1 nuclear entry, the Q63A/Q67A mutant virus appeared to be defective for nuclear import, as it exhibited decreased levels of 2-LTR circle formation as compared to WT virus in dividing cells [119]. Q63A/Q67A CA cores recovered from whole virions following detergent treatment were less stable than WT cores in vitro [120], but the mutant viral RTCs and PICs retained a greater complement of CA protein than did the WT virus during infection [45,57,119]. This apparent delay in Q63A/Q67A core uncoating appears related to the nuclear import and integration defects experienced by this mutant virus.

A number of additional CA-interacting host factors have been observed to affect HIV-1 nuclear import and integration. The rhesus Trim5α restriction factor normally restricts HIV-1 infection by targeting the viral core for disassembly and degradation prior

to the completion of reverse transcription [121,122]. Inhibition of cellular proteasome activity with the small molecule MG132 rescued reverse transcription while having no effect on the ultimate level of integration [123]. The MG132-rescued RTCs seemingly remain intact [124] and mature into integration-competent PICs [125]. These complexes also escape entrapment by proteasome-associated cytoplasmic bodies [126] yet accumulate fewer 2-LTR circles, consistent with a trafficking defect coincident with or shortly prior to nuclear import [123,125]. Various artificially engineered Trim-CypA fusion constructs have also been shown to cause defects to infection after reverse transcription, though these appear to occur after nuclear entry [127].

Perturbation of CA can also affect the post-reverse transcription steps of other retroviruses. Though MLV does not enter the nucleus via the NPC, it must also in large part dissolve its CA shell to effect IN-mediated integration. MLV CA is readily found in RTCs purified from infected cells, and remains stably associated with the PIC until it enters the nucleus [128]. MLV p12, a *gag*-encoded protein not found in HIV-1, is crucial for nuclear targeting as it tethers PICs to mitotic chromosomes [129-131]. While MLV CA dissociates from the PIC during mitosis, p12 mutants PM14 and S61A/S65A, which are defective for mitotic chromosomal tethering, each maintain CA in association with the PIC during mitosis [132]. Certain murine cells take advantage of RTC/PIC-associated CA to interrupt the MLV infection mechanism: the protein expressed from Friend virus susceptibility-1 (*Fv1*), which is a *gag*-related gene from a murine endogenous retroelement [133], is able to target MLV cores to inhibit infection [134-136]. Restricted MLV still reverse transcribes and forms PICs capable of integrating in vitro [137], yet does not form circular DNA byproducts [138,139]. The product of the Fv1 gene can also

inhibit HIV-1 infection when targeted to HIV-1 CA upon fusion to CypA, resulting in a quantifiable decrease in the number of integrated proviruses while leaving the accumulation of 2-LTR circles unchanged [140].

Together, these results show that the retroviral core shell is unlikely to passively fall apart upon viral entry, but instead functions at a critical juncture bridging reverse transcription and nuclear trafficking. Although premature CA disassembly and proteasomal targeting may exert their effects as early as reverse transcription, other perturbations to CA uncoating and CA-determined trafficking defects prevent PIC nuclear import, or even manifest as defects within the nucleus. MLV has specifically evolved to access chromosomes during mitosis, and accordingly, the combined functions exerted by MLV CA and p12 likely specifically link MLV uncoating and nuclear entry with mitosis. In the aforementioned chimeric HIV-1 encoding MLV *gag*, the PIC is likely forced into an MLV-type mechanism of nuclear entry. Contrastingly, the cell cycle dependence of HIV-1 CA missense mutations may be due to reasons stemming from various potential losses in function: for example, perturbed core engagement with host proteins may result in a virus blocked at one of many preintegrative steps of infection, and may require cellular rearrangements that occur during cell division to relieve this block. While the previously described phenotypes affecting CA reveal the effects the retroviral core may exert on the steps following reverse transcription, recent findings that CA protein physically associates with nuclear transport factors hints that CA takes a direct role in promoting the nuclear steps of HIV-1 infection.

RNA interference screens highlight specific nuclear transport proteins as HIV-1 host factors

A series of genome-wide RNAi screens [28-31] identified numerous nuclear transport factors as potential HIV-1 cofactors: TNPO3, NUP358/RANBP2, NUP155, NUP153, and NUP98 were each identified in two independent screens, while a number of additional NUPs (NUP50, NUP62, NUP85, NUP107, NUP133, NUP160, NUP210, NUP214, ELYS, and TPR) and soluble transporters (KPN β1, XPO1, and NXF1) each hit once [28-31,141] (**Figure 1-2**). The HIV-1 requirement for TNPO3, NUP358, and NUP153 were initially mapped to the nuclear steps of infection, either preceding or concomitant with integration [29].

TNPO3 (also referred to as Transportin-3 or Transportin-SR2) is a soluble transport receptor belonging to the KPN β superfamily. TNPO3 is responsible for the nuclear import of a subset of serine/arginine-rich host proteins required for pre-mRNA splicing, termed SR-proteins [142]. NUP358 (also referred to as RanBP2) is a large NUP that forms the cytoplasmic filaments which emanate from the cytoplasmic side of the nuclear pore complex [143-145]. The domains of this protein are involved in many different cellular functions: Ran-binding domains and FG repeats involved in controlling nucleocytoplasmic transport [146], zinc fingers required for nuclear envelope breakdown during mitosis [147], a SUMO E3 ligase domain necessary for sumoylation-based protein targeting [148], various domains for interacting with kinesins and microtubules to mediate organelle interaction with the cytoskeleton [149,150], and a C-terminal CypA homologous domain (CHD) likely involved in protein isomerization [151-153].

Nucleoporin NUP153 is a potential HIV-1 cofactor for HIV-1 PIC trafficking

My work has focused on NUP153, which is a relatively large (1475 amino acid) NUP found on the nuclear side of the NPC [154]. Its NTD is important for its localization and its functions in NPC scaffolding: it houses a nuclear localization signal [155], and it has separate regions involved in nuclear envelope binding [156], as well as protein interactions with nucleoporins NUP160, NUP50, and TPR [157-159]. Its central zinc-fingers bind Ran [160], but also recruit COPI for nuclear envelope breakdown during mitosis [147,161]. Most interestingly, NUP153 possesses a long, highly flexible CTD which reaches into the central channel [162] and can extend across to the cytoplasmic side of the NPC in a transport-dependent manner [163-165]. This domain contains 29 FG motifs of the patterns FG, FxF, or FxFG, and is involved in the nucleocytoplasmic transport of a variety of protein or nucleoprotein cargos [166,167].

In this thesis, I describe our investigation of the role of NUP153 during the process of HIV-1 ingress, particularly the postentry steps leading up to viral integration. I found that a direct interaction between the NUP153 FG motifs and the HIV-1 capsid protein underlie the viral requirement for NUP153 during its nuclear import, serving as a novel example of viral hijacking of a key feature of cellular nucleocytoplasmic transport. I propose that similar mechanisms of direct binding between viral capsids and host cell phenylalanine-glycine motifs extends to additional retroviruses, and may even extend to additional viral families.

Chapter 2

Human Immunodeficiency Virus Type 1 (HIV-1) Capsid Determines the Requirement for Cellular NUP153 during a Nuclear Step of HIV-1 Infection

Human Immunodeficiency Virus Type 1 (HIV-1) Capsid Determines the Requirement for Cellular NUP153 During a Nuclear Step of HIV-1 Infection

Kenneth A. Matreyek and Alan Engelman

Department of Cancer Immunology and AIDS, Dana-Farber Cancer Institute, and Department of Medicine, Harvard Medical School, Boston, Massachusetts 02215

* This chapter is adapted from the publication:

Matreyek KA, Engelman A. The requirement for nucleoporin NUP153 during human immunodeficiency virus type 1 infection is determined by the viral capsid. J Virol. 2011 Aug;85(15):7818-27

Contributions: I performed all of the experiments described in this manuscript. Alan Engelman and I both wrote the manuscript.

Abstract

Lentiviruses likely infect nondividing cells by commandeering host nuclear transport factors to facilitate the passage of their PICs through NPCs within nuclear envelopes. Genome-wide small interfering RNA screens previously identified karyopherin β transportin-3 (TNPO3) and NPC component NUP153 as being important for infection by HIV-1. The knockdown of either protein significantly inhibited HIV-1 infectivity, while infection by the gammaretrovirus MLV was unaffected. Here, we establish that primate lentiviruses are particularly sensitive to NUP153 knockdown and investigate HIV-1-encoded elements that contribute to this dependency. Mutants lacking functional Vpr or the central DNA flap remained sensitive to NUP153 depletion, while MLV/HIV-1 chimera viruses carrying MLV MA, CA, or IN became less sensitive when the latter two elements were substituted. Two CA missense mutant viruses, N74D and P90A, were largely insensitive to NUP153 depletion, as was WT HIV-1 when CypA was depleted simultaneously or when infection was conducted in the presence of cyclosporine A. The codepletion of NUP153 and TNPO3 yielded synergistic effects that outweighed those calculated based on individual knockdowns, indicating potential interdependent roles for these factors during HIV-1 infection. Quantitative PCR revealed normal levels of late reverse transcripts, a moderate reduction of 2-LTR circles, and a relatively large reduction in integrated proviruses upon NUP153 knockdown. These results suggest that CA, likely by the qualities of its uncoating, determines whether HIV-1 requires cellular NUP153 for PIC nuclear import.

Introduction

The early steps of the retroviral life cycle occur within the context of nucleoprotein complexes that are derived from the core of the infecting viral particle. The RT enzyme converts genomic RNA into linear double stranded viral DNA (vDNA) within the confines of the RTC [44,128]. Soon thereafter, the IN enzyme catalyzes its initial activity, 3' processing, whereby each vDNA 3' end is cleaved adjacent to the conserved dinucleotide sequence CpA. This marks the transition from the RTC to the PIC, wherein IN catalyzes its second catalytic function, DNA strand transfer [168,169]. Concomitantly, the complexes undergo morphological transitions, such as the dissolution of the viral CA core, as they traffic from the cellular periphery to desired regions of host DNA within the nucleus [44,49,56,128]. Well-studied but still-unresolved aspects of these steps are the mechanisms by which retroviruses bypass the nuclear envelope, which physically separates the nuclear and cytoplasmic compartments of the cell (reviewed in [170]). Although certain viruses, such as the gammaretrovirus MLV, are believed to require the dissolution of the nuclear membrane during mitosis [21], lentiviruses such as HIV-1 are able to infect nondividing cells and thus are believed to traverse the nuclear membrane by passing through the NPC [115,171]. As the HIV-1 PIC has been estimated to have a stokes radius of 28 nm [79] and thus grossly exceeds the ~9-nm diffusion limit [172] of the NPC, lentiviruses theoretically possess at least one mechanism to hijack the nuclear transport machinery and actively transport their PICs through the pore.

A number of HIV-1 PIC components, including MA, Vpr, IN, and the central DNA flap formed during reverse transcription, have been proposed to function during

nuclear import, although significant roles for any of these components during this step have not been well corroborated. This may, at least in part, be reflective of redundant PIC nuclear import mechanisms, although viruses with these elements mutated in combination did not exhibit obvious cell cycle-dependent infectivity or nuclear import defects [106,173]. In contrast, CA can determine the ability of HIV-1 to infect nondividing cells, suggesting that viral core uncoating is a rate-limiting step of lentiviral PIC nuclear import [57,174].

Numerous studies also have examined the requirements for specific cellular proteins during lentiviral/HIV-1 PIC nuclear import, including nuclear transport proteins NUP98 [175], importin 7 [176], KPN α2 Rch1 [76], and importin α3 [91]. A series of three genome-wide siRNA screens [28-30] highlighted nuclear transport proteins whose depletion strongly inhibited the early steps of HIV-1 infection. This included TNPO3 or transportin-SR2, a member of the KPN β superfamily responsible for transporting splicing factors with SR motifs into the nucleus. The depletion of TNPO3 resulted in a sizable HIV-1 nuclear import defect [70] while infection by MLV or the lentivirus feline immunodeficiency virus (FIV) remained largely unaffected [96,177,178], suggesting TNPO3 dependence to be specific to, although perhaps not obligatorily required by, lentiviruses. The mechanism by which HIV-1 physically hijacks TNPO3 remains unsolved; even though TNPO3 can bind HIV-1 IN [70], comparable levels of binding to MLV and FIV INs were observed [96,178], and analyses of HIV-1 proteins relevant during the infection of TNPO3 knockdown cells implicated the CA protein as the genetic determinant of TNPO3 dependency [96].

In addition to TNPO3, two major constituent proteins of the NPC, nucleoporins NUP358/RanBP2 and NUP153, were identified in two of the siRNA screens [28,29]. NUP358 composes the large cytoplasmic filaments emanating from eukaryotic NPCs [144], the knockdown of which was recently confirmed to result in a defect of HIV-1 nuclear entry during infection [179]. NUP153 is localized within the nucleus, linking central NPC scaffolding subcomplexes with their corresponding nuclear basket substructure, as well as anchoring individual NPCs with the nuclear lamina [180]. Additionally, NUP153 dynamically shuttles between NPC-localized and nucleoplasmic populations [181]. Although NUP153 knockdown also was interpreted to result in a defect in HIV-1 nuclear import, the lack of clear correlation between an approximately 85% reduction in acute infection and 20% reduction in 2-long terminal repeat 2- LTR-containing DNA circle levels, a marker for PIC entry into the nucleus [29], suggested to us that other factors were at play. NUP153 has been reported to bind HIV-1 IN and Vpr [98,182], suggesting potential mechanistic clues for the role of this host factor during HIV-1 infection. To investigate how NUP153 facilitates HIV-1 infection, we analyzed viral determinants that render HIV-1 sensitive to NUP153 depletion and additionally performed qPCR analyses of the viral DNA species formed during the infection of NUP153 knockdown cells.

Results

Depletion of NUP153 expression inhibits HIV-1 infection.

RNAi was used to knock down NUP153 expression and analyze the role of this host factor during HIV-1 infection. HeLa cells were transfected with one of two previously characterized NUP153-specific siRNAs [183,184] or a nontargeting siControl mismatch to siNUP153#1, and protein expression levels were measured 48 h later. Western blotting of whole-cell lysates showed NUP153 expression to be depleted greater than 8-fold by either siRNA (**Figure 2-1A**). NUP153 knockdown cells infected with HIV-1 or MLV revealed that siNUP153#1 and siNUP153#2 significantly reduced HIV-1 infectivity to 3.2 and 3.4% of siControl-treated cells, respectively (**Figure 2-1B**). MLV was less or not significantly inhibited in parallel infections. Because cells transfected with siNUP153#2 showed evidence of cytotoxicity (data not shown), siNUP153#1 was used for the remainder of the study.

To further address the specificity of NUP153 knockdown on HIV-1 infection, protein levels in depleted cells were restored via expression of an exogenously introduced siRNA-insensitive cDNA. siRNA-transfected HEK293T cells were retransfected with the inert pUC19 plasmid, an empty expression vector encoding an internal ribosome entry site (IRES)-controlled dsRed-Express fluorescent protein, or an engineered vector encoding NUP153 5’ of the IRES element. Western blot analysis of cells lysed at the time of infection showed more robust exogenous NUP153 expression than the endogenous protein in both knockdown and control cells (**Figure 2-1C**). As gross overexpression of NUP153 has been shown to distort the nuclear envelope [185], virus-infected green

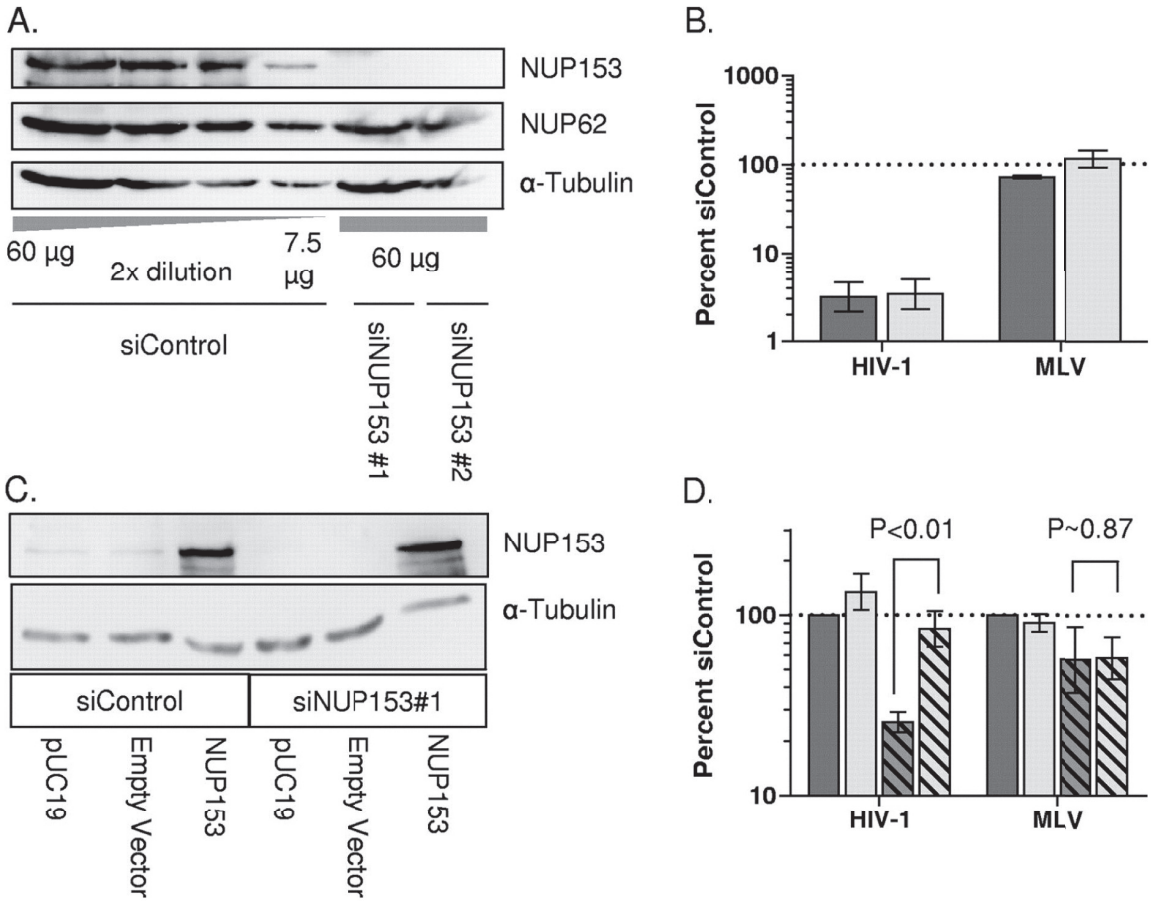

Figure 2-1. NUP153 expression and HIV-1 infection. (**A**) Twofold dilutions of a whole-cell extract from control cells (lanes 1 to 4) compared to extracts from NUP153-depleted cells (lanes 5 and 6). NUP62 cross-reacted with the utilized anti-NUP153 antibody. (**B**) Percent infectivity of GFP reporter viruses in HeLa cells transfected with siNUP153#1 (dark gray) or siNUP153#2 (light gray) compared to control cells. Results are averages from three experiments, each performed in triplicate; error bars denote 95% confidence intervals. (**C**) HEK293T cells transfected with siControl or siNUP153#1 were retransfected with either control DNA (pUC19), empty IRES-dsRed-Express vector, or the vector expressing siRNA-resistant NUP153 protein. (**D**) Cells in panel C were gated for dim dsRed-Express expression, and the infectivities of GFP reporter viruses were normalized to those of cells transfected with the empty vector. Solid and hatched bars, cells transfected with siControl and siNUP153#1, respectively; dark and light gray bars, cells transfected with empty and NUP153 expression vectors, respectively. The results are averages from four experiments performed in duplicate, with error bars denoting 95% confidence intervals.

fluorescent protein (GFP)-positive cells were quantitated within cell populations gated for the dim fluorescence of the dsRed-Express protein. HIV-1 infection of NUP153 knockdown HEK293T cells was significantly inhibited compared to the infection of control cells, while exogenous NUP153 expression restored infection to levels similar to those of controls (**Figure 2-1D**). Although MLV in this experiment was partially affected by NUP153 knockdown, this effect was inert to NUP153 reexpression.

Differential retroviral dependencies on cellular NUP153.

We investigated whether NUP153 dependency was specific or common to lentiviruses by testing the infectivities of a panel of retroviral reporter constructs. To determine whether the stark infectivity defect observed with HIV-1 extended to other primate lentiviruses, GFP reporter viruses for HIV-2_{ROD}, SIV_{MAC}, SIV_{AGM}Tan, and SIV_{AGM}Sab were analyzed. NUP153 depletion significantly inhibited infection by each of these viruses, with values ranging from 3.3% for SIV_{AGM}Tan to 10.6% for SIV_{MAC}, while infection by MLV was slightly enhanced under these conditions (**Figure 2-2A**). In contrast, similar experiments showed more-divergent retroviruses to be less sensitive to NUP153 depletion (**Figure 2-2B**). NUP153 knockdown significantly inhibited equine infectious anemia virus (EIAV) infection, to 33.4% of the level for the control. The alpharetrovirus Rous sarcoma virus (RSV) and betaretrovirus Mason-Pfizer Monkey Virus (MPMV) also were significantly affected but to even lesser extents, at 53.7 and 38.7% of the control level, respectively (**Figure 2-2B**). Consistently with results of Lee et al. [177], infection by FIV was largely unaffected by NUP153 knockdown.

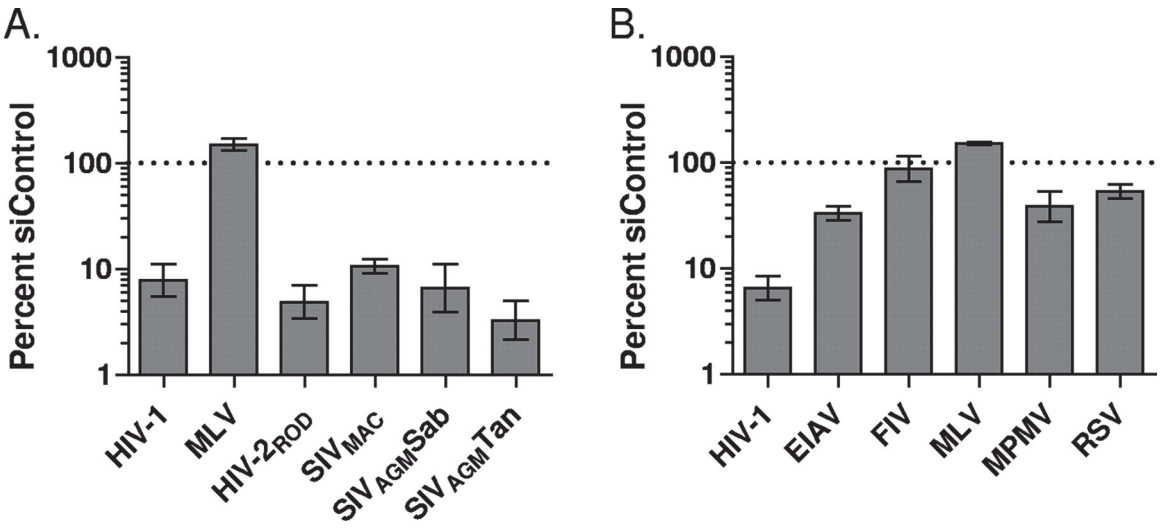

Figure 2-2. Retroviral susceptibilities to NUP153 knockdown. HeLa cells transfected with siNUP153#1 or siControl were infected with GFP reporter viruses specific to primate lentiviruses (**A**) or different types of retroviruses (**B**). Results are averages from at least three experiments performed in triplicate, with error bars denoting 95% confidence intervals.

Neither Vpr nor the central DNA flap play significant roles in NUP153 dependency during HIV-1 infection.

Viral elements implicated in HIV-1 nuclear import were analyzed to determine which ones might contribute to NUP153 dependency. Neither the central DNA flap nor Vpr are essential for HIV-1 infectivity, so mutations that completely abrogated function were analyzed here [114,186]. Reporter viruses with either or both elements mutated were applied to NUP153 or control knockdown cells at two levels of input: 5×10^6 or 5×10^4 RT-counts per minute (RTcpm). Similarly to previous observations, single and double mutant viral infectivities were comparable to that of the WT [106,114,186] (**Figure 2-3A**, dark gray bars). To determine whether sensitivity to NUP153 depletion was altered by these mutations, the infectivities of each mutant virus in knockdown cells were normalized to their corresponding control sample and regraphed (**Figure 2-3B**). Infections performed with either quantity of viral inocula were significantly decreased when NUP153 was knocked down, although as a group infections performed with less virus showed a slight, but not significant, increase in sensitivity to the knockdown. Although Vpr mutant viruses showed slight differences in sensitivity to the knockdown with both quantities of inocula, none of these values reached statistical significance.

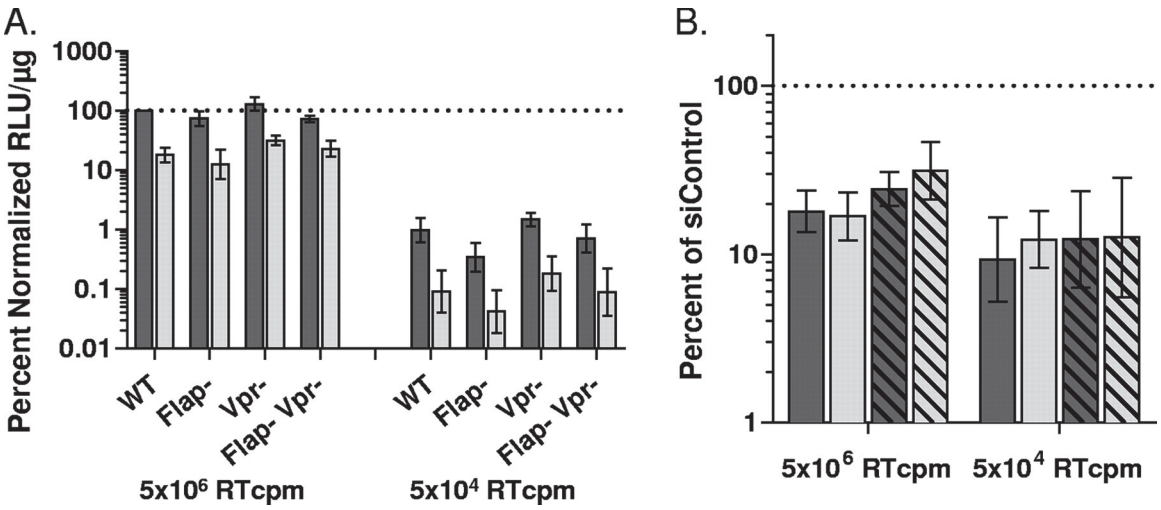

Figure 2-3. NUP153 dependency during HIV-1 infection is independent of Vpr and the central DNA flap. (**A**) Viral infectivities were normalized to the level obtained with 5×10^6 RTcpm of WT virus (set to 100%). Dark gray, siControl; light gray, siNUP153#1. (**B**) Regraph of panel A results, with infectivities in knockdown cells expressed as percentages of control cells, which were set at 100%. Solid dark gray, WT virus; light gray, DNA flap mutant; hatched bars, Vpr mutant viruses. Results are averages from four experiments performed in duplicate, with error bars denoting 95% confidence intervals. RLU, relative light units.

Replacement of HIV-1 IN or CA with MLV counterparts influences NUP153 dependency, while MA does not.

Essential roles of MA, IN, and CA proteins during the early and/or late steps of HIV-1 replication precluded the use of deletion constructs in infectivity assays. Because NUP153 depletion resulted in dramatically different levels of MLV and HIV-1 infection [29] (**Figure 2-1B**), we instead tested a set of HIV-1-based chimera viruses containing differing amounts of MLV Gag and/or Pol proteins [116,173] (**Figure 2-4A**). Chimera viral names indicate the swapped MLV protein(s). For example, mMAp12 carries MLV MA and p12, whereas mMAp12CA additionally harbors MLV CA.

Upon NUP153 depletion, the infectivity of the parental HIV-1_{LAI} isolate was significantly decreased to 2.1% of that of the control, while MLV remained unaffected at 112.1% (**Figure 2-4B**). The infectivity of mMAp12 was indistinguishable from that of HIV-1_{LAI}, while the addition of MLV CA reduced dependency on NUP153 about 10-fold, to 22.7% of that of the control. The separate replacement of the IN protein in mIN also yielded a significant, approximately 4-fold difference from HIV-1_{LAI} to 9.1% of that of the control, although this sample exhibited greater experimental variability. The combination virus containing MLV MA, p12, CA, and IN was not inhibited by NUP153 depletion, exhibiting 149.6% infectivity compared to that of the control.

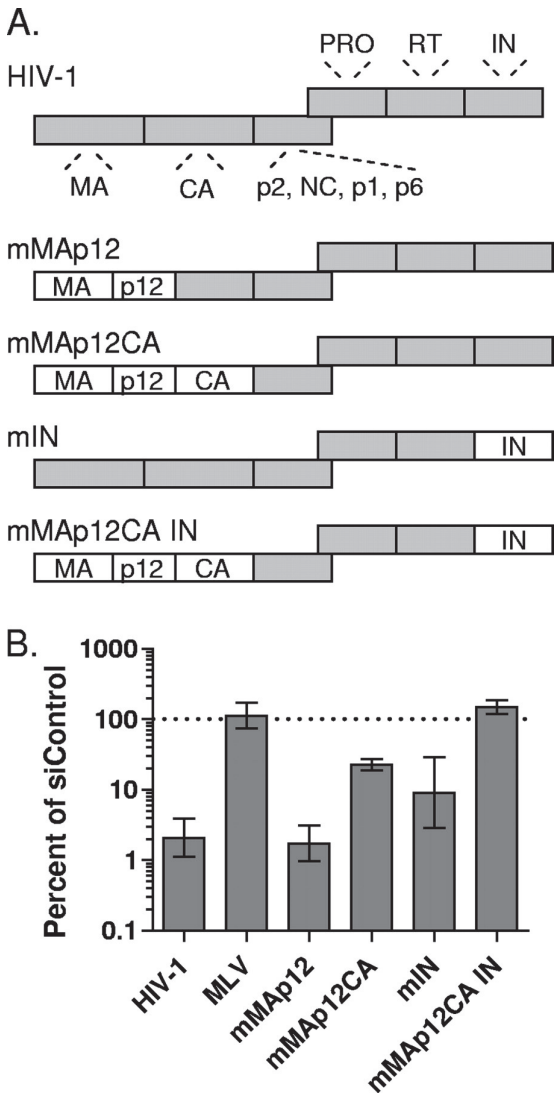

Figure 2-4. NUP153 dependencies of MLV / HIV-1 chimera viruses. (**A**) Illustration of constructs tested (not to scale), with major HIV-1 Gag and Pol proteins indicated in gray (NC, nucleocapsid; PR, protease) and MLV proteins in white. (**B**) Control or knockdown cells were infected with HIV-1_{LAI}, MLV, or HIV-1-derived MLV chimera viruses shown in panel A. Results are averages from three experiments performed in triplicate, with error bars denoting 95% confidence intervals.

Alteration of HIV-1 sensitivity to NUP153 depletion by CA missense mutations or cyclosporine treatment.

The preceding experiment revealed CA as a dominant determinant of NUP153 dependency, so we next surveyed a panel of previously characterized CA missense mutant viruses for NUP153 dependency during infection. Mutants of the CypA binding loop, encompassing HIV-1 residues His83 to Arg99, included G89V and P90A, which exhibit greatly diminished CypA binding [187], and A92E and G94D, whose infectivities are cell type specific [188,189]. Non-CypA loop mutants E45A and Q63A/Q67A, which exhibit altered core stability both in vitro and ex vivo [57,119,120,190], experience greatly decreased infectivities across cell types. A relatively large viral inoculum, 4×10^6 RTcpm, therefore was utilized to provide robust signals across the mutant virus set.

Consistently with previous reports, the infectivities of E45A and Q63A/Q67A were severely compromised, while G89V, A92E, and G94D yielded moderate defects and the N74D and P90A mutants infected HeLa cells at levels comparable to that of the WT (**Figure 2-5A**, dark gray bars). Comparison of infectivities in knockdown and control cells confirmed N74D to be insensitive to NUP153 depletion [177] (**Figure 2-5A and 2-5B,** light gray bars). E45A appeared moderately less sensitive to knockdown than the WT, while the Q63A/Q67A mutant was not distinguishable from the WT. A92E and G94D were at least as, if not more, sensitive to NUP153 depletion as the WT, while the CypA binding mutants G89V and P90A exhibited contrasting sensitivities: G89V was sensitive while P90A was resistant (**Figure 2-5A and 2-5B**, light gray bars). The P90A

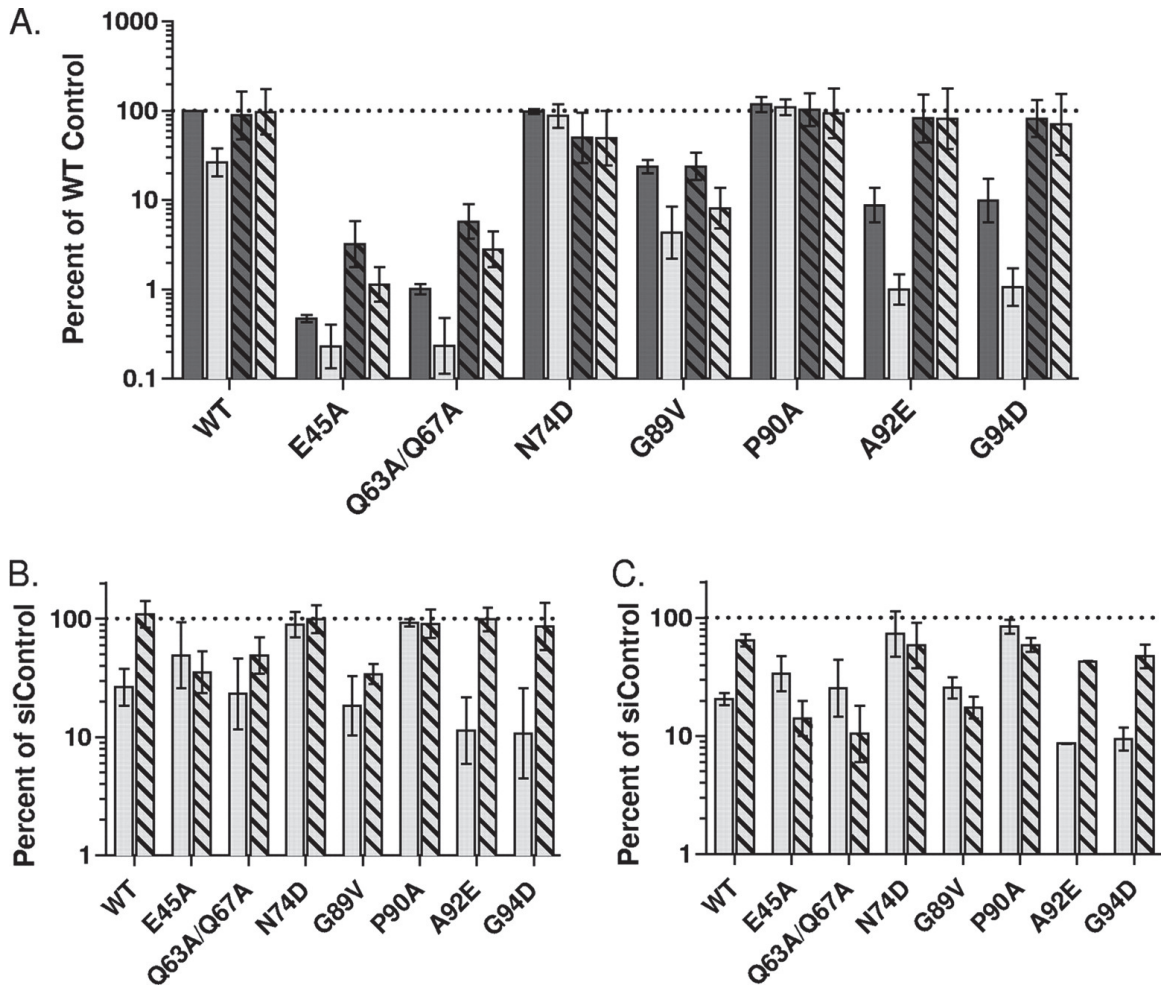

Figure 2-5. WT and CA mutant viral infectivities and cyclosporine dependences in control and NUP153 knockdown cells. (**A**) Control (dark gray) or NUP153 knockdown (light gray) cells were left untreated (solid bars) or were treated with 5 μM cyclosporine (hatched bars) at the time of infection. All samples were normalized to the infectivity of WT virus in untreated control cells, which was set at 100%. The results are averages from three experiments, each performed in duplicate, with error bars denoting 95% confidence intervals. (**B**) Regraph of panel A results, with infectivities in knockdown cells expressed as percentages of the infectivity of control cells; hatched bars denote infections in the presence of CsA. The results are averages from six experiments performed in duplicate, with error bars denoting 95% confidence intervals. (**C**) Infectivities in NUP153 knockdown cells compared to that of control cells, with hatched bars denoting cells in which CypA was simultaneously depleted. Results are averages from two experiments performed in duplicate, with error bars denoting 95% confidence intervals.

phenotype appeared to be cell type specific, as partial sensitivity to NUP153 knockdown was observed in HEK293T and GHOST-CXCR4 cells (data not shown).

As the interaction of CA with CypA can govern HIV-1 uncoating [191], WT and CA mutant viral dependencies were evaluated in the presence of cyclosporine to disrupt this protein-protein interaction. As previously observed in HeLa cells [188,192], the WT was relatively unaffected by cyclosporine treatment, while E45A, Q63A/Q67A, A92E, and G94D witnessed approximately 5- to 10-fold increases in infectivity (**Figure 2-5A**, compare dark gray hatched and solid bars). Interestingly, cyclosporine treatment rendered the WT, A92E, and G94D viruses fully insensitive to NUP153 depletion (**Figure 2-5A**, dark gray hatched bars, and **2-5B**, hatched bars). This effect was not observed with all NUP153-sensitive CA mutants, as the G89V mutant remained largely dependent on the host factor in the presence of the drug. Similar results were observed with CypA knockdown in place of cyclosporine treatment: CypA knockdown resulted in approximately 5- to 20-fold increases in the infectivities of E45A, Q63A/Q67A, A92E, and G94D mutant viruses (data not shown), and WT, A92E, and G94D viruses were rendered significantly less sensitive to NUP153 depletion when CypA was knocked down simultaneously (**Figure 2-5C**, compare hatched to solid bars).

Interdependent requirement for NUP153 and TNPO3 during HIV-1 infection.

Primate lentiviruses revealed strong dependencies on NUP153 and TNPO3, while MLV, FIV, and the N74D HIV-1 CA mutant virus were largely unaffected by either knockdown [96,177] (**Figure 2-2**). We therefore tested if these proteins would reveal evidence for interdependence during HIV-1 infection. Because Thys et al. [178] recently

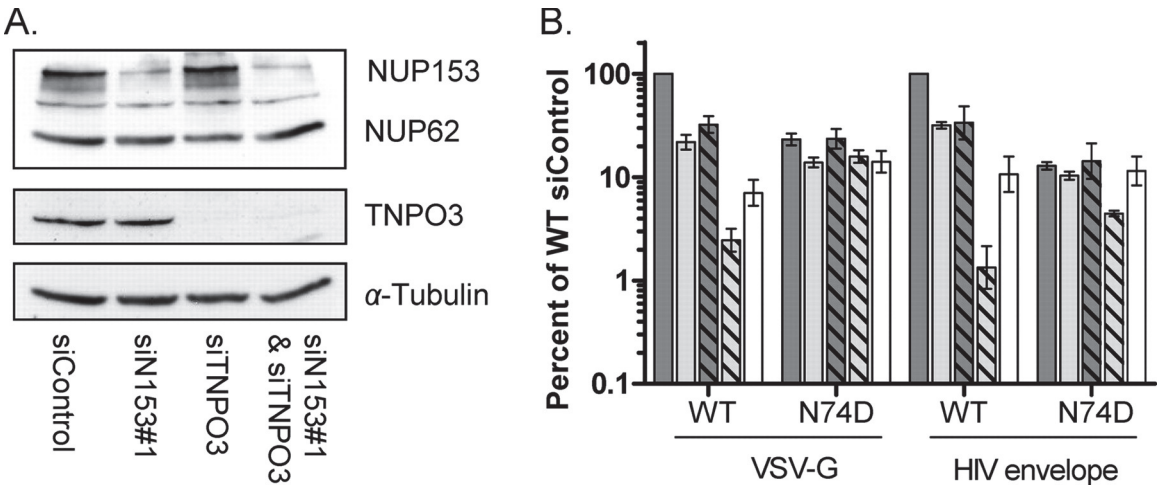

Figure 2-6. Interdependence of NUP153 and TNPO3 during HIV-1 infection. (**A**) Whole-cell extracts of control, NUP153-depleted, TNPO3-depleted, and combinatorially depleted cells were blotted with the indicated primary antibodies. (**B**) Control (dark gray) or NUP153 knockdown (light gray) cells simultaneously depleted for TNPO3 (hatched bars) were infected with 2×10^6 or 2×10^7 RTcpm of vesicular stomatitis virus (VSV)-G or HIV-1 envelope pseudotyped viruses, respectively, yielding numbers of RLU in control cells that were within 1 log of each other (not shown). All samples were normalized to the infectivity of the WT virus in control cells, which was set at 100%. White bars show the multiplicative product of infectivity defects exhibited upon individual protein knockdowns, representing the theoretical maximum expected assuming independent function. Results are averages from three experiments, each performed in duplicate, with error bars denoting 95% confidence intervals.

showed that the route of N74D entry influenced the requirement for TNPO3, experiments were conducted in CD4-positive GHOST-CXCR4 cells to enable comparisons of VSV-G and HIV-1 envelope pseudotyped particles. NUP153 and TNPO3 were knocked down either individually or in combination (**Figure 2-6A**). WT viruses carrying either envelope exhibited 3- to 5-fold decreases in infectivity when NUP153 (**Figure 2-6B**, light gray bars) or TNPO3 (dark gray hatched bars) was knocked down, while N74D was largely, if not completely, insensitive. Interestingly, a 40-fold decrease in infection by VSV-G-pseudotyped WT virus was observed when both proteins were knocked down (**Figure 2-6B**, light gray hatched bar), far greater than the ~ 14-fold defect expected based on the product of individual knockdowns (**Figure 2-6B**, white bar). The N74D mutant showed no such effect, with the dual knockdown inhibiting this virus no more than the slight decrease observed with NUP153 knockdown alone. The results with the HIV-1 envelope pseudotypes were similar, although slightly exaggerated: WT virus exhibited an approximately 75-fold infection defect when both factors were knocked down, while the N74D mutant exhibited a much smaller, though noticeable, 3-fold decrease in infectivity.

NUP153 depletion inhibits expression from an integration-defective reporter virus.

HIV-1 reporter viruses harboring mutations of IN active-site residues are unable to catalyze vDNA integration but still can yield a reproducible level of reporter gene expression. N/N active-site mutant viruses carrying either WT or N74D CA therefore were produced to determine if the inhibitory effects of NUP153 depletion were conferred in the absence of integration. Infection with N/N mutant viruses yielded ~ 2 to 3% reporter expression compared to that of the WT IN viruses, and as expected, these gene

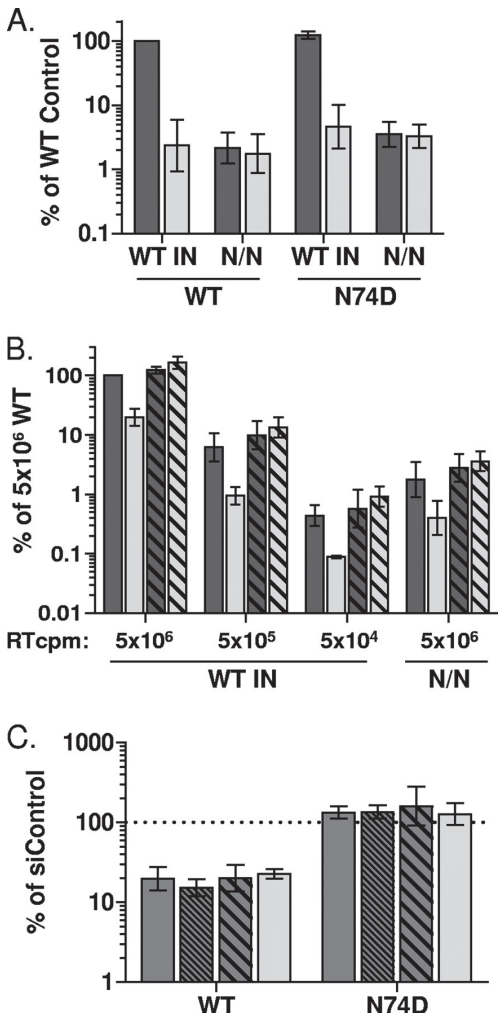

Figure 2-7. NUP153 dependencies of WT and IN active-site mutant viruses. (**A**) Relative differences in reporter expression of 5×10^6 RTcpm WT and N/N IN mutant, along with WT sequence or the CA N74D mutation, in the absence (dark gray) or presence (light gray) of 10 μM raltegravir. (**B**) Relative infectivities of WT and N/N mutant viruses in control (dark gray) or NUP153 knockdown cells (light gray), with WT infectivity (5×10^6 RTcpm) set to 100%. Viruses harbored either WT (solid bars) or N74D (hatched bars) CA. (**C**) Regraph of panel B results, with infectivities in knockdown cells expressed as percentages of respective control cells; solid, hatched, and boldface hatched bars denote infections with 5×10^6, 5×10^5, and 5×10^4 RTcpm of WT IN virus, respectively, while light gray bars denote infection with N/N virus. Results are averages from five experiments performed in triplicate, with error bars denoting 95% confidence intervals.

expression levels were completely refractory to the addition of 10 μM strand transfer inhibitor raltegravir, a dose ~ 100-fold in excess of that required to inhibit 95% of WT viral infection [193] (**Figure 2-7A**). Control and NUP153 knockdown cells next were challenged with N/N viruses alongside 10-fold dilutions of WT IN viruses to establish a comparable level of endpoint reporter expression (**Figure 2-7B**). The N/N virus harboring WT CA was significantly inhibited by NUP153 depletion to a level indistinguishable from that of its integration-competent counterpart at all viral inocula tested (**Figure 2-7C**). Additionally, similarly to the effects of the N74D change on integrating virus, the N74D CA mutation rendered the N/N virus insensitive to NUP153 depletion.

NUP153 depletion results in decreased 2-LTR circles and integrated proviruses.

Although NUP153 depletion was previously concluded to result in an HIV-1 PIC nuclear import defect, this interpretation was based on an approximately 20% reduction in 2-LTR circle levels at 24 hpi alongside an 8-fold infectivity defect [29]. To more comprehensively address the block to HIV-1 infection upon NUP153 depletion, LRT, 2-LTR circle, and integrated proviral DNA levels were measured at multiple time points by qPCR following infection with either WT or N/N mutant virus. As expected [194], cells infected with N/N virus supported a level of LRT products similar to that of WT-infected cells at 8 hpi, with a corresponding ~ 9.6 fold increase in 2-LTR circle levels at 24 hpi (data not shown). WT and N/N mutant viral reverse transcription were insensitive to the amount of cellular NUP153, as peak levels at 8 hpi were similar in control and knockdown cells (**Figure 2-8A and 2-8D**). NUP153 depletion resulted in an

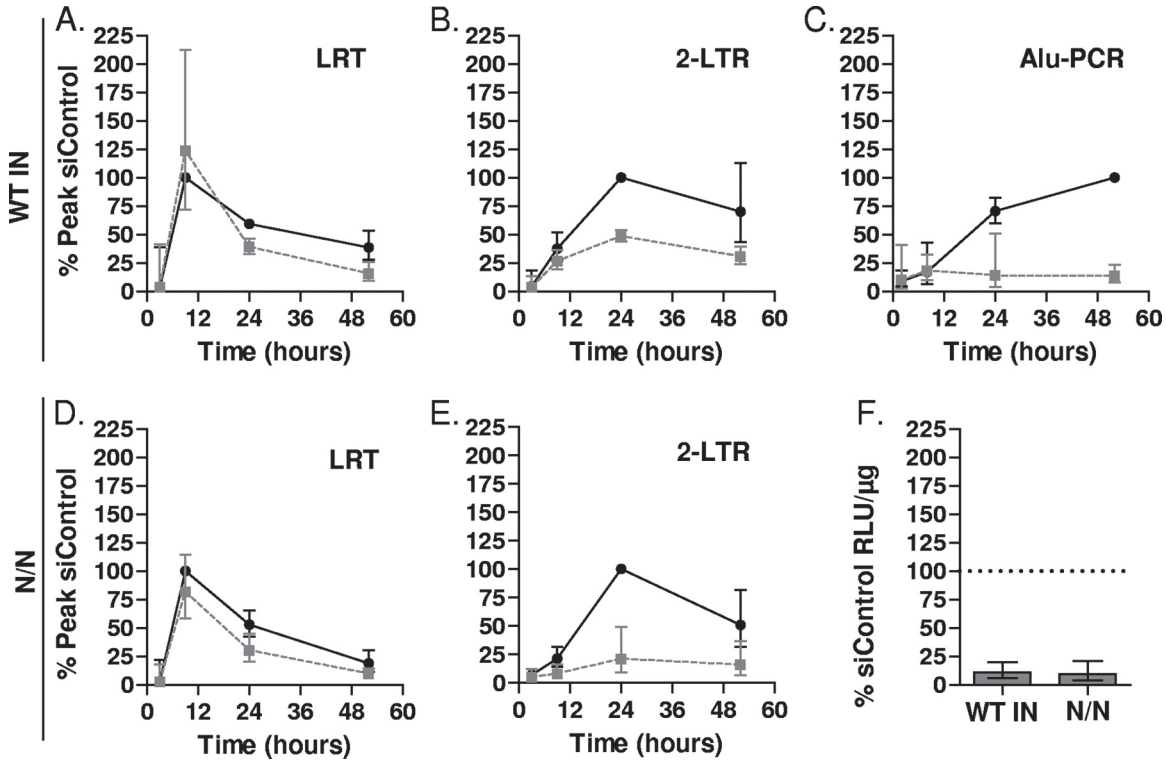

Figure 2-8. HIV-1 DNA species formed during acute infection of NUP153 knockdown cells. Viral DNAs were amplified from cells following infection with WT (**A, B, and C**) or N/N mutant (**D and E**) virus, with values from NUP153 knockdown cells (gray dashed line) normalized to peak LRT (8 hpi) (**A and D**), 2-LTR circle (24 hpi) (**B and E**), and integration (52 hpi) (**C**) values. (**F**) Levels of WT and N/N mutant virus infectivities upon NUP153 depletion, expressed as percent siControl-transfected cells (set at 100%). Results are averages from three experiments, with error bars denoting 95% confidence intervals.

approximately 4.7-fold decrease in N/N virus 2-LTR circle formation at 24 hpi, which leveled off somewhat, to 3.2-fold, by 52 hpi (**Figure 2-8E**). In contrast, NUP153-depleted cells infected with WT virus supported 2.1- and 2.3-fold lower 2-LTR circle levels than siControl transfected cells at 24 and 52 hpi, respectively (**Figure 2-8B**). WT viral integration was blocked more significantly than 2-LTR circles in NUP153 knockdown cells, about 5- and 7.2-fold lower than the levels of integrated proviruses in control cells at 24 and 52 hpi, respectively (**Figure 2-8C**). Comparison of luciferase activities at 52 hpi yielded approximately 9.3- and 10.7-fold reductions in WT and N/N mutant viral infectivities, respectively, upon NUP153 knockdown (**Figure 2-8F**).

Discussion

NUP153 is likely required for HIV-1 nuclear entry.

NUP153 expression has been shown to be required for HIV-1 infection [28,29], but its role(s) in this process has yet to be well characterized. Here, we show that NUP153 is required for efficient infection by primate lentiviruses and may play a role in infection by other retroviral genera (**Figure 2-2**). Our results with integration-defective N/N virus revealed NUP153 to be equally required for expression from integrated and unintegrated vDNA templates, implicating a step common to both processes. Our investigations tracking viral DNA accumulation in NUP153-depleted cells showed both WT and N/N IN mutant viral LRT levels similar to those of control cells, suggesting that NUP153 expression is not necessary for reverse transcription. In contrast, knockdown cells infected with the N/N mutant supported formation of about 5-fold fewer 2-LTR circles than NUP153-expressing cells (**Figure 2-8**). The nonhomologous end-joining machinery required for 2-LTR circle formation is expected to reside in the nucleus [61,62,195], which suggests that NUP153 is involved at a step(s) following reverse transcription which could precede or coincide with nuclear entry or a subsequent process that facilitates the formation and/or retention of 2-LTR circles. Because NUP153 is an NPC component, it seems most likely that the defect is at nuclear entry. Accordingly, knockdown cells infected with WT virus exhibited decreased levels of 2-LTR circles as well, albeit to a lesser extent than the N/N mutant. This discrepancy may be due to an overlying integration defect, which would be expected to contribute to the accumulation of vDNAs susceptible to circularization.

CA mutant viruses and cyclosporine treatment indicate a role for core uncoating in NUP153 dependency during HIV-1 infection.

Although the infection defect is likely at a nuclear step, the major functional determinant of NUP153 dependency identified thus far appears to be the CA protein [177] (**Figure 2-4 to 2-6**). It is possible that CA molecules associated with the PIC directly participate in steps at the NPC or within the nucleus, but because numerous point mutations across different faces of the HIV-1 CA monomer can dramatically alter NUP153 dependence, it is more likely that the dominant effects of CA are reflective of qualities conferred by a multimerized CA core. These results suggest that NUP153 dependency is an effect dictated by the manner in which the CA core uncoats in the cytoplasm or potentially at the nuclear pore itself [80]. Consistent with this interpretation, we found that the perturbation of cyclophilin binding, either by cyclosporine treatment or CypA knockdown, dictated the sensitivity of the WT and cyclosporine-dependent mutants A92E and G94D to NUP153 depletion (**Figure 2-5**). Thus, it appears as though the amount of CypA bound to the HIV-1 core is able to dictate whether the PIC undergoes downstream processes requiring NUP153, perhaps by altering the dynamics of uncoating [191].

Notably, this level of regulation by CypA does not appear to be a global requisite for infection, as SIV_{MAC} is highly sensitive to NUP153 knockdown in spite of its reported inability to bind CypA [196]. The route of cell entry taken by the N74D CA mutant, which has been documented to alter the requirement for TNPO3 during infection [178], may influence NUP153 dependency as well. Although the HIV-1-mediated entry of

N74D failed to reveal a requirement for NUP153 or TNPO3 in our hands, we did note a modest 3-fold effect upon the depletion of both proteins (**Figure 2-6**). Notably, there is precedence for a requirement of NUP153 and NUP153-like proteins during infection with other viruses and retrotransposons at a stage that interfaces capsid oligomerization with nuclear import. The *Saccharomyces pombe* ortholog Nup124p is important for the nuclear accumulation of the Tf1 retrotransposon [197,198]. Interestingly, residues adjacent to an N-terminal nuclear localization signal located in Tf1 Gag dictated whether Nup124p was necessary for Gag nuclear import, and this appeared to correlate with the ability of Gag to multimerize [199]. More recently, NUP153 was found to play a key role during hepatitis B virus nuclear import by signaling mature capsid proteins to dissociate within the NPC basket [200]. Interestingly, both Tf1 Gag and hepatitis B virus capsid have been demonstrated to directly bind their respective NUP153 orthologs. It therefore would be instructive to know if human NUP153 binds HIV-1 CA in an oligomerization-dependent manner.

A potential role for IN in NUP153 dependency.

Aside from the dominant effects conferred by CA, our functional studies of viral elements provide context to understand potential physical interactions relevant to NUP153 function during infection. Although NUP153 has been found to bind HIV-1 Vpr [182], viruses lacking virion-incorporated Vpr were not significantly altered in their NUP153 dependence compared to that of the WT virus, suggesting that this interaction is not relevant up to and including the nuclear import, integration, and early gene expression stages of infection (**Figure 2-3**). NUP153 also has been found to bind HIV-1

IN [98], and our results with MLV/HIV-1 chimera viruses support a role for HIV-1 IN during the infection of NUP153 knockdown cells (**Figure 2-4**). Additionally, the IN protein of FIV previously was found not to bind NUP153 [98], which appears to correlate with the insensitivity of this virus to NUP153 depletion (**Figure 2-2B**). As yet, the requirement for IN appears auxiliary to CA: despite carrying WT IN, HIV-1 CA mutants N74D and P90A were largely insensitive to NUP153 knockdown (**Figure 2-5 and 2-6**), while comparison between chimeras containing MLV IN or CA showed the replacement of CA to decrease the sensitivity of the virus to knockdown more than IN replacement (**Figure 2-4**).

Pleiotropic effects of NUP153 depletion.

It is currently unknown whether the effect of NUP153 knockdown on primate lentiviral infection is reliant on the cellular roles of NUP153 during nuclear transport or on other collateral pleiotropic effects caused by the depletion of this multifunctional protein. NUP153 is believed to be a major point of NPC interaction with translocating KPNs, including those for nuclear import via importin α/β and transportin, protein export via Crm1, and mRNA export via NXF1 (reviewed in [201]). Furthermore, NUP153 depletion has been shown to prevent the NPC from incorporating nucleoporins Tpr and NUP50 [159,184], and it also has been shown to perturb NUP62, NUP88, and NUP214 localization in certain contexts [184,202]. Thus, even if the disruption of a putative specific HIV-1 PIC-NUP153 interaction(s) is not the root cause of the infectivity defect, it may be due to the mislocalization of a subsequently required, potentially unidentified host factor. Furthermore, NUP153 can exert effects indirectly of nuclear transport, as its

depletion has been shown to disrupt the cytoskeleton [203], likely through the perturbation of the nuclear lamina, and it also has been found to delay cellular progression through mitosis [184,204]. Lastly, NUP153 is important during transcription and even has been found to be associated with large regions of transcriptionally active open chromosomes within the Drosophila genome [205]. Regardless, although NUP153 depletion is known to disrupt many processes within the cell, its overall relevance to HIV-1 infection must be relatively specific, as single point mutations in CA can render the virus completely unaffected (**Figure 2-5**).

It will be interesting to continue to determine the role of NUP153 in relation to other host factors implicated in HIV-1 nuclear transport, especially TNPO3 and NUP358. Numerous similarities have been observed upon the knockdown of individual components: HIV-1 exhibits a nuclear entry defect [29,70,179] (**Figure 2-8**), while MLV, FIV, and the N74D CA mutant virus are seemingly unaffected [28,29,70,96,177,178] (**Figures 2-2, 2-5, and 2-6**). Here, we determined that the simultaneous depletion of NUP153 and TNPO3 significantly enhanced the block to HIV-1 infection, suggesting interrelated functions. Perhaps these proteins represent multiple components of a concerted mechanism streamlining the early steps of HIV-1 infection, allowing for both optimal quantity and quality of proviral insertion into the host genome.

Materials and Methods

Plasmid constructs.

Infection assays utilized single-round viruses carrying either GFP or luciferase reporter genes. GFP-based constructs included: EIAV [206,207], HIV-1 [208], RSV [209] (Addgene plasmid 13878 obtained from Constance Cepko via Addgene), FIV [210,211], MLV [212,213], MPMV [214], HIV-2 strain ROD (HIV-2_{ROD}), and simian immunodeficiency virus from *Macaca mulatta* (SIV_{MAC}), *Chlorocebus sabaeus* (SIV_{AGM}Sab), and *Chlorocebus tantalus* (SIV_{AGM}Tan) [215]. Luciferase-based viruses included MLV/HIV-1_{LAI} chimeras [116,173] and HIV-1_{NL4-3}-derived D64N/D116N (N/N) IN active site and Vpr and/or DNA flap mutants of pNLX.Luc [102,216]. VSV-G and HIV-1_{NL4-3} glycoprotein expression vectors were as described [102,216].

HIV-1 CA mutations were generated through site-directed mutagenesis of the HIV-1_{NL4-3}-based pHP-dI-N/A packaging plasmid [217] (AIDS Research and Reference Reagent Program [ARRRP]), which was co-transfected in conjunction with either pHI-vec2.GFP [218] or pHI-Luc [219] transfer vectors. Sequencing was used to verify PCR-mutated DNAs. NUP153 expression vector pIRES-dsRedExpress-NUP153 was created by digesting pCMV-Sport6-NUP153 (Open Biosystems) with Sal I and Bgl II, and ligating the resulting NUP153-coding fragment with Sal I/BamH I-digested pIRES-dsRedExpress (Clontech Laboratories).

Cells and siRNA transfections.

HEK293T and HeLa cells were cultured in Dulbecco's modified Eagle's medium supplemented to contain 10% fetal bovine serum, 100 IU/ml penicillin, and 100 µg/ml streptomycin, while GHOST cells expressing CD4 and the CXCR4 co-receptor (GHOST-CXCR4) [220] (ARRRP) were additionally cultured with 500 µg/ml G418, 100 µg/ml hygromycin, and 1 µg/ml puromycin.. Approximately 75,000 HEK293T or 25,000 HeLa or GHOST-CXCR4 cells seeded per well of a 24-well plate were transfected the next day with a final concentration of 40 nM siNUP153#1 (GGACTTGTTAGATCTAGTT) [184], 10 nM siNUP153#2 (AGTGTTCAGTATGCTGTGTTTCT) [183], or 40 nM of mismatch control of siRNA #1, referred to as siControl (GGTCTTATTGGAGCTAATT; underlines indicate base mismatches with siNUP153#1)) (Dharmacon) using RNAiMax (Invitrogen) according to the manufacturers instructions. Simultaneous NUP153 and cyclophilin A (CypA) knockdown was performed by transfection with a final concentration of 20 nM siNUP153#1, 20 nM CypA siRNA (AAGGGTTCCTGCTTTCACAGA) [221], or the corresponding amount of siControl for a total siRNA concentration of 40 nM. Simultaneous NUP153 and TNPO3 knockdown was performed similarly, using siTNPO3 (CGACATTGCAGCTCGTGTA) [96]. Media was exchanged the following day. NUP153 re-expression was performed by $CaPO_4$ transfection of 1 µg DNA immediately after siRNA transfection.

Virus production.

Vector particles were generated by transfecting HEK293T cells in 10-cm plates with 10 µg total of various ratios of the aforementioned virus production plasmids using

either $CaPO_4$ or Fugene 6 (Roche Molecular Biochemicals). The cells were washed 16 h after transfection, and supernatants collected 12 to 60 h thereafter were clarified at 300 x *g*, filtered through 0.45μm filters (Nalgene), and either allotted and frozen or concentrated by ultracentrifugation using an SW28 rotor at 53,000 x *g* for 2 h at 4°C before freezing. Concentrations of Vpr, DNA flap, and CA mutant viral stocks were determined alongside concomitantly produced WT viruses using an exogenous ^{32}P-based RT assay [222].

Infectivity assays.

Control and siRNA knockdown cells seeded onto 48-well plates were infected overnight with various reporter viruses 48 h post-siRNA transfection. Percentages of GFP-positive cells were determined 36 h post infection (hpi) using a FACSCanto flow cytometer (BD) equipped with FACSDIVA software. GFP reporter experiments were performed with virus inoculates adjusted to yield < 40% GFP-positive cells in control samples. Cells were infected with equal RTcpm of WT or mutant HIV-1 luciferase reporter viruses, while MLV chimera viruses were adjusted such that all infections were approximately within 2 log RLU/μg/sec of control cells. Where applicable, cyclosporin A (CsA) (Sigma) was added at the time of infection to the final concentration of 5 μM. Cells infected with luciferase reporter viruses were lysed 48 hpi unless otherwise noted, and resulting levels of luciferase activity were normalized to the corresponding levels of total protein in cell extracts as described previously [96].

Normalized infectivity data were log transformed, and statistical analyses were performed by paired two-tailed Student's *t*-test. Mean infectivity values were then back

transformed for graphical representation, with error bars denoting 95% confidence intervals.

Western blot analysis.

At the time of infection, siRNA treated cells were lysed with radioimmunoprecipitation assay buffer (20 mM HEPES [pH 7.5], 150 mM NaCl, 1% NP-40, 1% sodium deoxycholate, 0.1% sodium dodecyl sulfate, 0.5 M EDTA, Complete protease inhibitor [Roche Molecular Biochemicals]). Following determination of protein concentration by Bradford assay, 60 μg or two-fold dilutions of each lysate were fractionated through 9% Tris-glycine gels, and proteins were transferred onto a polyvinylidene fluoride membrane. NUP153 and NUP62 were detected using a 1:2,500 dilution of mouse mAb414 antibody (Abcam Inc.), while TNPO3 was detected using a 1:150 dilution of mouse anti-TNPO3 antibody ab54353 (Abcam Inc.). A 1:5,000 dilution of rabbit anti-mouse horseradish peroxidase-conjugated served as secondary antibody (Dako North America Inc.), and a 1:5,000 dilution of mouse anti-α-tubulin antibody (Abcam Inc.) was used for loading control. Blots were developed using the ECL Plus detection reagent (GE Healthcare).

QPCR.

siNUP153#1 or siControl-transfected cells (500,000) were infected with ~$2x10^7$ RTcpm of DNase-treated WT or N/N mutant virus, with parallel infections conducted in the presence 100 μM azidothymidine (AZT) to define residual plasmid DNA levels potentially carried over from transfection. Two hours later, infected cells washed with

phosphate-buffered saline were re-plated into individual 24-wells. Cells were collected at various time points, and DNA was extracted with a QIAamp DNA Mini Kit as recommended by the manufacturer (Qiagen). Each sample was analyzed in triplicate by qPCR to determine levels of HIV-1 LRT-products, 2-LTR containing circles, and integrated proviruses via nested Alu-PCR essentially as described previously [51,223]. LRT and 2-LTR circle values were normalized to qPCR values for β-globin DNA performed in parallel, while all input DNAs for first-round Alu-PCRs were adjusted for equal β-globin amplification. Values obtained from corresponding AZT-treated samples, which averaged 2.6% of peak LRT and 2.5% of peak 2-LTR circles, were subtracted from non drug-treated values.

Plasmid pNLX.luc.R- was used to generate LRT standard curves while pUC19.2LTR was used for 2-LTR circles [216]. The integration standard was prepared by infecting HeLa cells at relatively low multiplicity of infection with the pHI-puro transfer vector [219], passage for two weeks in 2 μg/ml puromycin to permit loss of unintegrated HIV-1 DNA forms, and extraction of total DNA using the QIAamp DNA Mini Kit. Two-fold dilutions of infected cell DNA were mixed with complementary amounts of DNA prepared from uninfected HeLa cells to form the standard curve. Two-fold dilutions of uninfected cell DNA were used as the standard for β-globin.

QPCR primers and probes were: MH531, MH532, and MH535 for LRT [51]; 2-LTR circle junction [224]; AE3014, AE1066, AE3013, AE990, and AE995 for Alu-PCR [223,225]; and β-globin+ and β-globin- for HeLa genomic DNA [65]. SYBR green was used to measure β-globin amplification.

Chapter 3

Nucleoporin NUP153 phenylalanine-glycine motifs engage a common binding pocket within the HIV-1 capsid protein to mediate lentiviral infectivity

Nucleoporin NUP153 phenylalanine-glycine motifs engage a common binding pocket within the HIV-1 capsid protein to mediate lentiviral infectivity

Kenneth A. Matreyek, Sara S. Yücel, Xiang Li, Alan Engelman

Department of Cancer Immunology and AIDS, Dana-Farber Cancer Institute, and Department of Medicine, Harvard Medical School, Boston, Massachusetts, USA

* This chapter is adapted from the publication:

Matreyek KA, Yücel SS, Li X, Engelman A. (2013) Nucleoporin NUP153 phenylalanine-glycine motifs engage a common binding pocket within the HIV-1 capsid protein to mediate lentiviral infectivity. Plos Pathog, in press.

Contributions: I performed all of the experiments in this manuscript, except for Figure 3-1B (Performed by Sara S. Yücel) and Figure 3-15 (Performed by Xiang Li). Alan Engelman and I wrote the manuscript.

Abstract

Lentiviruses can infect non-dividing cells, and various cellular transport proteins provide crucial functions for lentiviral nuclear entry and integration. We previously showed that the viral CA protein mediated the dependency on cellular NUP153 during HIV-1 infection, and now demonstrate a direct interaction between the CA N-terminal domain and the phenylalanine-glycine (FG)-repeat enriched NUP153 C-terminal domain ($NUP153_C$). $NUP153_C$ fused to the effector domains of the rhesus Trim5α restriction factor (Trim-$NUP153_C$) potently restricted HIV-1, providing an intracellular readout for the $NUP153_C$-CA interaction during retroviral infection. Primate lentiviruses and EIAV bound $NUP153_C$ under these conditions, results that correlated with direct binding between purified proteins in vitro. These binding phenotypes moreover correlated with the requirement for endogenous NUP153 protein during virus infection. Mutagenesis experiments concordantly identified $NUP153_C$ and CA residues important for binding and lentiviral infectivity. Different FG motifs within $NUP153_C$ mediated binding to HIV-1 versus EIAV capsids. HIV-1 CA binding mapped to residues that line the common alpha helix 3/4 hydrophobic pocket that also mediates binding to the small molecule PF-3450074 (PF74) inhibitor and cleavage and polyadenylation specific factor 6 (CPSF6) protein, with Asn57 (Asp58 in EIAV) playing a particularly important role. PF74 and CPSF6 accordingly each competed with $NUP153_C$ for binding to the HIV-1 CA pocket, and significantly higher concentrations of PF74 were needed to inhibit HIV-1 infection in the face of Trim-$NUP153_C$ expression or NUP153 knockdown. Correlation between CA mutant viral cell cycle and NUP153 dependencies moreover indicates that the $NUP153_C$-CA interaction underlies the ability of HIV-1 to infect non-dividing cells. Our results

highlight similar mechanisms of binding for disparate host factors to the same region of HIV-1 CA during viral ingress. We conclude that a subset of lentiviral CA proteins directly engage FG-motifs present on NUP153 to affect viral nuclear import.

Introduction

Retroviruses integrate their reverse transcribed genomes into host cell chromosomes to provide a permanent vantage from which to amplify themselves for subsequent transmission. As the nuclear envelope physically separates the host chromosomes from the cytoplasm during interphase, retroviruses have evolved mechanisms to bypass this natural barrier to the nuclear compartment. The γ-retrovirus MLV is believed to await the dissolution of the nuclear envelope during mitosis, a mechanism that limits infection by this virus to actively dividing target cells [21,132,171]. Lentiviruses such as HIV-1 infect post-mitotic cell subtypes during the establishment of host systemic infection, and correspondingly harbor mechanisms to infect cells during interphase, likely circumventing the nuclear envelope by passing through the channel present in the NPC [22,226].

The vertebrate NPC is a large ~ 120 MDa macrostructure, composed of ~ 30 different proteins called nucleoporins (NUPs) that stack in rings of eight-fold symmetry to form the tubular pore as well as the attached cytoplasmic filaments and nuclear basket substructures [227,228]. Approximately one-third of the NUPs harbor domains rich in phenylalanine-glycine (FG) motifs, commonly observed as FxF, FxFG, or GLFG patterns [32]. These FG-rich domains line the central channel of the NPC, as well as the cytoplasmic and nuclear openings [229], and dictate the selective passage of macromolecules through the pore; small molecules are able to passively diffuse, while molecules greater than ~ 9 nm in diameter need to be ferried by specialized carrier proteins capable of interacting with the FG-based permeability barrier [230].

The HIV-1 nucleoprotein substrate for proviral integration, called the PIC, is estimated at ~ 56 nm in diameter [79], and thus requires active translocation into the nucleus. While initial studies suggested that HIV-1 IN, MA, and Vpr proteins, as well as a triple-stranded DNA structure of the reverse transcribed genome called the DNA flap, were key viral elements required for PIC nuclear import, subsequent studies found none of these factors to be essential [173]. Contrastingly, the viral CA protein was shown to be the major viral determinant for infecting non-dividing cells [57,116]. Various host proteins have also been shown to play roles in HIV-1 nuclear import, with perhaps the most promising candidates emerging from a series of genome-wide RNAi screens; factors identified in more than one of these screens include transportin-3 (TNPO3 or TRN-SR2), NUP358, and NUP153 [28,29,141]. We have been particularly interested in NUP153, which plays an important CA-dependent role in HIV-1 PIC nuclear import [177,231].

NUP153 is a FG nucleoporin that predominantly locates to the nuclear side of the NPC and exchanges dynamically with a nucleoplasmic population [181]. While NUP153 is anchored to the nuclear rim of the NPC through its N-terminal domain [156], its C-terminal FG enriched domain (referred to as $NUP153_C$ herein) is natively unfolded and highly flexible [162]. The ~ 200 nm long $NUP153_C$ potentially reaches through to the cytoplasmic side of the NPC channel [164], shifting in spatial distribution in a transport-dependent manner [163,165]. Human $NUP153_C$ contains 29 FG motifs (FxF, FG, and FxFG patterns), which provide a vital role in NUP153-mediated nucleocytoplasmic transport [166,167,185].

While numerous studies have demonstrated the functional significance of CA for HIV-1 nuclear import and integration, the mechanistic details for these connections are incompletely understood. Retroviral CA proteins are composed of two α-helical domains, the N-terminal domain (NTD) and C-terminal domain (CTD), separated by a short flexible linker. CA multimerizes into hexameric arrays during particle maturation, while twelve interspersed pentamers dictate the overall shape of the condensed viral core [40-43]. While relatively intact cores enter the cell upon viral-cell membrane fusion, little if any CA remains associated with the PIC within the nucleus [56,74,75,77,81]. The precise location and mechanism of CA core disassembly remains controversial: while initial steps of core uncoating are tied to reverse transcription [45], subsequent events may involve binding to host proteins. This may involve CypA and the NUP358 cyclophilin homologous domain (CHD), both of which bind the cyclophilin binding loop protruding from the top of the CA NTD [232,233], or CPSF6, which binds a hydrophobic pocket [234] located between α-helices 3 and 4 within the NTD. The small molecule PF-3450074 (PF74), which inhibits HIV-1 infection by destabilizing incoming CA cores, also engages this same pocket [235]. CA-containing protein complexes have been observed alongside the nuclear envelope [80], suggesting that the ultimate steps of core uncoating may occur at the nuclear periphery and/or during PIC nuclear transport.

Here, we find that the CA proteins from numerous lentiviruses, including HIV-1 and EIAV, directly bind $NUP153_C$, with subsequent mapping demonstrating the importance of individual FG-motifs themselves. A panel of HIV-1 CA mutants highlights the importance of side-chains lining the CA NTD helix 3/4 hydrophobic pocket, and competition with both CPSF6 and PF74 support this as the site of $NUP153_C$ binding.

Correlation between NUP153 binding and dependence on endogenous NUP153 expression additionally support the relevance of this interaction during infection. HIV-1 CA mutant viruses N57A and N57D were defective for $NUP153_C$ binding and acutely sensitive to the arrest of the cell-division cycle, with a significant correlation between cell cycle and NUP153 dependencies observed among an expanded set of CA mutant viruses. Our data support a model whereby partially uncoated cores directly engage NUP153 FG-motifs within the NPC to affect HIV-1 PIC nuclear import.

Results

NUP153$_C$ binds the NTDs of a subset of retroviral CA proteins

As we previously found CA to be the dominant viral determinant of the requirement for NUP153 during HIV-1 infection [231], we tested whether a physical interaction between NUP153 and HIV-1 CA exists. Our initial assay utilized a recombinant viral fusion protein consisting of HIV-1 CA and nucleocapsid (NC) proteins, which when assembled in vitro in the presence of high salt and single stranded nucleic acid forms large tube-like structures that readily pellet through cushions of sucrose [40]. In this way, CA-interacting proteins can co-sediment with the tube structures [122,177]. Full length or various fragments of HA-tagged NUP153 expression constructs were transfected into 293T cells, and the resulting proteins were tested for their ability to co-sediment with CA-NC assemblies. Full-length NUP153 (residues 1-1475) pelleted through the sucrose cushion in a CA-NC dependent manner (**Figure 3-1A and 3-1B**). The NUP153 N-terminal domain (residues 1-650) failed to bind CA-NC under conditions that supported efficient NUP153$_C$ (residues 896-1475) binding. The C-terminal NUP153 deletion mutant comprised of residues 1-1198 failed to bind, confirming the importance of the NUP153 FG-repeat domain in binding, and mapping the interaction to residues 1199-1475 of the full length protein.

We addressed whether the NUP153–CA-NC interaction was the result of direct protein binding through the use of purified, recombinant NUP153 protein. We attempted to express full-length NUP153 fused to glutathione *S*-transferase (GST) in bacteria, but despite extensive effort, were unable to define conditions that yielded usable quantities of

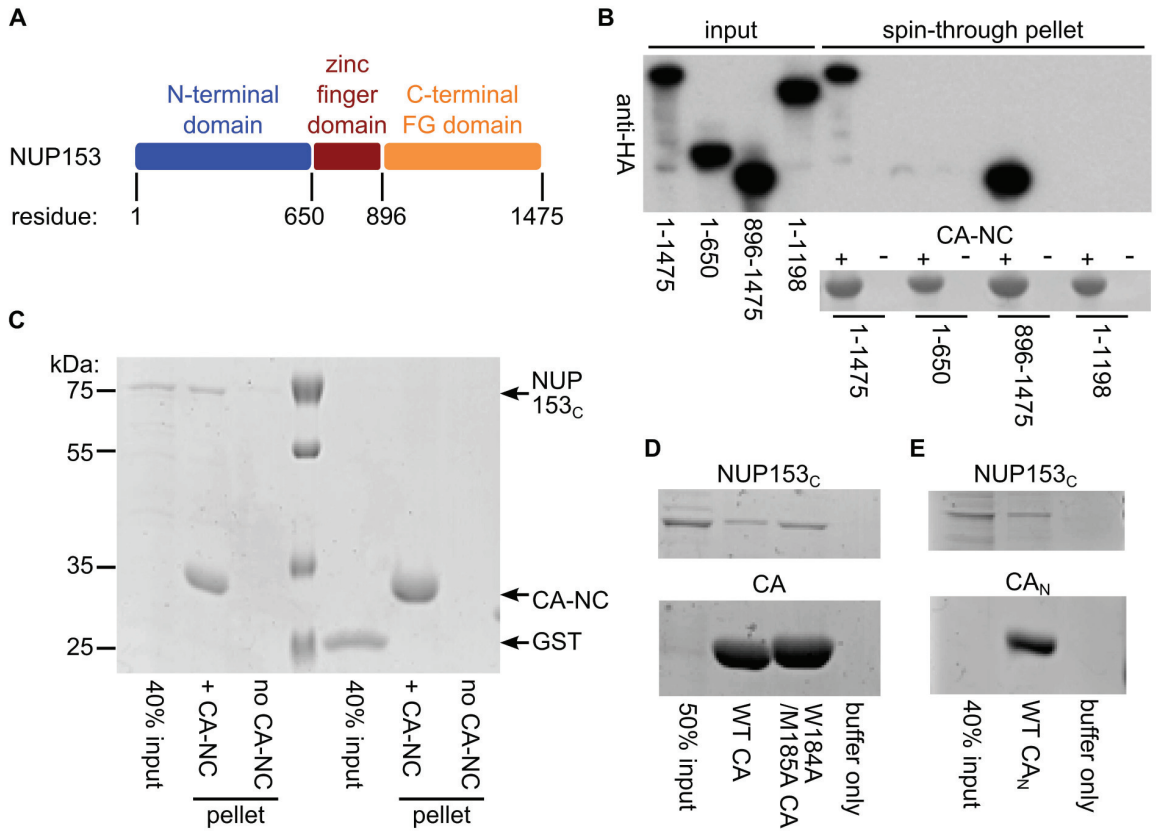

Figure 3-1. NUP153$_C$ directly binds the HIV-1 CA N-terminal domain. (**A**) Schematic of NUP153 protein, with residue numbers of domain boundaries indicated. (**B**) Full length or truncated fragments of HA-tagged NUP153 extracted from 293T cells were tested for binding to HIV-1 CA-NC. Pelleted proteins were resolved by SDS-PAGE and visualized by western blotting with anti-HA antibody 3F10 (top), or by Coomassie stain (bottom). Input, 20% of binding reaction. CA-NC was included in the binding reactions as indicated. (**C**) Recombinant, tag-free NUP153$_C$ and GST purified from *E. coli* were similarly tested for binding to CA-NC; proteins were detected with Coomassie stain. (**D**) Recombinant NUP153$_C$ pulled down with full length his-tagged wild-type (WT) or W184A/M185A HIV-1 CA, and detected with Coomassie stain. (**E**) Recombinant NUP153$_C$ pulled down with his-tagged CA$_N$, and detected with Coomassie stain. Each experiment was repeated at least 3 times, with a single representative result shown.

GST-NUP153 protein. Based on our preliminary binding data (**Figure 3-1B**), we instead expressed and affinity purified GST-NUP153$_C$. NUP153$_C$ was liberated from the GST tag by site-specific proteolysis, with the remaining CA binding studies utilizing tag-free NUP153$_C$ protein. Approximately 40% of the input recombinant NUP153$_C$ protein was recovered during co-sedimentation under conditions where binding of a negative control GST protein was undetected **(Figure 3-1C**). To test whether NUP153$_C$ binds CA in the absence of NC and nucleic acid, his-tagged HIV-1 CA expressed and purified from *E. coli* was utilized in Ni-nitrilotriacetic acid (NTA) pulldown assays. Approximately 30% of input NUP153$_C$ was pulled down by his-tagged HIV-1 CA protein. Notably, this interaction is likely independent of CA oligomerization, as double mutant W184A/M185A CA, which is unable to dimerize and form higher-ordered assemblies [236], pulled-down comparable amounts of NUP153$_C$ (**Figure 3-1D**). The isolated CA NTD (CA$_N$) was expressed as a his-tagged protein and purified to next probe the binding region within HIV-1 CA; CA$_N$ pulled down ~ 30% of input NUP153$_C$ protein (**Figure 3-1E**). Although these data do not quantitatively address potential CA oligomerization-based affects on NUP153$_C$ binding, the relatively robust interaction with CA$_N$ suggests that NUP153 may efficiently engage monomeric CA during HIV-1 infection.

The preceding results established a direct interaction between NUP153 and HIV-1 CA proteins in vitro. We next examined whether an assay could be constructed to visualize the interaction in the context of HIV-1 infection. We scored for potential intracellular interaction by relying upon the potent capability of rhesus Trim5α (rhTrim5α) to inhibit HIV-1 infection. RhTrim5α is a cytoplasmically localized restriction factor, capable of blocking HIV-1 infection at an early post-entry step [121].

Figure 3-2. Restriction of HIV-1 infection by Trim5-NUP153$_C$ fusion proteins. (**A**) Schematic of Trim-NUP153$_C$ fusion and control constructs. Color code: Trim5 RBCC, brown; rhTrim5α SPRY, auburn; HA-tag, blue; NUP153$_C$, orange. (**B**) Western blot of HOS cells stably transduced with HA-tagged Trim-NUP153$_C$ fusion or control constructs, detected with antibody 3F10. (**C**) Western-blot detection of Trim-NUP153$_C$ fusion proteins with anti-HA monoclonal antibodies 3F10 and 16b12. Antibody 3F10 detects full-length Trim-NUP153$_C$-HA whereas antibody 16b12 more faithfully detects full-length Trim-HA-NUP153$_C$. (**D**) Infectivity of various doses of HIV-1 (left) or MLV (right) GFP reporter viruses on HOS cells stably expressing various Trim-based constructs. The results are an average of two experiments, with error bars denoting standard error. Asterisks in panels B and C mark bands that correspond to the expected mobilities of full length Trim-NUP153$_C$ constructs.

(**Figure 3-2,** continued)

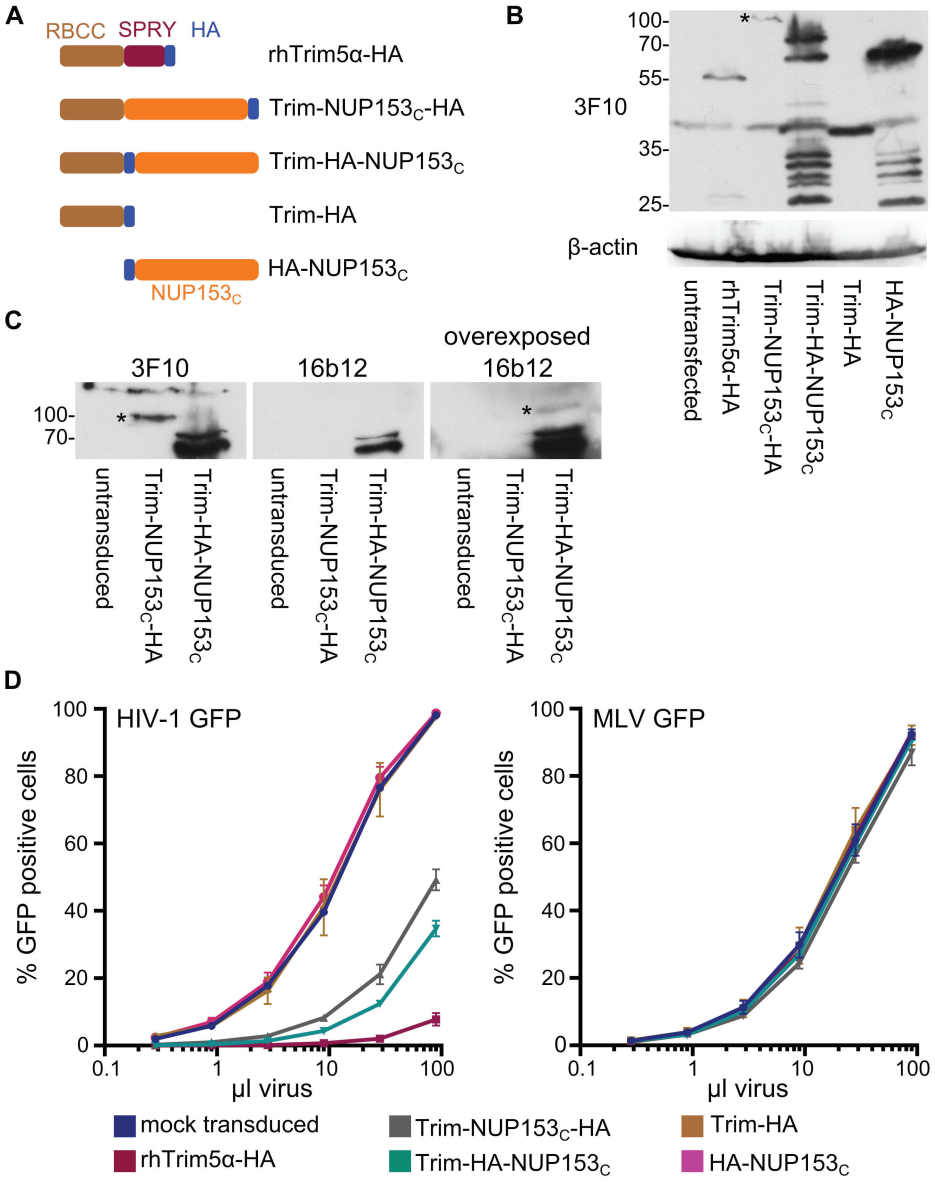

While the C-terminal B30.2 (SPRY) domain recognizes patterns present on the surface of retroviral CA cores [237,238], the N-terminal RING, B-box 2, and coiled coil (RBCC) effector domains block infection by eliciting a combination of inhibitory activities, including premature disassembly of the viral core [122], proteasomal targeting [123], and triggering of innate immune signaling [239]. Both naturally occurring, as well as artificially engineered variants of Trim5 have been discovered wherein the SPRY domain is replaced by heterologous coding sequences, retaining viral restriction while changing the method by which the viral core is recognized [233,240,241]. In this vein we tested for intracellular recognition between $NUP153_C$ and HIV-1 CA by replacing the SPRY domain of rhTrim5α with $NUP153_C$, concomitantly introducing either an internal- or C-terminal HA epitope tag to enable detection of the fusion proteins by western blotting (**Figure 3-2A**). These constructs, as well as control constructs encoding only the epitope-tagged rhTrim5 RBCC or $NUP153_C$, were stably introduced into human osteosarcoma (HOS) cells (**Figure 3-2B**). While a single species of C-terminally HA tagged Trim-$NUP153_C$ of the expected molecular weight was detected by western blot, the internally tagged construct revealed the protein susceptible to degradation, with the full-length protein representing only a minority of the expressed products at steady state (**Figure 3-2B and 3-2C**). Regardless, Trim-$NUP153_C$ expressing cells potently restricted HIV-1 infection, yielding consistent 5-10 fold reductions in viral titer (**Figure 3-2D**). The combination of both rhTrim5 RBCC and $NUP153_C$ domains was necessary, as neither domain expressed alone inhibited HIV-1 infection. Knockdown of endogenous NUP153 acutely attenuates HIV-1 infection with little or no effect on MLV [231]. Importantly, the observed attenuation of HIV-1 infection by Trim-$NUP153_C$ expression was specific, as

Figure 3-3. Trim-NUP153$_C$ localizes to the cell cytoplasm and restricts HIV-1 reverse transcription. (**A**) Immunofluorescence confocal microscopy of HOS cells transduced with empty vector or the indicated HA-tagged construct. Hoescht 33342 stains DNA and therefore highlights cell nuclei. (**B**) Fractionation of rhTrim5α-HA, Trim-HA-NUP153$_C$, and HA-NUP153$_C$ expressing cells. Gels were probed with antibodies against the HA tag (top panels), histone H3, α-tubulin, or NUP62 (bottom panels). Cytoplasmic α-tubulin and nucleus-associated NUP62 and histone H3 marker proteins were predominantly found in fractions 1 and 3, respectively. Asterisks mark bands that correspond to the expected mobilities of full length constructs. (**C-E**) Levels of R-U5 DNA synthesis (early reverse transcripts) (C), U5-*gag* DNA synthesis (late reverse transcripts) (D), and 2-LTR circle formation (E), in cells transduced with empty vector, rhTrim5α-HA, or Trim-HA-NUP153$_C$ expressing constructs at 1, 6, 24, and 48 h post HIV-1 infection, as detected by qPCR. Results (averages of three experiments, with error bars denoting standard error) were normalized to levels of peak DNA amplification, which was set at 100%. (**F**) Corresponding infectivity of GFP reporter viruses, measured 48 h post infection. Data were normalized to infectivity in cells transduced with empty expression vector. Results are an average of three experiments, with error bars denoting standard error.

(**Figure 3-3,** continued)

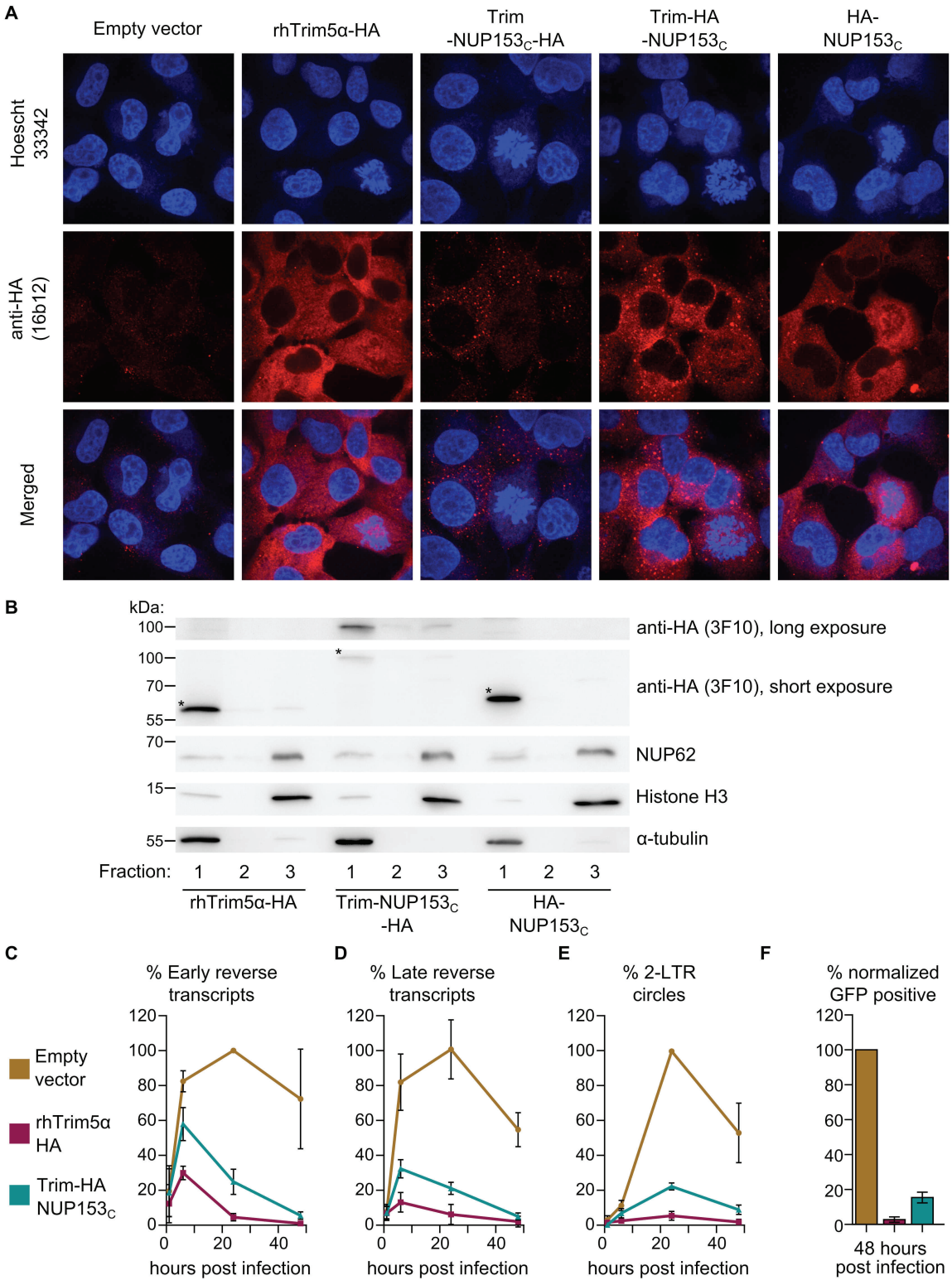

infection by an MLV reporter virus was unaffected (**Figure 3-2D**). Similar to parental rhTrim5α, Trim-NUP153$_C$ located to the cell cytoplasm (**Figure 3-3A and 3-3B**) and prevented HIV-1 from completing reverse transcription (**Figure 3-3C-F**), suggesting that it likely recognizes the HIV-1 CA core in the cytoplasm shortly after viral entry. We conclude that although NUP153$_C$ in the context of the Trim5 protein likely engages HIV-1 CA earlier than endogenous NUP153 protein, the novel fusion nonetheless affords the analysis of the NUP153-CA interaction in the context of HIV-1 infection. Due to the marginally greater level of restriction imparted by the internally tagged construct, the Trim-HA-NUP153$_C$ variant was used in subsequent experiments.

The readout for intracellular CA core recognition was further validated by subjecting a panel of divergent retroviral reporter viruses to Trim-NUP153$_C$ inhibition. Primate lentiviruses SIVmac, SIVagmSab, SIVagmTan, and HIV-2 were similarly sensitive to Trim-NUP153$_C$ inhibition (**Figure 3-4A**). Though EIAV was also sensitive, not all lentiviruses were: neither bovine immunodeficiency virus (BIV) nor FIV was inhibited by Trim-NUP153$_C$. The more distantly related α-retrovirus RSV was also unresponsive. To correlate the results of Trim-mediated restriction of virus infection to direct protein binding, a subset of the sensitive (EIAV) and nonresponsive (MLV and FIV) CA$_N$ proteins were purified following their expression in bacteria. EIAV CA$_N$ bound NUP153$_C$ as efficiently as HIV-1 CA$_N$, whereas binding to either MLV or FIV CA$_N$ was significantly less efficient ($P < 0.01$) **(Figure 3-4B and 3-4C**). Reliance on NUP153 during retroviral infection was compared with CA-NUP153$_C$ binding (**Figure 3-4A**) by correlating percent infectivity in the face of NUP153 knockdown [231] (repeated here using HOS cells; **Figure 3-4D**).

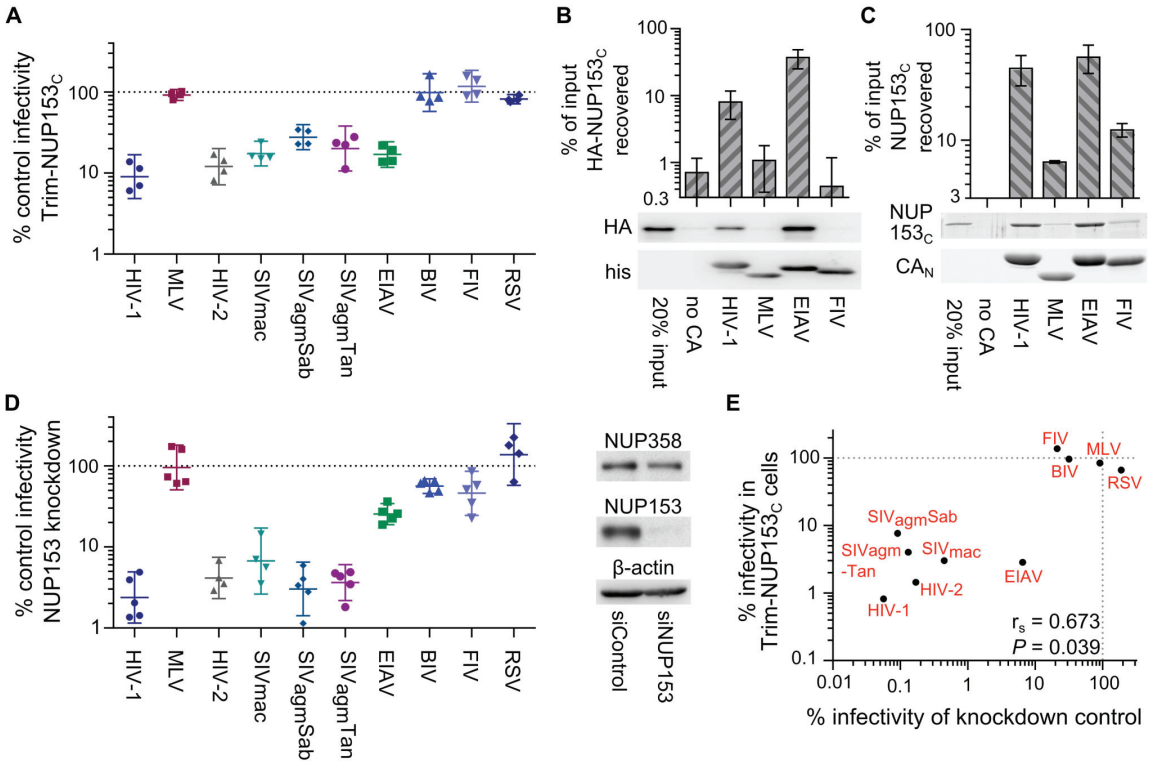

Figure 3-4. Diverse lentiviruses bind NUP153$_C$. (**A**) Transduction efficiencies of retroviral GFP reporter viruses in Trim-NUP153$_C$ expressing cells normalized to infection in mock transduced cells, which were set to 100%. Results are the geometric mean of 4 experiments, with error bars denoting 95% confidence intervals. (**B**) HA-NUP153$_C$ expressed in 293T cells was pulled down by the indicated his-tagged retroviral CA$_N$ proteins. Captured proteins resolved by SDS-PAGE were western blotted with antibody 3F10 alongside a standard curve of input protein. The results are an average of 5 experiments, with error bars denoting 95% confidence intervals. A representative western blot is shown. (**C**) SYPRO Ruby detection of retroviral CA$_N$ pull-down of purified NUP153$_C$. The results are an average of two experiments, with error bars denoting standard error. A representative western blot is shown. (**D**) (left) Retroviral infectivities in HOS cells knocked down for NUP153 expression as compared to cells treated with a non-targeting siRNA control [231]. The results are the geometric mean of at least 4 experiments, with error bars denoting 95% confidence intervals. (right) Western blot detection of control or NUP153 knockdown HOS cells with antibody mab414. (**E**) Scatter plot comparing relative retroviral infectivities under each condition.

The resulting Spearman rank coefficient of 0.673 was statistically significant ($P = 0.039$) (**Figure 3-4E**).

FG motifs within NUP153 dictate CA binding

Mutations within $NUP153_C$ were made to decipher the components of NUP153 critical for binding. As the HIV-1 restriction assay was higher throughput than the expression and purification of separate $NUP153_C$ proteins, we first engineered mutations within the Trim-$NUP153_C$ fusion construct. Since the starting fusion construct contained the entire ~ 580 amino acid $NUP153_C$, we generated cell lines stably expressing Trim fusion proteins with roughly quarter-size deletions of $NUP153_C$, and determined the extent to which these constructs inhibited HIV-1 and EIAV infection, using MLV and FIV as negative controls (**Figure 3-5A and 3-5B**). Relative levels of HIV-1 and EIAV infection were compared to ease the interpretation of results to Trim-$NUP153_C$ mediated restriction; parental Trim-$NUP153_C$ yielded an HIV-1 to EIAV infectivity ratio of ~ 0.41 (**Figure 3-5B**). Deletion of residues 896 to 1045 at the N-terminus of $NUP153_C$ resulted in a construct that potently inhibited HIV-1 infection to a level ~ 8 fold greater than the full-length construct, yet lost the ability to inhibit EIAV, yielding an HIV-1 to EIAV infectivity ratio of ~ 0.01 (**Figure 3-5B**). Contrastingly, deletion of C-terminal residues 1350 to 1475 resulted in a protein still capable of inhibiting EIAV infection to a level comparable to the full-length construct, yet incapable of inhibiting HIV-1 infection beyond the level of the control viruses, resulting in an infectivity ratio of ~ 4.70. These effects were specific to sequences deleted in the preceding constructs, as neither internal deletion noticeably perturbed the original Trim-$NUP153_C$ restriction pattern; both

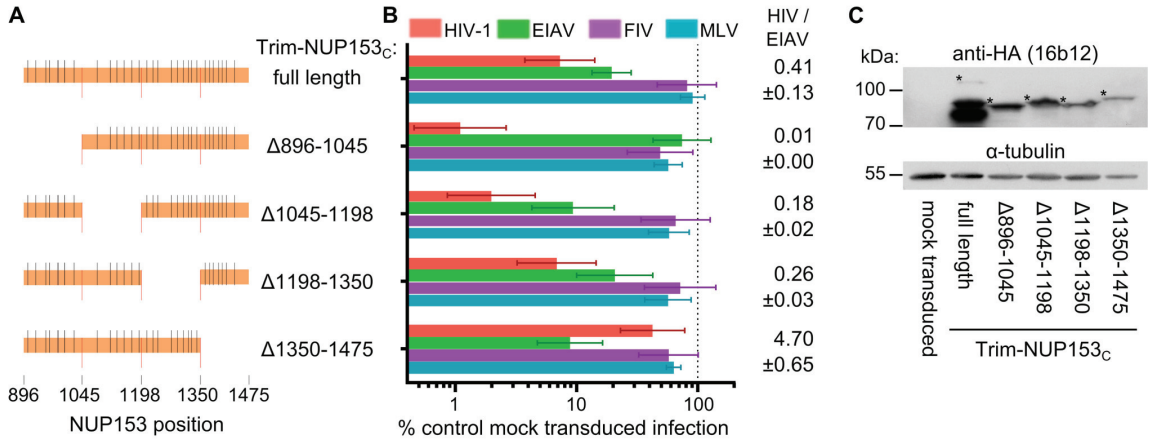

Figure 3-5. Different NUP153$_C$ sub-regions mediate Trim-NUP153$_C$ restriction of EIAV versus HIV-1 infection. (**A**) To-scale schematic of NUP153$_C$ sequences encoded in various Trim-NUP153$_C$ constructs. Red lines represent boundaries of quarter-sized NUP153$_C$ sub-regions, while black lines denote the locations of FG motifs. (**B**) Infectivity of retroviral GFP reporter viruses on HOS cells stably expressing full-length or quarter-deleted Trim-NUP153$_C$ constructs, normalized to infection in mock transduced cells. Data represent the geometric mean of 5 experiments, with error bars denoting 95% confidence intervals. HIV-1 to EIAV ratios of infectivity are shown, with associated standard error. (**C**) Western blot of HOS cells stably transduced with Trim-NUP153$_C$ fusion constructs detected with antibody 16b12. Asterisks denote bands corresponding to the expected mobilities of full length or mutated Trim-NUP153$_C$ constructs.

constructs displayed the same slight advantage to inhibit HIV-1 infection over EIAV, with HIV-1 to EIAV infectivity ratios similar to the full-length construct. Western blotting confirmed that each deletion construct was expressed at roughly similar levels (**Figure 3-5C**). The mapping of the HIV-1 binding determinant on $NUP153_C$ to residues 1350-1475 by Trim-mediated restriction notably coincides with our preliminary identification of the region C-terminal to residue 1198 using CA-NC tubes and HA-tagged NUP153 deletion constructs (**Figure 3-1B**).

We next focused on the initial quarter of $NUP153_C$ for its importance in mediating restriction of EIAV infection. Stable cell lines expressing only the first quarter of $NUP153_C$ fused to the Trim RBCC, as well as smaller derivatives of the $NUP153_C$ sequence, were generated (**Figure 3-6A**). Residues 896-949, which yielded the smallest construct capable of restricting EIAV infection (**Figure 3-6B**), harbored only two of the 29 FG motifs present within $NUP153_C$. The importance of these FG motifs in mediating EIAV restriction was tested by substituting four consecutive alanine residues for each corresponding FKFG sequence. The combination octa-alanine 903A/924A Trim-$NUP153_C$ mutant construct lost its ability to inhibit EIAV infection despite being expressed at a level equal to or greater than unmodified Trim-$NUP153_C$ (**Figure 3-6B and 3-6C**). The 903A/924A mutant moreover retained potent HIV-1 restriction. Separate mutation of each motif revealed 924-FKFG-927 as the dominant FG sequence for mediating EIAV restriction.

Sequence components of $NUP153_C$ that mediated restriction of HIV-1 infection were investigated next. Attempts to recover cells expressing the responsible C-terminal quarter of $NUP153_C$ (residues 1350-1475) fused to Trim RBCC were unsuccessful. We

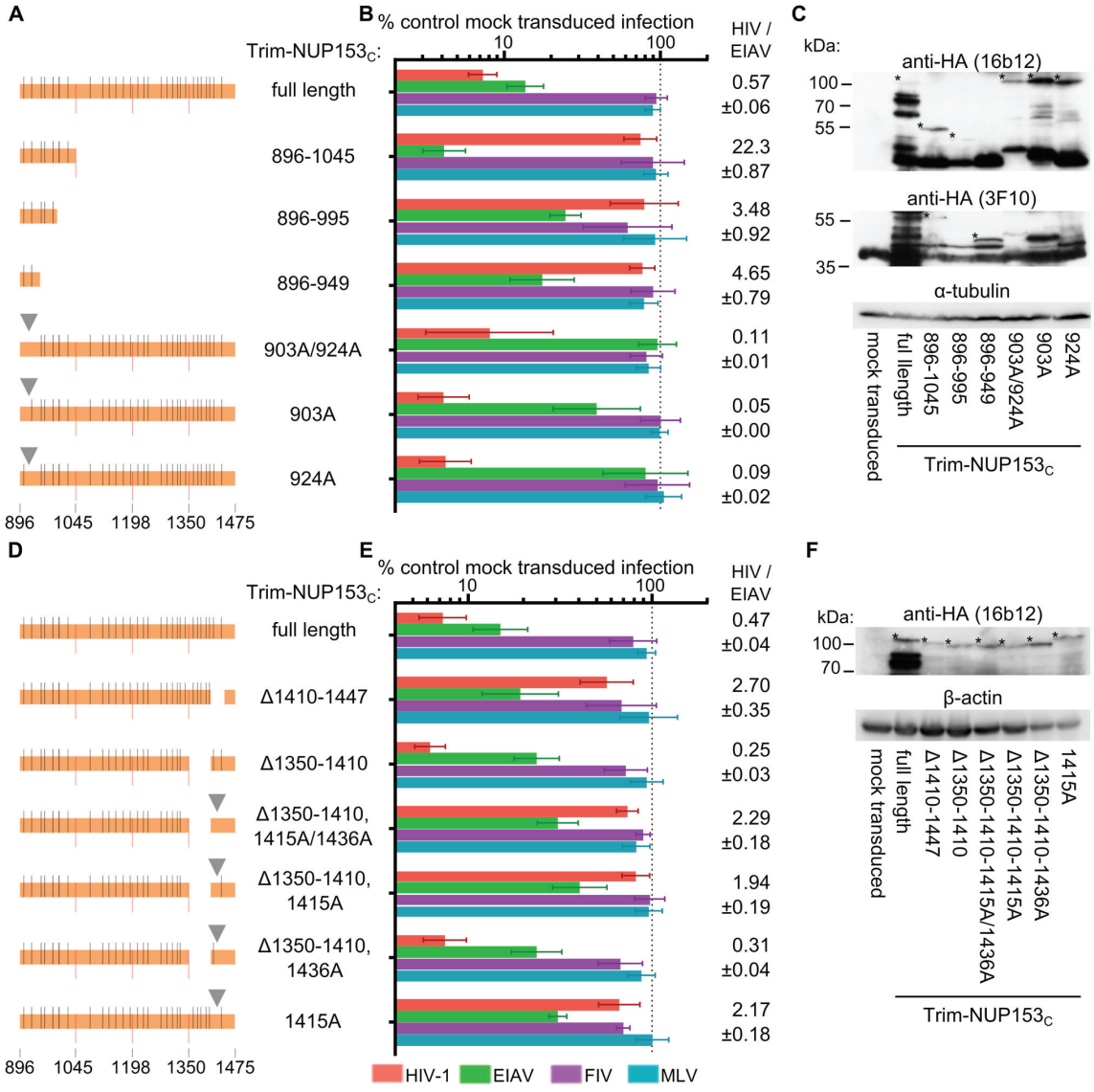

Figure 3-6. The importance of FG motifs for Trim-NUP153$_C$ mediated inhibition of HIV-1 and EIAV infection. To-scale schematics (**A and D**), normalized infection data (**B and E**), and western blotting (**C and F**) as described for Figure 3-5. Infection data are the geometric mean of at least 4 experiments, with error bars denoting 95% confidence intervals. Inverted grey triangle (panels A and D) denotes area of missense mutation.

instead undertook the alternative strategy to internally delete segments of residues 1350-1475 from the full-length Trim-NUP153$_C$ construct (**Figure 3-6D**). Deletion of residues 1410-1447 selectively diminished inhibition of HIV-1 without affecting EIAV, yielding an increased HIV-to-EIAV infectivity ratio of 2.7, while deletion of residues 1350-1410 did not drastically alter the ratio from that observed with the full length construct (**Figure 3-6E and 306F**). As residues 1410-1447 contained only one FxFG and one FxF motif, these were mutated to alanine residues, initially in the context of the Δ1350-1410 construct. Combinatorial alteration of both tetra- and tri-peptides reduced restriction of HIV-1 without significantly affecting EIAV restriction (HIV-1/EIAV infectivity ratio = 2.29). Separate mutation showed this effect was largely, if not entirely due to 1415-FTFG-1418, and the 1415A mutation largely prevented restriction of HIV-1 in the full-length construct as well (infectivity ratio = 2.17). Combined, these results highlight the importance of FG motifs for Trim-NUP153$_C$ mediated restriction of HIV-1 and EIAV infection. Moreover, different FG motifs appear to selectively recognize HIV-1 versus EIAV CA proteins.

We subsequently tested for Trim-NUP153$_C$ FG motif recognition of EIAV and HIV-1 CA proteins in vitro. HA-tagged NUP153$_C$ or analogous quarter deleted fragments expressed in 293T cells were used as bait for pull-down by various his-tagged retroviral CA$_N$ proteins (**Figure 3-7A**). The construct lacking residues 1045-1198 was expressed far less than the other constructs, and was not interpreted. As expected (**Figure 3-4B**), none of the constructs bound MLV CA$_N$ to levels greater than those observed with beads alone. Consistent with the results from Trim-NUP153$_C$ restriction, the protein lacking residues 1350-1475 was selectively bound less well by HIV-1 CA$_N$. Contrastingly, EIAV

Figure 3-7. FG motifs determine NUP153$_C$ binding to HIV-1 CA$_N$. (**A**) Pull-down of full-length or quarter deleted HA-NUP153$_C$ by HIV-1, EIAV, or MLV CA$_N$ proteins, detected with antibody 3F10. (**B**) Pull-down of WT NUP153$_C$, FG-motif tetra-alanine mutant 1415A, or combinatorial 7xFG/A mutant by beads alone (none, grey), HIV-1 (red), MLV (blue), or EIAV (green) CA$_N$ proteins, as detected by western blot with antibody 3F10. Results are an average of at least 4 experiments, with error bars denoting standard error. (**C**) Purified NUP153$_C$ (black circles, solid line), NUP153$_C$Δ1350-1475 (purple triangles, fine dotted line), and NUP153$_C$7xFG/A (brown diamonds, coarse dotted line) were incubated with various concentrations of HIV-1 CA$_N$ and a constant amount of Ni-NTA beads. Data points represent the mean and standard error of at least three experiments, fit with non-linear regression curves. The dissociation constant of NUP153$_C$ binding was calculated by averaging concentrations of half-maximal binding for 5 individual experiments, with associated standard error. (**D**) Sedimentation of WT NUP153$_C$, FG-motif tetra-alanine mutant 1415A, combinatorial 7xFG/A mutant, or NUP153$_C$Δ1350-1475 after incubation with buffer alone or assembled CA-NC. Results are an average of 6 experiments, with error bars denoting 95% confidence intervals. Representative western blotting results are shown.

(**Figure 3-7,** continued)

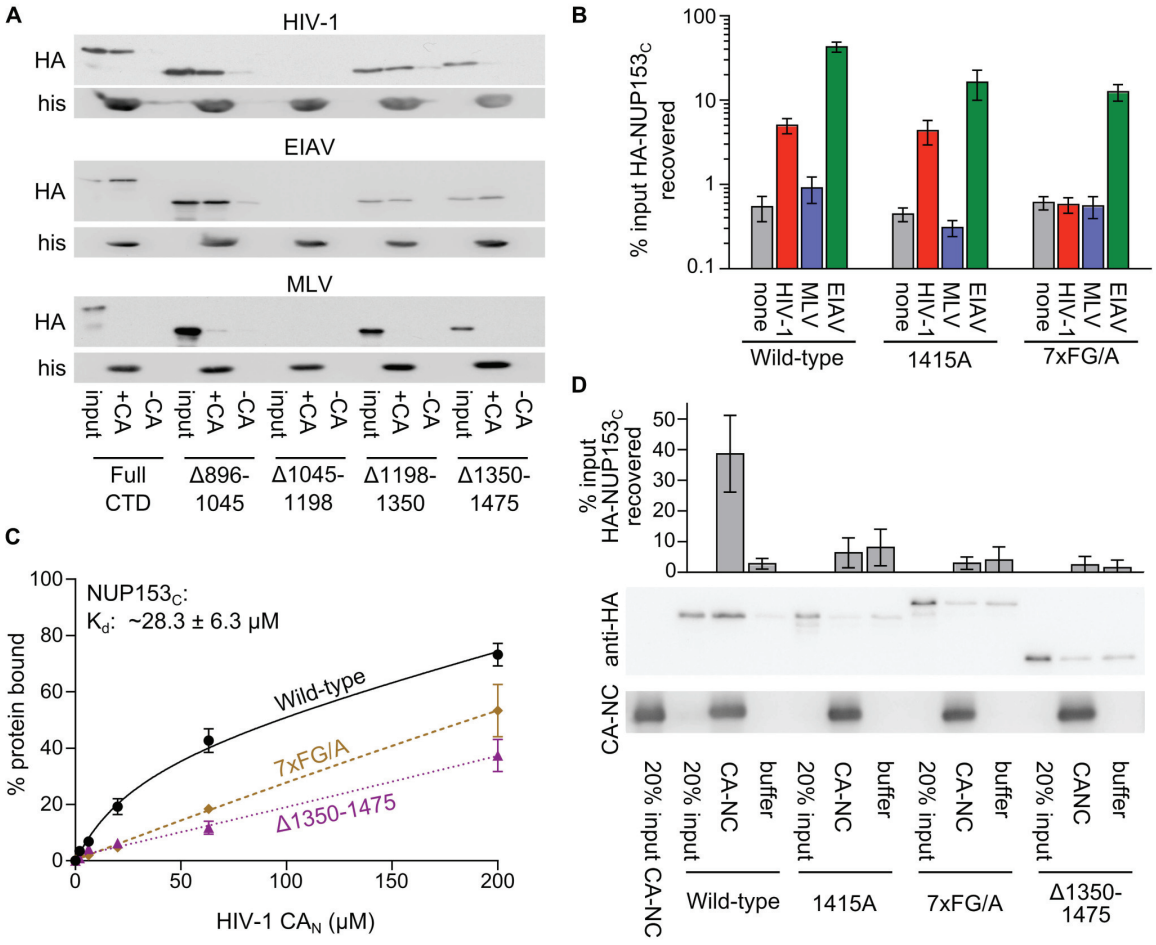

CA_N bound all of the fragments tested, including the fragment that lacked residues 896-1045.

We further tested whether HIV-1 CA_N binding was traceable to specific FG motifs. HA-$NUP153_C$ containing the 1415-FTFG-1418 tetra-alanine replacement bound HIV-1 CA_N essentially as well as the unmutated fragment (**Figure 3-7B**). Since we observed strongly diminished binding when the last quarter of HA-$NUP153_C$ was deleted (**Figure 3-7A**), we next mutated all 7 of the FG motifs within this segment to alanines (HA-$NUP153_C$7xFG/A). The combination of these mutations selectively abrogated binding of HA-$NUP153_C$ to HIV-1 CA_N; importantly, effective binding of the mutant protein to EIAV CA_N was retained (**Figure 3-7B**). Decreased Δ1350-1475 and 7xFG/A mutant binding to HIV-1 CA_N was also observed with purified $NUP153_C$ proteins. HIV-1 CA_N bound purified $NUP153_C$ (0.5 μM) in a dose-dependent manner, revealing a corresponding K_d of ~ 28.3 μM at half-maximal saturation (**Figure 3-7C**). Although CA_N displayed some affinity for $NUP153_C$Δ1350-1475 and $NUP153_C$-7xFG/A, the shapes of these linear response curves were notably different from the unmutated protein, and half-maximal saturation was not reached under these assay conditions.

We hypothesized that differing states of CA multimerization might contribute to the partially overlapping specificities observed in the CA_N pull-down (**Figure 3-7A and 3-7B**) versus Trim-$NUP153_C$ restriction (**Figure 3-6E**) assays. To test this, assembled CA-NC tubes were substituted for monomeric CA_N protein. Under these conditions, both the $NUP153_C$-7xFG/A and 1415A mutant proteins displayed significantly diminished binding, similar to the effect observed for the Δ1350-1475 deletion ($P < 0.01$) (**Figure 3-**

7D). These findings seemingly agree with the results of the Trim-NUP153$_C$ mediated restriction assays (**Figure 3-5B and 3-6E**).

Side-chains proximal to a common hydrophobic pocket in HIV-1 CA$_N$ mediate NUP153$_C$ binding

We and others previously observed that various CA mutant viruses exhibit altered sensitivity to NUP153 knockdown [177,231]. We next characterized an expanded set of CA mutant viruses for altered sensitivity to Trim-NUP153$_C$ restriction. Mutants were selected based on prior descriptions of pre-integrative defects during HIV-1 infection. Alteration of CA residue(s) Pro38, Glu45, Thr54/Asn57, or Gln63/Gln67 can effect core stability [45,57,119,120], whereas Thr54, Asn57, Lys70, Asn74, Gly89, Pro90, Ala92, Gly94, and Thr107 mutants can alter dependencies on various host proteins, including CPSF6, TNPO3, NUP358, CypA, or NUP153 [177,187,191,231,233,234,242,243]. As a number of these mutants exhibit drastically diminished overall levels of infectivity (**Figure 3-8A**), an unrelated IN mutant virus (D167K), which infects cells at ~ 8% of the level of wild-type (WT) HIV-1 [244], was included to control for our ability to reproducibly measure restriction at reduced viral titers. While the IN mutant virus was as sensitive as the WT virus to Trim-NUP153$_C$ restriction, a number of CA mutant viruses exhibited significantly reduced susceptibility ($P < 0.001$) (**Figure 3-8B**). Included among these were CypA and NUP358 CHD binding mutants G89V and P90A [187,233], as well as mutants E45A, T54A/N57A, N57A, N57D, Q63A/Q67A, Q67A, K70R, and N74A.

As these CA mutant viruses could resist Trim-NUP153$_C$ restriction for any number of reasons, we tested for direct binding defects by pulling down NUP153$_C$ with

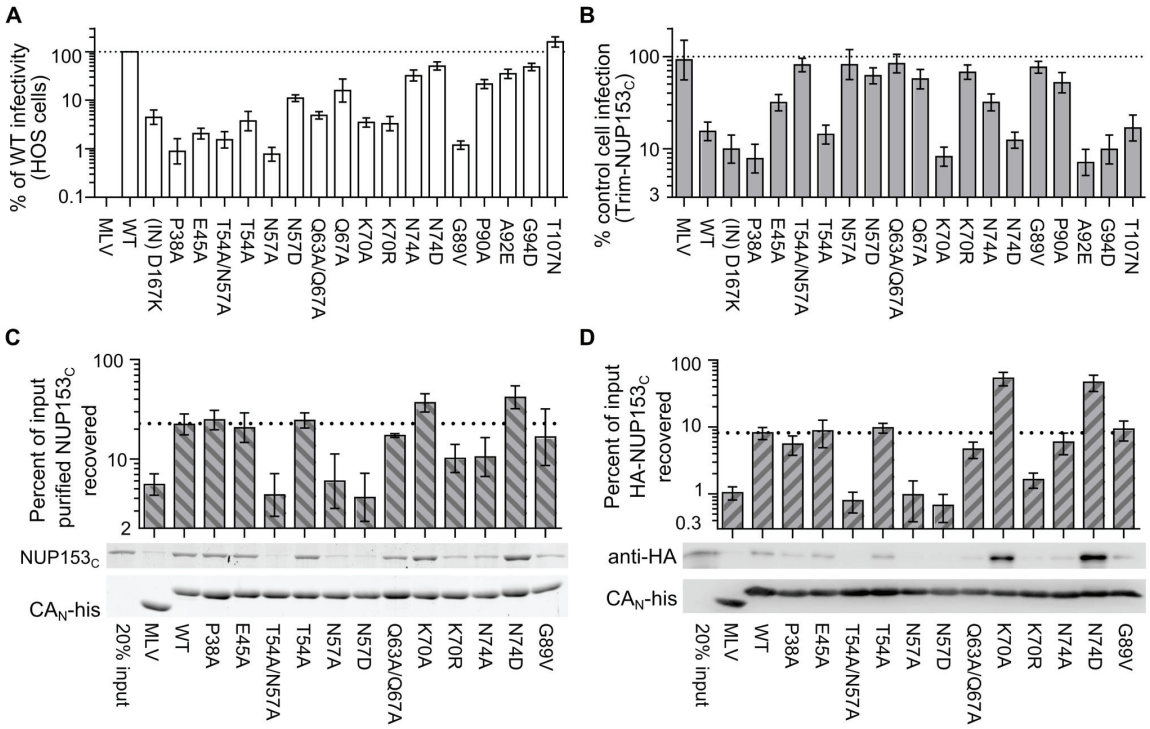

Figure 3-8. HIV-1 CA mutant-NUP153$_C$ binding and sensitivity to Trim-NUP153$_C$ restriction. (**A**) Equal RTcpm of WT and HIV-1 mutant viruses plated on HOS cells, with resulting infectivities normalized to WT virus. (**B**) Percent infectivity of viruses in Trim-NUP153$_C$ expressing HOS cells, normalized to mock transduced control cells. Graphs show the mean of at least 5 experiments, with error bars denoting 95% confidence intervals. (**C**) Purified NUP153$_C$ pull-down by WT or the indicated mutant his-tagged HIV-1 CA$_N$ protein, with recovered proteins resolved by SDS-PAGE and detected by SYPRO Ruby stain. Results are an average of 5 experiments, with error bars denoting 95% confidence intervals. A representative staining result is shown. The dotted line highlights the level of NUP153$_C$ binding to WT CA$_N$ protein. (**D**) HA-NUP153$_C$ in 293T cell lysates pulled-down by WT or various mutant his-tagged HIV-1 CA$_N$ proteins, with recovered protein resolved by SDS-PAGE and detected by 3F10 and anti-his antibodies. Results are an average of 4 experiments, with error bars denoting standard error. A representative western blot result is shown. The dotted line highlights the level of HA-NUP153$_C$ binding to WT CA$_N$ protein.

correspondingly purified CA_N mutant proteins. Residue Asn57 was critical for binding, as mutant proteins T54A/N57A, N57A, and N57D were strongly diminished in their abilities to pull down $NUP153_C$ (**Figure 3-8C**). Although not critical for binding, both Lys70 and Asn74 appeared to participate: mutation of Lys70 to arginine diminished binding while mutation to alanine enhanced binding; contrastingly, mutation of Asn74 to alanine diminished binding, while mutation to aspartic acid enhanced binding to $NUP153_C$. The Q63A/Q67A mutation marginally diminished binding by ~ 1.3 fold. This binding hierarchy was also observed for HA-$NUP153_C$ protein expressed in mammalian cells, with Asn57 again proving key for the interaction, and mutants K70A and N74D yielding hyper-binding activity (**Figure 3-8D**). Overall, CA mutant viral sensitivities to Trim-$NUP153_C$ restriction correlated well with CA_N mutant binding to $NUP153_C$ protein in vitro (**Figure 3-9A**).

As we predict that mutant viruses that require NUP153 for infection also bind $NUP153_C$, we compared the sensitivities of CA mutant viruses to NUP153 knockdown with their susceptibility to Trim-$NUP153_C$ mediated restriction. We observed that CA mutant viruses that require endogenous NUP153 for infection were also sensitive to Trim-$NUP153_C$ mediated restriction. A strong correlation supported this relationship across the entire panel of CA mutant viruses (**Figure 3-9B**). This included $NUP153_C$ loss-of-binding mutants T54A/N57A, N57A and N57D, which retained approximately 85%, 102% and 58% of their infectivity, respectively, upon NUP153 knockdown.

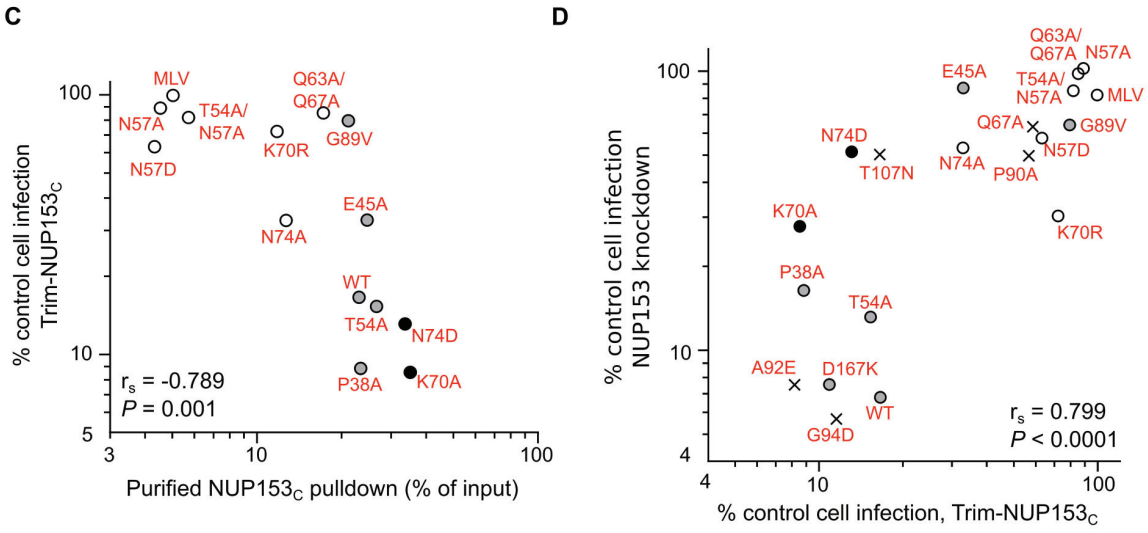

Figure 3-9. Comparison of HIV-1 CA mutant-NUP153$_C$ sensitivity to Trim-NUP153$_C$ restriction with binding to NUP153$_C$, or sensitivity to NUP153 depletion. (**A**) Scatter plot of NUP153$_C$ recovery in pull-down assays (Figure 3-8C) compared to percent infectivity in Trim-NUP153$_C$ expressing cells (Figure 3-8B). Points are color-coded based on NUP153$_C$ binding phenotype: grey, not significantly different from WT; white, significantly decreased from WT; black, significantly increased from WT. (**B**) Scatter plot of normalized infectivity of CA mutant viruses in Trim-NUP153$_C$ expressing cells compared to the average infectivity of three experiments when endogenous NUP153 was knocked down. The comparison exhibited a significant Spearman rank correlation ($P < 0.0001$). Points are color-coded as in panel C, except for CA mutants not tested for binding, which are denoted with "x" symbols.

The NUP153$_C$ binding site overlaps with those for PF74 and CPSF6

Residues Asn57, Lys70, and Asn74, highlighted in our binding assays, surround a hydrophobic pocket within CA$_N$ formed by α helices 3 and 4, and this pocket has been shown to be the binding site of the small molecule inhibitor PF74 [235] (**Figure 3-10A**). To probe potentially similar binding modes, we tested whether PF74 could compete for HA-NUP153$_C$ binding to CA$_N$ (**Figure 3-10B**). PF74 indeed competed for binding to CA$_N$ in a dose-dependent manner, with an IC$_{50}$ of ~ 13.6 μM. While PF74 binds WT and N74D CA$_N$ proteins similarly [234], the small molecule was less effective at competing for HA-NUP153$_C$ binding to N74D CA$_N$, yielding an IC$_{50}$ of 145.3 μM, perhaps due to the increased binding observed between NUP153$_C$ and N74D CA$_N$ (**Figure 3-8C and 3-8D**). PF74 does not bind K70A mutant CA$_N$ [234], and accordingly did not compete for HA-NUP153$_C$ binding to this mutant protein (**Figure 3-10B**).

This same pocket also engages the mRNA splicing cofactor CPSF6 [177,234,240], which was first implicated in HIV-1 biology by the ability for an exogenously expressed C-terminal truncation mutant CPSF6$_{358}$ to restrict PIC nuclear import [177]. Though vastly differing molecules, co-crystal structures of PF74-CA$_N$ and CPSF6 (residues 313-327)-CA$_N$ complexes revealed that each exhibit nearly identical insertions of methyl benzyl residues (Phe321 in the case of CPSF6) within the helix 3/4 pocket, in both cases forming two hydrogen bonds with the carboxamide side-chain of CA residue Asn57 (**Figure 3-10A and 3-10C**). Based on these observations, we tested whether purified NUP153$_C$ could compete with full-length CPSF6 protein for binding to CA. HA-tagged CPSF6 expressed in 239T cells was incubated with HIV-1 CA-NC tubes prior to centrifugation through a 20% sucrose cushion. CPSF6 pelleted only in the

Figure 3-10. $NUP153_C$ competes with molecules that bind the HIV-1 CA_N hydrophobic pocket. (**A**) X-ray crystal structure (pdb: 2xde) of compound PF74 (yellow) bound to HIV-1 CA_N (green). Critical CA_N side-chains (labeled) are shown as sticks, with oxygen and nitrogen atoms colored red and blue, respectively. Hydrogen bonds are shown as black dashes, with distances labeled. The phenylalanine moiety in PF74 is indicated by the black arrow. (**B**) PF74 competition of HA-$NUP153_C$ binding to WT or mutant his-tagged HIV-1 CA_N. Recovered HA-$NUP153_C$ was detected with antibody 3F10 and quantitated alongside a standard curve of serially diluted HA-$NUP153_C$-containing lysate. Baseline background signal observed with T54A/N57A CA_N pulldown was subtracted, and all values were normalized to that of the DMSO control (2% DMSO final concentration in each sample). Results are an average of at least 2 experiments, with error bars denoting standard error. Representative western blotting results are shown. (**C**) X-ray crystal structure (pdb: 4b4n) of a peptide from CPSF6 (backbone carbon atoms shown as sticks in grey) bound to CA_N (green) in the same orientation as in panel A. Side-chains and hydrogen bonds are represented as in panel A. The CPSF6 Phe321 side chain is indicated by the black arrow. (**D**) Binding of HA-tagged, full-length CPSF6 protein in 293T cell extract to HIV-1 CA-NC protein, and competition with purified $NUP153_C$ or mutants thereof. Results of 5 experiments were normalized to the level of CPSF6 binding observed in the absence of competing factors, with error bars denoting standard error.

(**Figure 3-10,** continued)

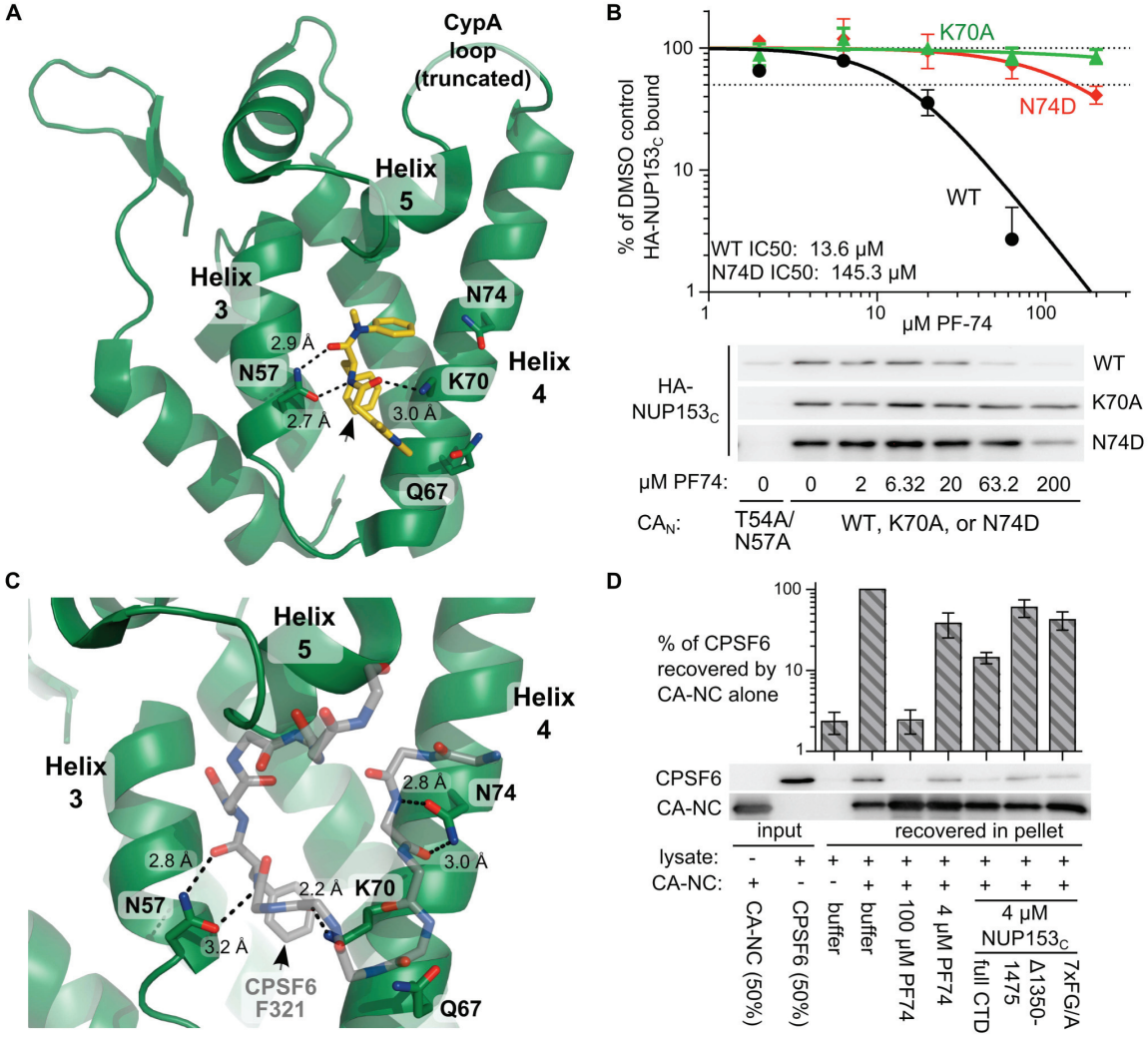

presence of CA-NC (**Figure 3-10D**). This interaction indeed required binding to the CA_N hydrophobic pocket, as excess PF74 counteracted it. We additionally observed that co-incubation with purified $NUP153_C$ significantly diminished CPSF6 binding ($P < 0.0001$) by ~ 7 fold as compared to the level observed in the absence of competing factors. This competition was specific, as $NUP153_C$ mutants Δ1350-1475 and 7xFG/A, both of which exhibit greatly diminished binding to CA-NC (**Figure 3-7**), were significantly less effective at competing for CPSF6 binding ($P < 0.05$) (**Figure 3-10D**).

CA residues that mediate binding to $NUP153_C$ and CPSF6 were further analyzed by assessing CA mutant sensitivities to restriction by the artificial restriction factor Trim-$CPSF6_{358}$ (**Figure 3-11A**), a larger derivation of the Trim-CPSF6 fusion proteins previously tested [240]. Though conferring similar levels of restriction, far fewer of the CA mutant viruses were able to resist Trim-$CPSF6_{358}$ inhibition (**Figure 3-11B**, red data points) compared to Trim-$NUP153_C$ (black points). CypA binding mutants G89V and P90A were partially resistant to Trim-$CPSF6_{358}$ restriction, whereas N57A, N74A, and N74D in large part conveyed full resistance. The N57A and N74D changes were notably previously shown to prevent binding of CA_N to the CPSF6 peptide [234]. Interestingly, changes at Asn57 and Asn74 conferred distinguishable resistance profiles to Trim-$NUP153_C$ versus Trim-$CPSF6_{358}$: both conservative N74D and non-conservative N74A changes rendered HIV-1 resistant to Trim-$CPSF6_{358}$, while only N74A rendered the virus partially resistant to Trim-$NUP153_C$ (**Figure 3-11B**). Contrastingly, both conservative and non-conservative Asn57 changes prevented Trim-$NUP153_C$ recognition, while the conservative N57D mutant remained as sensitive to Trim-$CPSF6_{358}$ restriction as the WT virus.

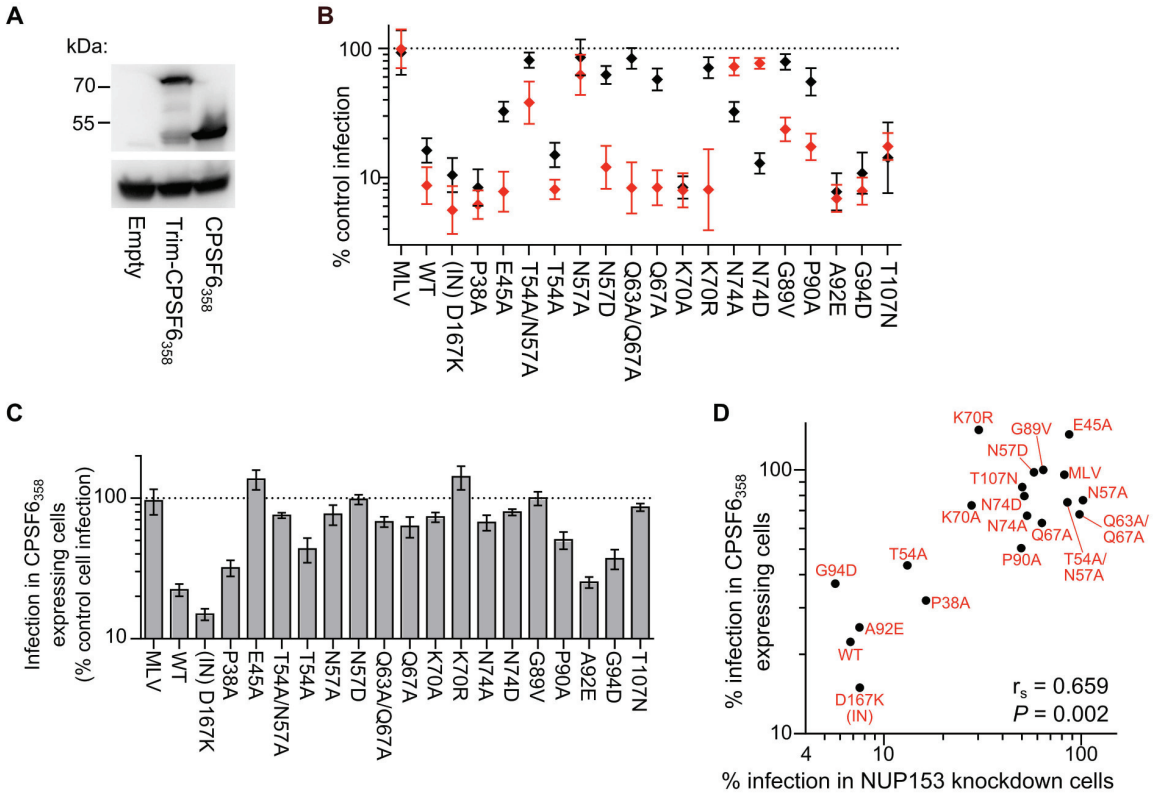

Figure 3-11. HIV-1 CA mutant sensitivities to Trim-NUP153$_C$ as compared with sensitivities to CPSF6$_{358}$ and Trim-CPSF6$_{358}$. (**A**) Western blot of HOS cells stably expressing Trim-CPSF6$_{358}$ or CPSF6$_{358}$, detected with antibody 3F10. (**B**) CA mutant virus sensitivities to Trim-NUP153$_C$ (black) and Trim-CPSF6$_{358}$ (red), as compared to cells transduced with an empty vector. Results are an average of at least 3 experiments, with error bars denoting 95% confidence intervals. (**C**) Scatter plot of CA mutant sensitivities to NUP153 knockdown compared with sensitivities to inhibition by CPSF6$_{358}$. (**D**) Percent infectivity of CA mutant viruses on CPSF6$_{358}$ expressing HOS cells compared to mock transduced cells. Results are the average of 3 experiments, with error bars denoting standard error.

The breadth of CA mutants restricted by Trim-CPSF6$_{358}$ in HOS cells appeared to contrast with prior results of CPSF6$_{358}$-mediated restriction of HIV-1 in Hela cells, where many of the same CA mutations conferred resistance to inhibition [66]. We confirmed these phenotypes in HOS cells, where we observed that many additional CA mutant viruses resist CPSF6$_{358}$-mediated restriction (**Figure 3-11C**). Many of the CA mutant viruses selectively resistant to CPSF6$_{358}$ over Trim-CPSF6$_{358}$ restriction were also insensitive to endogenous NUP153 knockdown, resulting in a moderate correlation between CA mutant sensitivities to CPSF6$_{358}$ restriction and NUP153 knockdown (**Figure 3-11D**).

PF74 destabilizes the structure of purified CA cores and can inhibit reverse transcription, which likely accounts for at least part of its antiviral activity [245]. We assessed whether PF74 could additionally antagonize NUP153$_C$ engagement by CA in the context of HIV-1 infection, given the caveat that we could not unambiguously correlate data from protein binding assays (**Figure 3-10B**) with effects from PF74-induced capsid destabilization in cells. PF74 exhibited dose-dependent inhibition of WT HIV-1 and N74D CA mutant viral infection, but had no effect on CA mutant T54A/N57A, which lacks the critical Asn57 side-chain necessary for PF74 binding [234] (**Figure 3-12A, upper panel**; results replotted below to reveal EC$_{90}$ values under conditions of Trim-NUP153$_C$ restriction). WT virus was noticeably less sensitive to PF74 in Trim-NUP153$_C$ expressing cells, with an EC$_{90}$ of 5.65 μM as opposed to 0.65 μM in control cells (**Figure 3-12A**). The competing effect of PF74 on Trim-NUP153$_C$ inhibition seemingly occurred between the concentrations of 0.1 and 1 μM (light green shading in **Figure 3-12A**), as the inhibition curves within the two cell lines were nearly

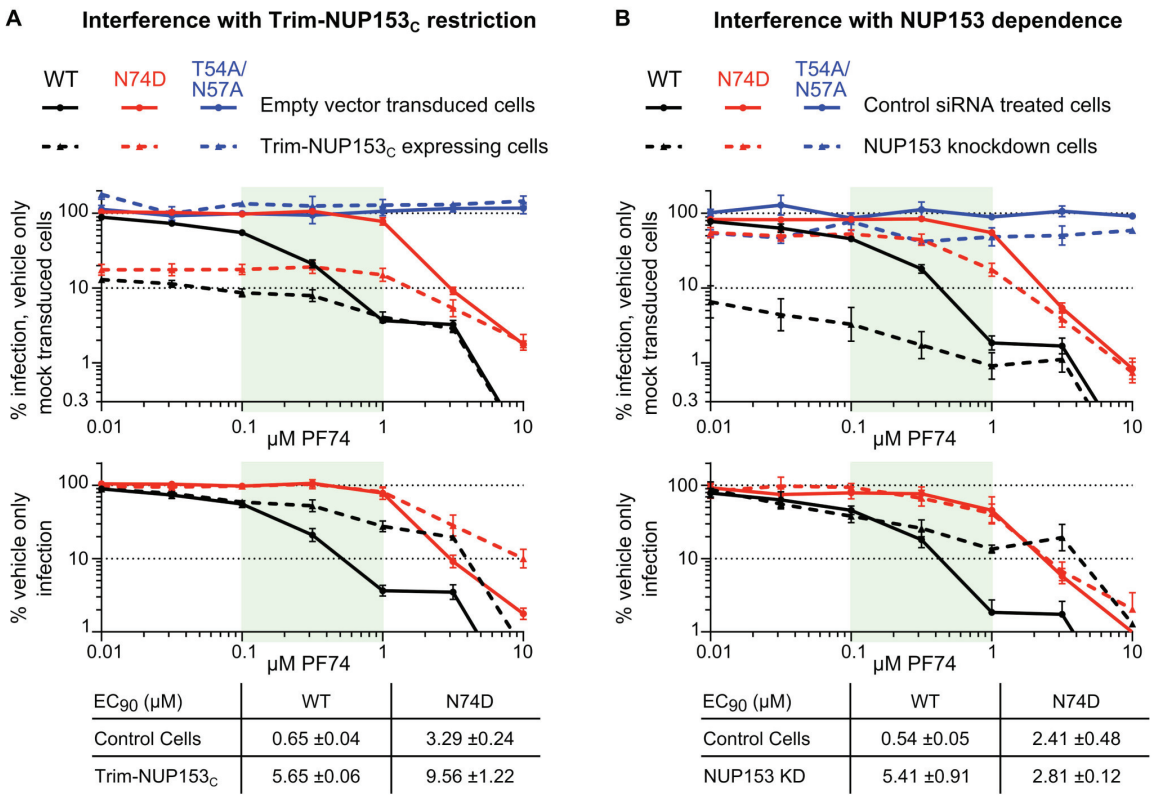

EC_{90} (μM)	WT	N74D
Control Cells	0.65 ±0.04	3.29 ±0.24
Trim-NUP153$_C$	5.65 ±0.06	9.56 ±1.22

EC_{90} (μM)	WT	N74D
Control Cells	0.54 ±0.05	2.41 ±0.48
NUP153 KD	5.41 ±0.91	2.81 ±0.12

Figure 3-12. PF74 similarly counteracts HIV-1 in the face of Trim-NUP153$_C$ restriction and NUP153 knockdown. Mock transduced and Trim-NUP153$_C$ expressing (**A**) or non-targeting control and NUP153 knockdown (**B**) HOS cells were infected with equal RT-cpm of denoted viruses in the presence of various PF74 concentrations. Results are shown as infectivity normalized to vehicle only control cells (top), or vehicle only infection for each cell type (bottom) to calculate EC_{90} values. Dashed lines represent Trim-NUP153$_C$ or NUP153 knockdown results in panels A and B, respectively. Results are an average of at least 3 experiments, with error bars denoting standard error. Calculated EC_{90} values are displayed with standard error.

superimposable outside of these concentrations. N74D CA mutant virus also exhibited a shift in the PF74 EC_{90} concentration in Trim-$NUP153_C$ cells, though this occurred at higher PF74 concentrations than with the WT virus. Interestingly, an almost identical effect was observed with WT virus when PF74 was titrated onto NUP153 knockdown cells; the EC_{90} shifted from 0.54 μM to 5.41 μM, with the same window of concentrations likely accounting for the discrepancy in inhibition curves (**Figure 3-12B**). While the exact mechanism of NUP153 antagonism – direct, or indirect through the alteration of the state of CA multimerization – is difficult to discriminate, the nearly superimposable interference profiles of PF74 in Trim-$NUP153_C$ expressing and NUP153 knockdown cells support the relevance of the Trim-$NUP153_C$ restriction assay as a surrogate readout for the engagement of endogenous NUP153 protein.

An analogous pocket in EIAV CA mediates binding to $NUP153_C$

Retroviral CA_N proteins exhibit remarkable similarity in secondary and tertiary structure despite marked differences in primary sequence [246,247]. With the exception of HIV-1 residue Gln67, the previously described polar residues flanking the helix 3/4 hydrophobic pocket (Asn57, Lys70, and Asn74 in HIV-1) exhibit variability across divergent retroviruses (**Figure 3-13A**, yellow boxes). While HIV-2 and SIVmac only differ at these positions with Arg69 in place of HIV-1 Lys70, EIAV exhibits greater difference: Leu71 corresponds to HIV-1 Lys70, and EIAV Asp58 and Asp75 correspond to HIV-1 Asn57 and Asn74, respectively (**Figure 3-13B**). These differences may account for the resistance of EIAV to inhibition by PF74 (**Figure 3-13C**) and $CPSF6_{358}$ [240], which we confirmed using HOS cells expressing Trim-$CPSF6_{358}$ (**Figure 3-13D**). As

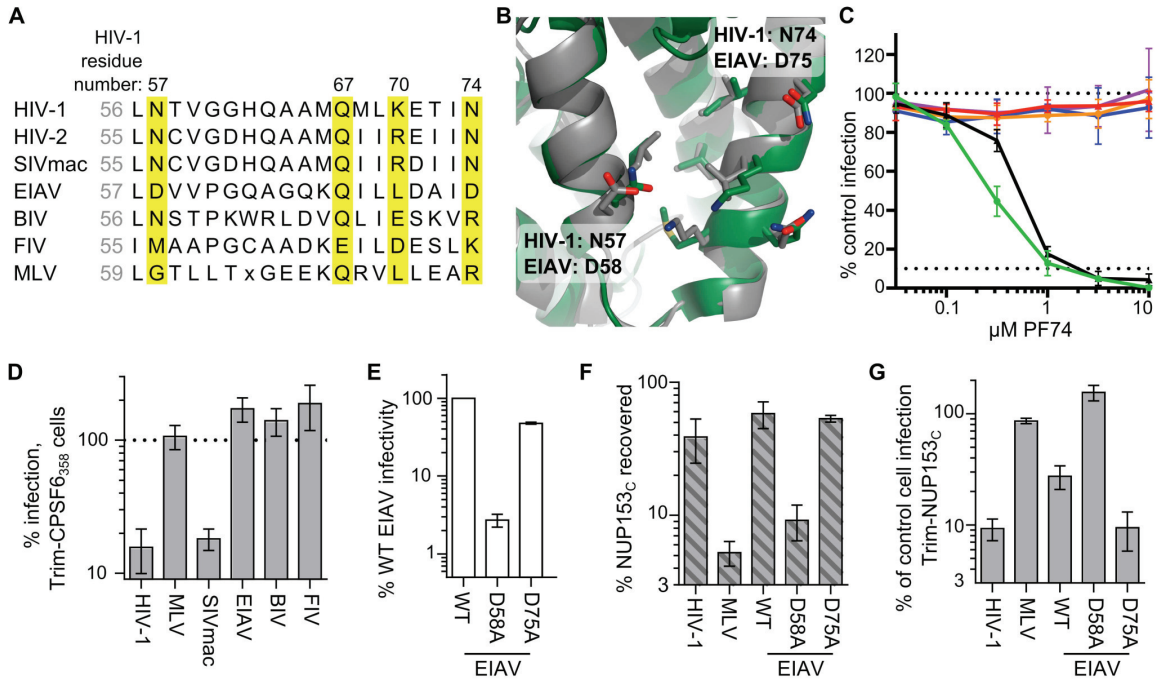

Figure 3-13. Mode of NUP153$_C$ binding to EIAV CA. (**A**) Alignment of residues corresponding to HIV-1 CA Leu56 through Asn74 among various retroviruses. Residues that significantly affected HIV-1 CA$_N$ binding with NUP153$_C$ are highlighted in yellow. (**B**) Alignment of HIV-1 CA$_N$ (green, pdb: 3mge) and EIAV CA$_N$ (gray, pdb: 1eia), with side-chains surrounding the pocket shown as sticks. (**C**) Retroviral sensitivities to inhibition by PF74. Color codes: HIV-1, green; SIVmac, black; MLV, red; EIAV, orange; BIV, blue; FIV, purple. Results are an average of two experiments. (**D**) Retroviral sensitivities to inhibition by Trim-CPSF6$_{358}$. Results are an average of 3 experiments. (**E**) Infectivity of RT-cpm matched EIAV GFP-reporter viruses carrying CA point mutations. Results are an average of 3 experiments. (**F**) Pull-down of purified NUP153$_C$ by EIAV point mutant CA$_N$ proteins. Results are an average of 2 experiments. (**G**) Sensitivity of EIAV CA point-mutant viruses to Trim-NUP153$_C$. Results are an average of 4 experiments. Error bars in each panel denote standard error.

Asp58 exhibits similar physiochemical properties as its HIV-1 Asn57 counterpart, we mutated this as well as residue Asp75 to test their contributions to $NUP153_C$ binding. Similar to HIV-1 mutant N57A, EIAV CA mutant D58A was poorly infectious (**Figure 3-13E**), and the corresponding CA_N protein was unable to pull down appreciable levels of $NUP153_C$ protein (**Figure 3-13F**). Contrastingly, EIAV CA mutant D75A behaved similar to WT EIAV (**Figure 3-13E and 3-13F**). The Trim-$NUP153_C$ sensitivities of these viruses corresponded with the binding profiles of their CA_N proteins: D58A was completely insensitive to Trim-$NUP153_C$ mediated restriction, while D75A remained as sensitive as WT EIAV (**Figure 3-13G**).

Comparison of NUP153 requirement and cell cycle dependence

Changes at Asn57 in HIV-1 CA have previously been associated with cell cycle dependence: T54A/N57A infection was attenuated in both chemically arrested cell lines and non-dividing primary macrophages [57,117], and the N57A mutant virus was recently shown to lose infectivity upon chemical arrest of Hela cells [233]. We confirmed the importance of Asn57, as well as other previously observed cell cycle dependent phenotypes, with our panel of CA mutant viruses; alanine substitution of residue Glu45, Thr54, Asn57, or Gln67 rendered the virus significantly sensitive to growth arrest (**Figure 3-14A and 3-14B**). Notably, we found even the conservative N57D substitution rendered the virus as, if not more sensitive, than these mutants to growth arrest. A handful of CA mutant viruses have been described to be sensitive to cell cycle arrest in Hela cells in a CypA-dependent manner [117,118]. We found N57A and N57D CA mutant viruses to remain highly cell cycle dependent when the interaction with CypA

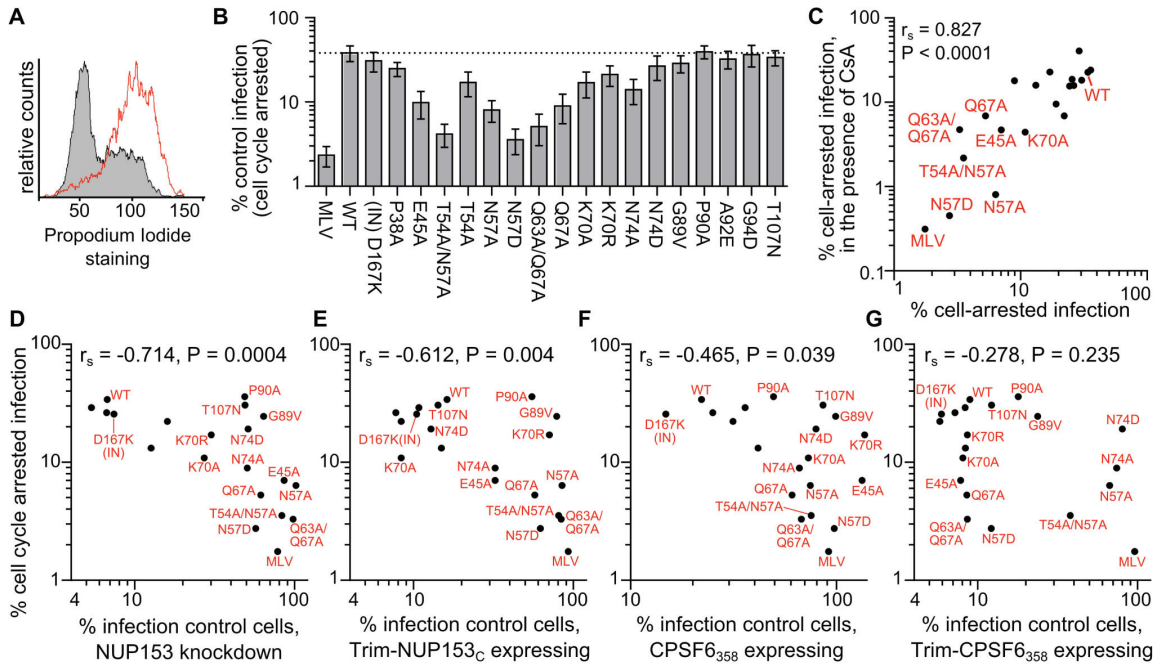

Figure 3-14. Association between NUP153 dependency and cell cycle independence. (**A**) Propidium iodide staining of HOS cells untreated (grey) or treated for 24 h with 5 µM Etoposide phosphate (red line). (**B**) Infectivity of CA mutant viruses in HOS cells arrested with 5 µM Etoposide phosphate, normalized to infectivity in control HOS cells. Error bars denote standard error of 4 experiments. (**C**) Scatter plot comparison of CA mutant sensitivities in cell cycle arrested HOS cells in the absence or presence of 5 µM CsA. Mutant viruses most sensitive to cell cycle arrest are indicated. (**D to G**) Scatter plots comparing sensitivities of mutant viruses to cell cycle arrest versus NUP153 knockdown (D), or restriction by Trim-NUP153$_C$ (E), CPSF6$_{358}$ (F), or Trim-CPSF6$_{358}$ (G). Spearman rank correlation coefficients and measures of significance are indicated. Data points for CA mutant viruses P38A, T54A, A92E, and G94D clustered with the WT virus within these panels, so their labels were omitted to aid legibility.

was blocked by the addition of cyclosporine during infection (**Figure 3-14C**).

Based on the coincident NUP153-insensitive and cell cycle dependent phenotypes of Asn57 mutant viruses, we tested the association between NUP153 requirement and cell cycle dependency in the context of our expanded panel of mutant viruses. We observed a moderately strong inverse correlation between requirement for NUP153 and cell cycle dependence during infection (**Figure 3-14D**). Notably, of the viruses tested in our panel, all of the ones that were cell cycle dependent were NUP153 independent. The correlation however was not absolute, as N74D, G89V, P90A, and T107N mutant viruses did not require NUP153 for infection yet remained cell cycle independent. There was a moderate correlation between cell cycle dependence and Trim-NUP153$_C$ resistance (**Figure 3-14E**). We observed a moderate to low correlation between cell cycle dependence and CPSF6$_{358}$ mediated restriction, and no correlation with Trim-CPSF6$_{358}$ mediated restriction (**Figure 3-14F and 3-14G**). These results reveal that cell cycle dependence is associated with NUP153 independence, and that this relationship likely depends on CA-NUP153 binding.

Discussion

NUP153 FG motif binding within the CA helix 3/4 cavity

GFP-tagged NUP153 expressed in animal cell lysate was recently shown to co-sediment with HIV-1 CA-NC tubes in vitro [248]. We confirmed this observation for HA-tagged protein, and extended it by using purified recombinant protein to demonstrate direct binding between the FG-enriched $NUP153_C$ and the HIV-1 CA NTD. Mutation of CA residue Asn57, Lys70, or Asn74, which each flank the hydrophobic pocket between CA α helices 3 and 4, perturb binding of $NUP153_C$ protein to HIV-1 CA_N. Furthermore, $NUP153_C$ competes with PF74 and CPSF6 for binding, both of which engage the same pocket. Notably, co-crystal structures between HIV-1 CA_N and the latter two molecules exhibit an almost identically situated benzyl ring within the hydrophobic cavity, with the amide nitrogen and carbonyl oxygens of this phenylalanine moiety each forming a hydrogen bond with the side chain of Asn57 [234] (**Figure 3-10**). This observation, in conjunction with our finding that FG motifs within $NUP153_C$ strongly contribute to binding with CA_N, suggest that the phenylalanine moieties of specific FG motifs found in $NUP153_C$ likely take on a similar conformation during binding. We accordingly speculate that hydrogen bonding with Asn57 underlies the FG motif interaction, as both N57A and N57D mutations abrogated binding. While originally described to support CPSF6 binding [234], the high degree of amino acid conservation within this region of CA amongst primate lentiviruses likely also reflects the requirement for binding to NUP153 during virus infection [231].

Relevance of FG motif binding for NUP153 dependency during HIV-1 infection

Supporting the relevance of the NUP153-CA interaction, both a divergent set of retroviruses and a targeted set of CA missense mutants exhibited significant correlations between CA binding to $NUP153_C$ – either tested in vitro or inferred through Trim-$NUP153_C$ recognition – and requirement for endogenous NUP153 protein during infection (**Figures 3-4 and 3-9**). Notably, loss-of-binding CA mutant viruses T54A/N57A, N57A, and N57D infected cells independent of endogenous NUP153 expression. The relationship between NUP153 binding and host factor requirement was consistent with PF74 sensitivity as well; while potentially mediated through an indirect effect on uncoating, PF74 interfered with Trim-$NUP153_C$ restriction at the same concentrations that it antagonized the inhibition of infection caused by NUP153 knockdown (**Figure 3-12**).

Woodward and colleagues reported that ectopically-expressed $NUP153_C$ protein imparted an approximate twofold defect on HIV-1 infection [98], a result we did not reproduce despite efficient $NUP153_C$ expression (**Figure 3-2**). By contrast, appending $NUP153_C$ to the RBCC domains of rhTrim5α resulted in potent HIV-1 restriction, allowing us to infer the results of $NUP153_C$ binding to the CA shell during virus infection. NUP153 has been shown to bind HIV-1 IN [98], and though we observed minimal binding (≤1% of input IN recovered by GST-$NUP153_C$ pull-down; **Figure 3-15**), it was comparably weaker than our findings with HIV-1 CA (30-40% of input $NUP153_C$ recovered), and was less correlative with lentiviral requirement for endogenous NUP153 (**Figure 3-4D**) as FIV IN bound more robustly than HIV-1 IN to $NUP153_C$ in our hands (**Figure 3-15**). Thus, while NUP153 may bind more than one HIV-1

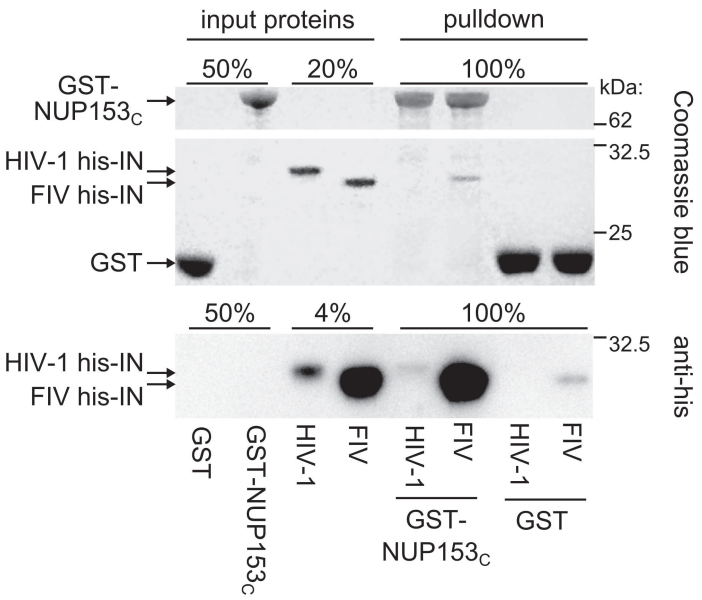

Figure 3-15. GST-NUP153$_C$ pull-down of HIV-1 and FIV IN. GST-NUP153$_C$ pulled-down an average of ~ 0.85 % of input his-tagged HIV-1 IN and ~ 5.55 % of input his-tagged FIV IN over 3 experiments. A representative experiment is shown. Note preferential western blot detection of the FIV IN N-terminal his-tag over that of the HIV-1 tag.

determinant, our results are consistent with a direct interaction between $NUP153_C$ and viral CA_N underlying the requirement for NUP153 during HIV-1 infection.

Potentially degenerate binding of NUP153 FG motifs

Different FG motifs within Trim-$NUP153_C$ mediated restriction of EIAV versus HIV-1 infection (**Figure 3-6**). Contrastingly, correspondence to protein binding in vitro was less strict: $NUP153_C\Delta$896-1045 effectively bound EIAV CA_N, though this deletion variant could not inhibit EIAV as a Trim-fusion. The 1415-FTFG-1418 tetra-alanine mutant, which lost the ability to inhibit HIV-1 as a Trim-fusion, was little if at all reduced for pull-down by HIV-1 CA_N, though alteration of all seven FG motifs in the last quarter of $NUP153_C$ yielded a protein greatly deficient for binding to HIV-1 CA_N (**Figure 3-7**). Because the tetra-alanine 1415-FTFG-1418 $NUP153_C$ mutant protein was significantly defective for binding assembled CA-NC tubes, we infer that this specific FG motif is important for $NUP153_C$ binding to multimerized CA.

We believe our results reflect the nature of the $NUP153_C$-CA interaction during HIV-1 infection. Unlike a bimolecular interaction between two well-folded domains, each with a single binding site, $NUP153_C$ exhibits no appreciable secondary structure and is highly repetitive in its primary sequence, particularly for phenylalanine-based FG motifs. As FG sequences appear to dictate $NUP153_C$ binding to CA_N, each of the 29 motifs may possess some affinity for CA_N. Residues adjacent to the phenylalanine, such as glycine, may allow proper flexibility to fit into the helix 3/4 pocket for Asn57 engagement. We envision that residues peripheral to the motif may also contribute intra- and inter-molecular interactions. This interpretation is consistent with the mode of CPSF6

binding: the CPSF6 FG dipeptide (residues Phe321 and Gly322) is critical for $CPSF6_{358}$ mediated restriction [240], while upstream residues Val314 and Leu315 fulfill important secondary roles through engaging additional hydrophobic patches located between CA_N α helices 4 and 5. CPSF6 backbone functional groups also interact to varying degrees with the side-chains of CA residues Asn74, Thr107, Lys70, and Gln67 [234] (**Figure 3-10C**).

Given this model, we hypothesize that differential accessibility of the CA_N helix 3/4 pocket might factor into the contrasting binding specificities observed between monomeric and oligomerized CA: while the pocket is likely exposed as a soluble NTD fragment in the pull-down assay, it may be less available within the context of a multimeric CA array. The CTD of the adjacent CA subunit covers the bottom edge of the cavity (**Figure 3-16A**), and the interacting $NUP153_C$ peptide would need to reach into the crevice between CA subunits, past the cyclophilin-binding loop, and under helix 5 to reach the pocket (**Figure 3-16B**). These steric requirements likely limit the number of $NUP153_C$ FG motifs capable of forming energetically favorable interactions with the oligomerized CA array present on the viral core.

Association with core uncoating and sensitivity to cell cycle arrest

Accordingly, alterations in the rate or extent of CA core uncoating may alter engagement of NUP153 during infection. Though both Trim-$NUP153_C$ and Trim-$CPSF6_{358}$ presumably encounter CA cores shortly after entry (**Figure 3-3**) [240], Trim-$CPSF6_{358}$ restricted the hyperstable CA mutant viruses E45A and Q63A/Q67A [45,57,119,120,249] as efficiently as WT cores, while Trim-$NUP153_C$ was less effective at restricting either of these mutants. Both mutant CA_N proteins in large part retained

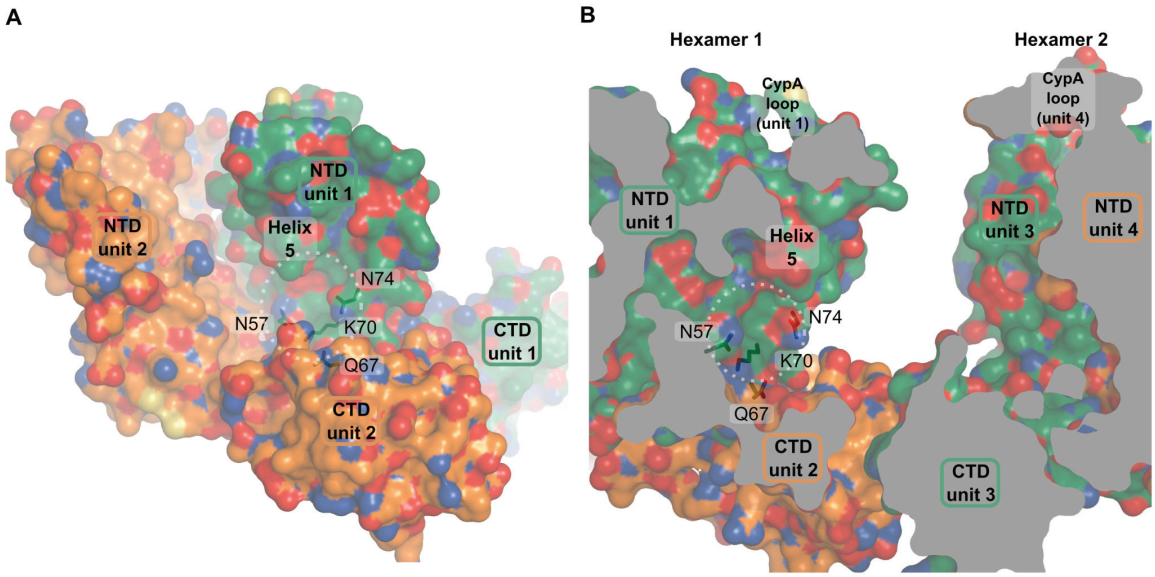

Figure 3-16. Location of NUP153$_C$ binding site within multimerized CA. (**A**) Model of the HIV-1 CA hexamer (pdb: 3j34) [43], with surface representations of two adjacent CA units shown. Side chains involved in NUP153$_C$ binding are shown as sticks and labeled, with the binding pocket highlighted by a dashed white circle. (**B**) Model of the HIV-1 inter-hexameric CA interface (pdb: 3j34). The two molecules in panel A were rotated 90º around the y-axis, -10º around the x-axis, and juxtaposed with two CA molecules from the adjacent hexamer. The z-plane was clipped to expose the NUP153$_C$ binding site within the interface.

$NUP153_C$ binding in vitro, suggesting that some CA disassembly may be needed for interaction with $NUP153_C$ within cells.

These hyperstable CA mutant viruses acutely depend on the cycling state of the cell. Comparison between cell cycle dependence and NUP153 reliance resulted in a strong negative correlation within the panel of CA mutant viruses (**Figure 3-14D**). This correlation was stronger than the relationship between $CPSF6_{358}$ sensitivity and cell cycle dependence (**Figure 3-14F**), suggesting a more direct association with NUP153 engagement. Consistent with this, CPSF6 binding mutant virus N74D was cell cycle independent, while N57A and N57D mutant viruses, both of which are also defective for NUP153 binding, were sensitive. While the direct cause of cell cycle dependence is not clear, we suspect that defective NUP153 binding is a key contributor, and that hyper-stable CA cores may phenotypically mimic this effect.

Competitors of NUP153-CA binding

The HIV-1 CA side-chains involved in $NUP153_C$ binding overlap those identified to interact with CPSF6. Accordingly, we found recombinant $NUP153_C$ able to compete with CPSF6 for binding to HIV-1 CA_N in vitro (**Figure 3-10D**). The overlapping binding sites suggest these proteins may take interdependent or even antagonistic roles during infection. While the role of endogenous CPSF6 protein in HIV-1 infection is unknown, the cytoplasmic $CPSF6_{358}$ truncation variant potently restricts HIV-1 [66,177,234,240,250]. Like Trim-$NUP153_C$, $CPSF6_{358}$ likely interacts with the viral core shortly after entry; both a Trim-fusion protein containing the CPSF6 binding domain [240], and the cytoplasmically expressed $CPSF6_{375}$ isoform [251], yield proteins capable

of preventing the completion of reverse transcription. Interestingly, $CPSF6_{358}$ does not inhibit reverse transcription, but instead blocks HIV-1 nuclear import. Additionally, $CPSF6_{358}$ appears to inhibit only a subset of CA mutant cores that it is able to bind [66] (**Figure 3-11B and 3-11C**). This may reflect an incomplete understanding of the mechanism of $CPSF6_{358}$ restriction, which could involve antagonism of the CA-NUP153 interaction (**Figure 3-11D**). While $CPSF6_{358}$-mediated stabilization of the CA core [66,250] may contribute to the nuclear import defect, it seems possible that direct competition for NUP153 binding may also be at play.

Small molecules that bind the helix 3/4 pocket in CA may also preclude NUP153 binding during HIV-1 infection. At least part of the PF74 antiviral mechanism occurs before nuclear entry, as it can inhibit HIV-1 reverse transcription [245]. Yet, its altered dose-response curve in NUP153 depleted cells suggests that it antagonizes CA engagement with NUP153 as well (**Figure 3-12**). Notably, recently identified pyrrolopyrazolone small molecules BI-1 and BI-2 bind the same pocket, yet inhibit HIV-1 nuclear import [252]. As both PF74 and the pyrrolopyrazolone compounds bind CA_N with similar affinity [234,252], we speculate that the contrasting phenotypes observed with these small molecules is due to their similar abilities to directly compete with host factors that bind the helix 3/4 pocket juxtaposed with their differential affects on CA core stability: PF74 destabilizes incoming capsids [235], whereas BI-1 and BI-2 can stabilize capsid structures in vitro [252]. TNPO3 depletion is proposed to mis-localize endogenous CPSF6 into the cytoplasm, recreating the phenotypes conferred by $CPSF6_{358}$ expression [66]. Resembling our observations with NUP153 knockdown cells, infection of TNPO3 depleted cells exhibited a similar profile of reduced sensitivity to PF74 [253].

Materials and Methods

Plasmid constructs

Infection assays utilized single-round viruses carrying either GFP or luciferase reporter genes. GFP-based constructs included HIV-1, EIAV, BIV, RSV, FIV, MLV, HIV-2 strain ROD, simian immunodeficiency viruses SIVmac, SIVagmSab, and SIVagmTan, all described previously [96,231]. HIV-1 CA mutations were generated through site-directed mutagenesis of the HIV-1_{NL4-3}-based pHP-dI-N/A packaging plasmid [217] (AIDS Research and Reference Reagent Program [ARRRP]), which were co-transfected with either pHI-vec2.GFP or pHI-Luc transfer vectors [231].

Human NUP153 (accession number NM_005124.3), or deletion mutants thereof, fused to N-terminal HA tags were expressed from the pIRES-dsRed Express HA-NUP153 expression vector [231]. Trim-fusion constructs, which were built within pLPCX-rhTrim5α-HA [121], were created by engineering a BamHI site at nucleotides corresponding to residues 301 and 302 of rhesus Trim5α, and ligating the digested vector with sequences encoding HA-$NUP153_C$, $NUP153_C$-HA, or $CPSF6_{358}$-HA [177]. Truncated Trim-HA was engineered by modifying the Trim-HA-$NUP153_C$ vector to encode two stop codons at the nucleotides corresponding to the first two residues of $NUP153_C$. All deletion and missense mutations within animal-cell expressed $NUP153_C$ were engineered by site-directed-mutagenesis of plasmids pLPCX-Trim-HA-$NUP153_C$ or pLPCX-HA-$NUP153_C$.

HIV-1_{NL4-3} CA carrying C-terminal his and FLAG tags was expressed from the pET11a-HIV1-CA-his-flag bacterial expression vector. The vector encoding tagged HIV-

1 CA NTD (pET11a-HIV1-CA_N-his-flag) was constructed by removing nucleotides corresponding to CA residues 147-231 from the full-length expression vector. Bacterial expression vectors for FIV CA were generated by amplifying DNA encoding full-length FIV CA (residues 1-223; pET11a-FIV-CA-his) or NTD only (residues 1-140; pET11a-FIV-CA_N-his) from pFP93 [254] with a primer encoding a C-terminal his-tag, and ligating with digested pET11a DNA. pET22b-based bacterial expression vectors encoding C-terminally his-tagged N-tropic MLV (pET22b-NMLV-CA-his) and EIAV (pET22b-EIAV-CA-his) were obtained from the laboratory of Dr. Joseph Sodroski, and CA NTDs were engineered from full-length his-tagged constructs by removing nucleotides corresponding to residues 133-263 of N-MLV, and residues 149-231 of EIAV, by site-directed mutagenesis.

A construct encoding an N-terminal GST protein fused to $NUP153_C$ (pGEX2T-GST-$NUP153_C$) was created by deleting sequences encoding residues 1-895 from a bacterial expression construct (pGEX2T-hNUP153) encoding the full-length human protein [180]. Plasmid pGEX2T-his-GST-pp-$NUP153_C$, which was utilized to obtain tag-free $NUP153_C$ protein, was derived from pGEX2T-GST-$NUP153_C$ by sequentially engineering a PreScission protease site between GST and $NUP153_C$ and then appending a his-tag N-terminal to GST. A stop codon was introduced at the nucleotides corresponding to residue 1350 to generate the Δ1350-1475 truncation mutant. The 7xFG/A mutant $NUP153_C$ was engineered for bacterial expression by swapping the WT sequence present in pGEX2T-his-GST-pp-$NUP153_C$ with a fragment encoding NUP153 residues 1178-1475 amplified from pLPCX-HA-$NUP153_C$-7xFG/A. All coding sequences were verified through DNA sequencing.

Cells

293T and HOS cells were cultured in DMEM (Invitrogen) supplemented with 10% FBS, 100 U/ml penicillin, and 0.1 mg/ml streptomycin. HOS cells stably transduced with MLV-derived LPCX transfer vectors were subsequently selected and maintained with 2 μg/ml puromycin. Approximately 25,000 HOS cells seeded per well of a 24-well plate were transfected the next day with a final concentration of 40 nM siNUP153#1 (GGACTTGTTAGATCTAGTT) or a mismatch control of siNUP153#1, referred to as siControl (GGTCTTATTGGAGCTAATT) (Dharmacon) [231], using RNAiMax (Invitrogen) according to the manufacturer's instructions. Dividing or cell cycle arrested cells were collected at the time of infection, fixed in 70% ethanol, and incubated for 30 min at room temperature in staining solution [0.1% Triton X-100, 0.2 mg/ml RNAse A (Invitrogen), and 20 μg/ml propidium iodide in phosphate-buffered saline (PBS)]. The cells were washed, and cellular DNA content was assessed with a FACSCanto flow cytometer (Becton, Dickenson and Company) equipped with FACSDIVA software.

Virus production

Viral vector particles were produced by transfecting 293T cells in 10-cm plates with 10 μg total of various ratios of the aforementioned virus production plasmids using $CaPO_4$. The cells were washed 16 h after transfection, and supernatants collected from 24 to 72 h thereafter were clarified at 300 x g, filtered through 0.45 μm filters (Nalgene), and either allotted and frozen or concentrated by ultracentrifugation using an SW32Ti rotor at 50,000 x g for 2 h at 4°C before freezing. Concentrations of HIV-1 and EIAV CA mutant

viral stocks were determined alongside concomitantly produced WT viruses using an exogenous ^{32}P-based assay for RT activity [222].

Infectivity assays

HOS cells (10,000 or 2,500) seeded onto 48-well or 96-well plates, respectively, were infected with various reporter viruses. Percentages of GFP-positive cells were determined 48 h post-infection (hpi) using a FACSCanto flow cytometer equipped with FACSDIVA software. GFP reporter experiments comparing retroviral genera were performed with virus inoculates adjusted to yield ~ 40% GFP-positive cells in control samples. HIV-1 or EIAV CA mutant viruses (2 x 10^5 RTcpm) were used to infect 96-well and 48-well plates of cells, respectively. HIV to EIAV infectivity ratios were calculated after initially normalizing to the average of MLV and FIV negative control viruses to account for slight differences in overall infectivities between stable cell lines. Cyclosporine (5 μM, Sigma) was introduced to cells at the time of infection. Cell cycle arrest experiments were performed by plating 2,500 control or 5,000 experimental cells treated with 5 μM Etoposide-phosphate (Calbiochem) the day before infection. Quantitative PCR for the accumulation of viral late reverse transcripts and 2-LTR-containing circles were performed as previously described [231]. The quantitation of early reverse transcripts was performed using primers AE989 and AE990 and Taqman probe AE995 [255].

Western blot analysis

Cells stably expressing Trim-fusion proteins were lysed in Buffer A [25 mM Tris-HCl pH 7.5, 200 mM NaCl, 1 mM DTT, 1 mM EDTA, Complete protease inhibitor (Roche)] and sonicated for 30 s total with a misonix sonicator. Protein concentration of the bulk lysate was determined by Bradford assay (Bio-rad), and 75 µg of each sample were electrophoresed through Tris-glycine polyacrylamide gels, and transferred onto polyvinylidene fluoride membranes. Transiently expressed HA-tagged proteins were either extracted with buffer H [10 mM Tris-HCl pH 8.0, 10 mM KCl, 1.5 mM $MgCl_2$] followed by repeated freeze-thaws, or Triton buffer [50 mM Triethanolamine, 250 mM NaCl, 0.5% Triton X-100], and pelleted in a microcentrifuge for 20 min at 21,000 x g at 4°C. Stably expressing cells were also fractionated by initial lysis in Buffer F1 [20 mM Tris-HCl pH 7.5, 10 mM NaCl, 1.5 mM $MgCl_2$, 0.25 % Triton X-100, and Complete Protease Inhibitor], followed by centrifugation at 6,000 x g. The supernatant was removed as Fraction 1, and the process was repeated, with the resulting supernatant combined with the previous fraction. The subsequent pellet was resuspended in Buffer F2 [Buffer F1 lacking Triton X-100, but with 0.5% sodium deoxycholate and 1% Tween-40], and pelleted at 21,000 x g for 15 min. The supernatant was removed as Fraction 2, and pellet was resuspended in 1x Turbo DNase buffer and treated with 40 U/ml Turbo DNase (Ambion) for 10 min at 37° C. Two parts fraction 1, one part fraction 2, and one part of the remaining fraction (Fraction 3) were each mixed with sample loading buffer and separated on Tris-glycine polyacrylamide gels. Exogenously expressed HA-tagged proteins were detected using a 1:4,000 dilution of HRP-conjugated 3F10 antibody (Roche) or 1:4,000 dilution of mouse 16b12 antibody (Covance) and developed with ECL prime (GE Healthcare) or Femto (Thermo Scientific) detection reagents. NUP153,

NUP62, and NUP358 were detected with a 1:4,000 dilution of mouse monoclonal antibody mab414 (Abcam). HRP-conjugated mouse anti-β-actin antibody or mouse anti-α-tubulin antibody (Abcam) were used at 1:10,000 dilutions to confirm equal lysate loading across samples. His-tagged HIV-1 CA was detected with 1:15,000 α-his HRP (Clontech). CA-NC protein was detected with 1:5,000 mouse anti-p24 antibody ab9071 (Abcam). Histone H3 was detected with 1:2,000 rabbit histone H3 antibody #9715 (Cell Signaling Technology). All mouse and rabbit primary antibodies were detected using 1:10,000 dilutions of anti-mouse or anti-rabbit HRP secondary antibodies (Dako).

Immunofluorescence confocal microscopy

Cells transduced with empty LPCX vector or stably expressing HA-epitope tagged rhTrim5α, $NUP153_C$, or fusion proteins thereof, were cultured on eight-well chamber slides. After 24 h, the cells were fixed with 4% paraformaldehyde for 10 min, washed, and permeabilized with PBS containing 0.5% Triton X-100. The permeabilized cells were blocked with PBS containing 10% FBS for 1 h, and stained with a 1:100 dilution of anti-HA antibody 16b12. After a 30 min wash with PBS, the cells were incubated for 1 h with a 1:1,000 dilution of an Alexa Fluor 555 conjugated goat anti-mouse IgG antibody (Invitrogen), as well as Hoechst 33342 (Invitrogen) diluted to a concentration of 0.2 μg/ml. After an additional 30 min wash with PBS, the samples were covered with mounting medium [150 mM NaCl, 25 mM Tris pH 8.0, 0.5% N-propyl gallate, and 90% glycerol]. The processed samples were analyzed on a Nikon Eclipse spinning disk confocal microscope.

NUP153 protein purification

GST-NUP153$_C$ was expressed in BL21-CodonPlus (DE3)-RILP *E. coli* (Agilent) grown in 2X YT media and induced at an optical density of 0.8 at 600 nm (OD_{600}) with 1 mM isopropyl β-D-1-thiogalactopyranoside (IPTG) for 1 h at 18°C. Cells were pelleted at 6,000 x g, and sonicated for 5 min in buffer A. The lysate was centrifuged for 30 min at 35,000 x g, and the pellet was resuspended in buffer B [1 M NaCl, 25 mM Tris-HCl pH 7.5, 1 mM DTT, 1 mM EDTA, Complete protease inhibitor] with a dounce homogenizer. The lysate was again spun at 35,000 x g, and the pellet was resuspended in Buffer C [2 M Urea, 200 mM NaCl, 25 mM Tris-HCl pH 7.5, 1 mM DTT, 1 mM EDTA, Complete protease inhibitor] with a dounce homogenizer. After a last centrifugation at 35,000 x g, the supernatant was collected and incubated with glutathione-sepharose beads (GE Healthcare) overnight at 4°C. The beads were washed with buffer D [200 mM NaCl, 25 mM Tris-HCl pH 8.0, 1 mM DTT, 1 mM EDTA, Complete protease inhibitor], and the protein was eluted with buffer D containing 20 mM glutathione. Eluted protein was dialyzed against buffer D to remove excess glutathione, spin concentrated by ultrafiltration through a 10,000 nominal molecular weight limit (NMWL) Amicon filter (Millipore), and flash frozen in liquid nitrogen for storage at -80ºC.

BL21-CodonPlus (DE3)-RILP *E. coli* transformed with pGEX2T-his-GST-pp-NUP153$_C$ was grown to an OD_{600} of 0.8, followed by induction with 1 mM IPTG for 1 h at 18°C. Cells were pelleted at 6,000 x g, and sonicated for 5 min in buffer A. The lysate was then centrifuged for 30 min at 35,000 x g, and the pellet was resuspended in buffer E [6 M Urea, 200 mM NaCl, 25 mM Tris-HCl pH 7.5, 1 mM DTT, 1 mM EDTA, Complete protease inhibitor] with a dounce homogenizer. The lysate was then

centrifuged at 40,000 x g for 1 h, and the resulting supernatant was incubated with Ni-NTA conjugated agarose beads (Qiagen) overnight. The beads were then initially washed with buffer E, and then progressive dilutions of buffer E into cleavage buffer [150 mM NaCl, 50 mM Tris-HCl pH 7, 1 mM DTT, 1 mM EDTA] (3:1, 1:1, 1:3), with a final wash in cleavage buffer only, each supplemented with 7.5 mM imidazole. The beads were incubated with 5 U of PreScission protease (GE Healthcare) for 48 h. The supernatant, which was cleared with 0.1 volumes of Ni-NTA beads and glutathione-sepharose beads each at 4°C to remove uncleaved protein and residual PreScission protease, was centrifuged at 21,000 x g for 15 min at 4°C. The resulting supernatants were quantitated following fractionation by sodium dodecyl sulfate-polyacrylamide gel electrophoresis (SDS-PAGE) and staining with SYPRO Ruby (Invitrogen) or Coomassie blue, as compared to a standard curve of bovine serum albumin (BSA), using ChemiDoc MP imager (Bio-Rad) with Image Lab software. Cleaved full length $NUP153_C$ was recovered at ~ 50% purity, with the predominant contaminants degradation products of the full-length protein, as inferred through comparison with western blots using mab414 antibody.

CA binding assays

Recombinant HIV-1 CA-NC was expressed in *E. coli*, purified, and assembled into CA-NC complexes as previously described [40]. Expression constructs encoding full-length HA-NUP153 or fragments thereof were transiently transfected into 293T cells using X-tremeGENE 9 DNA transfection reagent (Roche). Cells were collected after 48 h, lysed with successive freeze thaws in buffer H, and clarified by centrifugation at

21,000 x g at 4°C. CA-NC complexes were incubated with clarified lysates for 1 h at room temperature before ultracentrifugation for 30 min at 100,000 x g through a 50% sucrose cushion prepared in PBS. The resulting pellet was resuspended in 1x sample loading buffer, and fractionated by SDS-PAGE. Experiments with purified proteins were stained with Coomassie blue or SYPRO Ruby, while experiments using a lysate component were developed by western blot. Quantification was performed with a ChemiDoc MP imager using Image Lab software.

His-tagged HIV-1, MLV, EIAV, and FIV capsid proteins, either full length or NTD only, were expressed in BL21-CodonPlus (DE3)-RILP *E. coli*, grown to an OD_{600} of 0.6, and induced for 4 h with 1 mM IPTG. Bacteria pelleted by centrifugation were resuspended in Buffer A, sonicated, and centrifuged at 30,000 x g for 30 min. The supernatants were incubated overnight with Ni-NTA-sepharose beads, eluted with 20 mM Tris-HCl pH 8.0, 200 mM imidazole elution buffer, and dialyzed into Tris Buffer (20 mM Tris-HCl pH 8.0). Dialyzed protein was concentrated by ultrafiltration through a 10,000 NMWL filter, centrifuged at 21,000 x g, and the resulting soluble protein was quantitated by spectrophotometer.

Pull-down assays with full-length CA or CA_N proteins were performed by mixing 20 µl reactions with the following final concentrations: 0.02 µl packed volume Ni-NTA beads per µl (0.4 µl total), 20 µM CA, 25 mM Tris-HCl pH 8.0, and either 0.5 µM purified $NUP153_C$ with 0.1% NP-40 and 150 mM NaCl, or 100 µg 293T lysate overexpressing HA-tagged NUP153 with 0.25% Triton X-100 and 200 mM NaCl. Mixtures were left rocking at room temperature for 1 h after which the samples were washed twice in buffer M [25 mM Tris-HCl pH 8.0, 150 mM NaCl, and 0.1% NP-40],

allowing the beads to settle by gravity, and finally resuspended in 1x sample loading buffer. Saturation curves were achieved by mixing 3 µl packed volume Ni-NTA beads with 0.5 µM purified WT or mutant $NUP153_C$, 150 mM NaCl, 25 mM Tris-HCl pH 8.0, and 0.1% NP-40, with half-log increments of HIV-1 CA_N from 2 µM to 200 µM. Both bead-bound and supernatant fractions were separated by SDS-PAGE and stained with SYPRO Ruby, with the percent of $NUP153_C$ protein bound calculated at each concentration. The K_d of $NUP153_C$ binding was calculated by subtracting nonspecific binding to beads and fitting the resulting data-points with a one-site saturation binding nonlinear regression using Prism6 software (GraphPad).

CPSF6 competition experiments were performed through modification of the CA-NC protocol. Assembled CA-NC was diluted to a final concentration of 0.8 µM in the reaction mixture. WT or mutant $NUP153_C$ was added to a final concentration of 4 µM, along with 10 µg total 293T extract expressing C-terminally HA-tagged CPSF6, resulting in final concentrations of 170 mM NaCl, 75 mM Tris-HCl pH 8.0, and 0.025% Triton X-100. Mixtures (20 µl) were incubated at room temperature for 20 min, after which they were spun over a 30 µl 20% sucrose cushion in a microcentrifuge at 21,000 x g for 20 min at 4°C. The resulting pellet was resuspended in sample loading buffer and separated by SDS-PAGE. Western blotting with p24 antibody indicated ~ 35% of input CA-NC was recovered in the pellet. CA-NC co-sedimentation assays with WT or FG mutant $NUP153_C$ were performed similarly, but were instead centrifuged over a 25% sucrose cushion.

IN pull-down assay

His-tagged HIV-1 and FIV IN [96] and GST [256] were expressed and purified as previously described. Pull-down of soluble IN was performed as previously described for GST-LEDGF$_{326-530}$ [244], with 0.8 μM of his-tagged HIV-1 or FIV IN incubated with 0.47 μM GST-NUP153$_C$ or control GST pre-bound to glutathione-sepharose beads in PD buffer [150 mM NaCl, 25 mM Tris-HCl pH 7.4, 5 mM $MgCl_2$, 5 mM DTT, 0.1% NP-40]. BSA (5 μg) was included as an additional specificity control. The reaction was incubated for 2 h at 4°C, after which the beads were washed 4 times with PD buffer, and settled each time for 20 min in the absence of centrifugation. Recovered samples were resolved by SDS-PAGE, and stained with Coomassie blue and western blotted with anti-his antibody.

Statistical analysis

Dependencies between variables were assessed by Spearman rank correlation using Prism6 software. The significances of pair-wise differences were calculated by Student's t-test (two-tailed) using Prism6 software.

Chapter 4

General Discussion

Model of NUP153 FG engagement during lentiviral infection

Current data and the known biology of this protein suggest NUP153 is likely important for trafficking the HIV-1 PIC through the nuclear pore and into the nucleus [29,82,231] (**Figure 4-1**). The viral nucleoprotein complex is likely to initially dock to the NPC by engaging NUP358 [82,233]. While intact HIV-1 cores are too large to enter the central channel, CA cores in various stages of disassembly may enter far enough for remaining CA to be accessed by the FG domains present in $NUP153_C$.

CA binding with $NUP153_C$ may serve two distinct roles during infection. Firstly, NUP153 may be responsible for physically translocating the PIC by engaging CA molecules that may associate with it. The relatively short half-life of NUP153 at the NPC may contribute to the release of the PIC into the nucleoplasm [181]. Secondly, as even a partially disassembled core could remain too large to efficiently pass through the NPC channel, CA interaction with NUP153 may be required to fully uncoat the viral core at the NPC and prime the PIC for nuclear import. Indeed, CA cores have been shown to dock to NPCs for several hours before PIC nuclear translocation [80]. CA oligomers may interact with a limited subset of $NUP153_C$ FG motifs, while increased CA pocket accessibility from progressive core disassembly may expose monomeric CA to an expanded number of $NUP153_C$ FG repeats. While CA mutant viruses such as N74D may uncoat differently and circumvent this mechanism without penalty in various transformed cell lines, they apparently incur steep costs to infectivity in other cell types, such as primary macrophages [233,257].

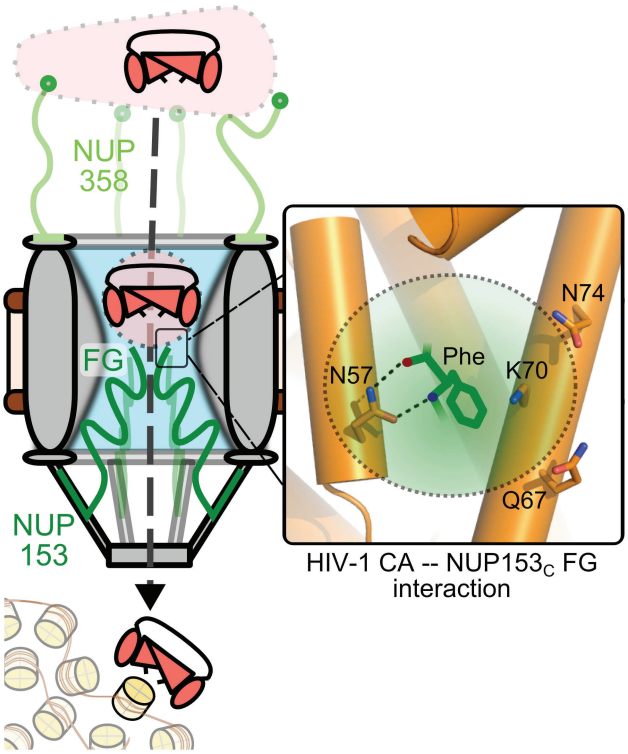

Figure 4-1. The NUP153-CA interaction during HIV-1 infection. Partially uncoated HIV-1 cores dock at the NPC through engaging NUP358 (light green). Once docked, NUP153 (dark green) FG motifs bind CA through phenylalanine insertion into the hydrophobic pocket of the NTD, forming hydrogen bonds with CA residue Asn57, as well as adjacent polar side-chains (enlarged to the right). CA engagement with NUP153 is required for HIV-1 nuclear import, either directly during PIC translocation, or for completion of a prerequisite uncoating step. Perturbation of NUP153 engagement may affect multiple steps, such as intranuclear trafficking and integration site selection [231,248,258].

Convergence in NUP153 use amongst viral families

Divergent viruses have adapted to use NUP153 for their own devices. Our results suggest EIAV, which presents different amino acid residues flanking the CA_N hydrophobic pocket, may have either retained, or convergently evolved NUP153 binding. Hepatitis B virus (HBV) has also been reported to bind NUP153 during its nuclear transport; though the HBV core is sufficiently small to traverse the NPC channel, NUP153 binding is believed to be important for HBV core conformational change and genome release within the nuclear basket [200]. This interaction may also require binding to NUP153 FG motifs, as both of the broadly defined regions mapped for HBV capsid binding overlapped parts of $NUP153_C$. The *S. pombe* homolog of NUP153, Nup124p, is important for Tf1 retrotransposition and binds the Tf1 Gag protein, though binding did not necessarily appear to map to Nup124p FG motifs [197,259]. Perhaps akin to effects caused by differential HIV-1 uncoating, the requirement for Nup124p appears to be related to the state of Tf1 Gag multimerization [199].

It remains to be determined whether FG motifs found on additional nucleoporins may bind HIV-1 and aid its infection. While the effects of NUP98 depletion on HIV-1 infection are relatively modest [175,177,248], this protein can also co-sediment with HIV-1 CA-NC tubes in vitro [248]. Similarly, the GLFG-motif enriched domain of *S. cerevisiae* NUP100, predicted to be orthologous to vertebrate NUP98, binds Ty3 Gag protein [260]. Alternatively, while CA binding with the CHD is proposed to determine the requirement for NUP358 [233], it remains to be seen whether its own FG domains may bind CA and contribute to its function during infection [261]. While numerous FG nucleoporins exist, it is likely that certain characteristics specific to NUP153, including

its length, flexibility, and its relatively high dissociation rate from the NPC, along with its spatial location around the nuclear rim of the NPC, makes this protein particularly important for lentiviral passage through the nuclear pore.

Interdependence of CA-determined host factors during infection

A number of phenotypic similarities suggest the roles of TNPO3, NUP153, NUP358, CPSF6, and CypA during HIV-1 infection are interrelated. CA mutant virus N57A is NUP153 and CPSF6 binding-defective but detectably binds the NUP358 CHD, yet does not require NUP358 expression for infection. Perhaps most starkly, the N74D CA mutant virus is insensitive to knockdown of TNPO3, NUP153, and NUP358, despite possessing a CA protein capable of binding all three proteins with similar affinities to WT CA (**Figure 3-8** and [233]). As the N74D mutation clearly counteracts CPSF6 binding [177,234], it seems plausible that CPSF6 engagement licenses HIV-1 to employ NUP358 and NUP153 during infection. CPSF6 is currently believed to be exclusively nuclear at steady state, suggesting that it may not exert its effects on HIV-1 until the virus engages the NPC. Curiously, siRNA depletion of CPSF6 does not affect HIV-1 infection [177].

CypA also appears to alter nuclear transport factor dependence during HIV-1 infection. The CypA and NUP358 CHD binding mutants G89V and P90A are comparably less sensitive to NUP153 depletion and $CPSF6_{358}$ restriction than WT virus [66,231,233]. Consistent with this, abrogation of CA binding with CypA, either through CypA depletion or competition with the small molecule cyclosporine, rescued viruses inhibited by NUP153 or NUP358 knockdown [231,233]. While cyclosporine treatment

can partially rescue WT HIV-1 infection in TNPO3 depleted cells [233,253], the lack of complete rescue may reflect its multiple potential roles in promoting HIV-1 infection. CypA binding to HIV-1 CA can alter its disassembly [191], suggesting that its effect on NUP153, NUP358, and TNPO3 may be indirect through modulating the rate and extent of CA core uncoating.

Effects of nuclear transport proteins on integration site selection

While HIV-1 appears to predominantly utilize NUP153, NUP358, and TNPO3 to affect its import into the nucleus, these factors can also affect post-nuclear trafficking as evidenced by differences in HIV-1 integration site distributions upon factor knockdown. Numerous different forces can influence integration site distribution. IN favors certain nucleotide patterns at the site of integration [262,263]. Integration also favors the distorted major grooves that occur when DNA is wrapped around the nucleosome core [264,265], as well as certain epigenetic modifications [265]. Lens epithelium-derived growth factor (LEDGF)/p75, which is a lentiviral IN-binding cofactor, in large part dictates integration along active transcriptional units [255,266,267]. Interestingly, TNPO3, NUP358, and NUP153 appear to contribute to an even broader level of integration site preference [68]: depletion of TNPO3, NUP358, and to a lesser extent, NUP153, reduced the extent of integration in gene dense regions of chromatin [233,248,258,268]. This pattern was consistent with the involvement of CA, as the HIV-1 chimeric virus encoding MLV CA, as well as CA missense mutants N57A and N74D, showed a similar shift in integration site distribution [233,258,268]. Notably, CypA binding was also found to affect integration site selection, as disruption of CypA binding

to CA by cyclosporine treatment resulted in an increase in the number of integration events in chromosomal regions enriched in transcriptional units [233].

It is possible that these proteins are directly involved in directing the PIC to distinct regions of chromatin; NUP153 has been shown to associate with large regions of active chromatin in drosophila [205], and TNPO3 may engage the HIV-1 intasome to effect integration [94]. On the other hand, NUP358 appears more important for integration targeting than NUP153, yet this protein does not appear to be found within the nucleus during interphase [150]. Furthermore, depletion of a number of other nuclear host proteins including IK, ANAPC2, WDHD1, SNW1, and PRPF38A similarly redirected integration away from gene dense chromosome regions [268]. It remains formally possible that the roles of some host factors in dictating integration to these regions may be indirect, instilled through alteration of global chromosomal environment as compared to specific affects on HIV-1 PIC trafficking. Still, ablation of gene dense region targeting by CA mutations such as N74D highlights a specific role for CA in post-nuclear PIC trafficking. The mechanism of nuclear import may be linked with integration site targeting by affecting the chromosomal environments first encountered by the PIC upon nuclear entry.

Model of CA and nuclear transport factors during HIV-1 nuclear entry

We propose the following working model to coalesce recently reported results from the rapidly evolving field of HIV-1 PIC nuclear transport (**Figure 4-2**). While the initial steps of uncoating likely occur shortly after entry [45], the final events of uncoating may occur at the NPC [80]. The partially uncoated PIC likely docks at the NPC

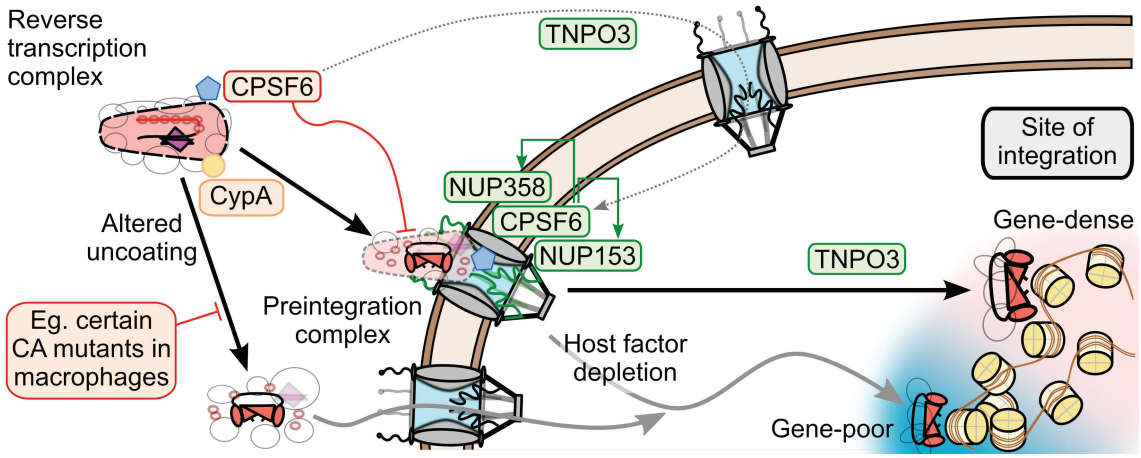

Figure 4-2. Model of the potential roles of the CA-dependent nuclear transport factors during HIV-1 infection. NUP358, NUP153, and CPSF6 at the nuclear pore likely act on PIC-associated CA to aid HIV-1 infection. TNPO3 is required to localize CPSF6 to the nucleus; premature cytoplasmic CPSF6 binding to CA can prevent nuclear import. TNPO3 may affect integration by interacting with IN within the nucleus. CypA modulates CA uncoating, altering dependencies on NUP358, NUP153, and TNPO3. Perturbation of this pathway by CA mutation or TNPO3, NUP153, or NUP358 knockdown results in altered integration site selection away from gene-dense regions of chromatin.

by engaging the NUP358 CHD with its remaining CA proteins [82,233]. Once docked, CPSF6 and NUP153 then engage the PIC. The combined actions of these proteins are necessary for PIC nuclear import. TNPO3 expression is required for proper nuclear localization of CPSF6; CPSF6 binding to CA cores too early during infection misregulates the upstream steps of uncoating [66,250] and NPC engagement, blocking infection at the step of nuclear import. TNPO3 may also have an additional intra-nuclear role permitting proper nuclear trafficking and integration, perhaps related to its interaction with IN. These concerted steps of uncoating and nuclear import appear to influence the downstream steps of nuclear trafficking and integration. It will be instructive to see if CPSF6 depletion similarly influences HIV-1 integration site distribution.

The precise mechanistic requirements for NUP358, NUP153, and CPSF6 for nuclear import remain unclear: these proteins may be critical for a prerequisite uncoating step prior to nuclear import, or they may be directly involved in the act of PIC nuclear translocation. As these three proteins have each been published to bind CA, the latter model presupposes that CA would need to be concomitantly imported into the nucleus with the PIC. This point remains highly controversial; CA has historically been noticeably absent from the nucleus, with only a couple recent reports observing potential PIC-associated CA signals within the nuclear fraction [81,82]. Notably, TNPO3, NUP358, and NUP153 are not absolutely required for HIV-1 infection of transformed cell lines: while the WT virus is highly dependent on these factors, certain CA mutant viruses such as N74D can bypass CPSF6 binding and infect cells depleted for NUP358, NUP153, or TNPO3 without a concomitant loss of infectivity. While the N74D CA

mutant virus was previously proposed to bypass these requirements by relying on an alternative set of NUPs (including NUP155 and NUP98) [177], it is not clear whether these proteins indeed fulfill critical roles for N74D mutant virus infection [248].

Alternatively, if the main function of these nuclear transport factors is to uncoat the PIC as a prelude for nuclear import, then alterations to viral uncoating may obviate the need for this mechanism during infection. CypA modulates HIV-1 core stability [191], and is accordingly capable of modulating the viral requirement on NUP153 and the other nuclear transport factors [231,233,253]. While a mechanism for active PIC nuclear transport would be required in all cell types, optimal CA uncoating may be particularly important in certain cell types, such as macrophages. Indeed, the N74D CA mutant virus exhibits a significant infectivity defect in monocyte-derived macrophages [233,257], where its reverse transcription is defective [257]. Because Asn74 is highly conserved among primate lentiviruses, HIV-1 may very well rely on these nuclear transport factors in vivo [177].

Curiously, while HIV-1 appears to rely upon NUP358, NUP153, TNPO3, and CPSF6 during infection, other lentiviruses only appear to share certain aspects of this mechanism. SIVmac does not bind NUP358, and accordingly does not rely on this protein for infection. Furthermore, EIAV utilizes NUP153 and TNPO3, though it does so in the apparent absence of CPSF6 binding. FIV likely utilizes an entirely different mechanism, as it does not seem to require any of these factors. Thus, although recent years have witnessed significant advances on the role of CA and particular nuclear transport proteins in HIV-1 PIC nuclear import, there is clearly much left to learn about

how HIV-1 and some of the other lentiviruses circumvent the nuclear envelope to reach their chromosomal targets of integration.

Concluding remarks

Despite two decades of research, the identities of the critical molecular interactions between viral and host proteins governing HIV-1 nuclear import has remained elusive. We find the CA proteins of HIV-1 and a subset of other lentiviruses directly bind NUP153, a major functional component of the nuclear pore complex. Determinents of CA interaction with the NUP153 FG motifs correlate well with the viral requirement for this nucleoporin during infection. Specific FG motifs within NUP153 were necessary for the interaction, highlighting a mechanism wherein certain lentiviral capsids have likely evolved to recognize the unique biophysical properties of the nuclear pore. Our findings demonstrate a key facet of lentiviral nuclear entry, and posit comparable mechanisms to occur across viruses and viral elements that require entry into the host nucleus.

References:

1. Barre-Sinoussi F, Chermann JC, Rey F, Nugeyre MT, Chamaret S, Gruest J, Dauguet C, Axler-Blin C, Vezinet-Brun F, Rouzioux C, Rozenbaum W, Montagnier L (1983) Isolation of a T-lymphotropic retrovirus from a patient at risk for acquired immune deficiency syndrome (AIDS). Science 220: 868-871.

2. Popovic M, Sarngadharan MG, Read E, Gallo RC (1984) Detection, isolation, and continuous production of cytopathic retroviruses (HTLV-III) from patients with AIDS and pre-AIDS. Science 224: 497-500.

3. Levy JA, Hoffman AD, Kramer SM, Landis JA, Shimabukuro JM, Oshiro LS (1984) Isolation of lymphocytopathic retroviruses from San Francisco patients with AIDS. Science 225: 840-842.

4. UNAIDS (2010) UNAIDS Report on the Global AIDS Epidemic.

5. McDougal JS, Kennedy MS, Sligh JM, Cort SP, Mawle A, Nicholson JK (1986) Binding of HTLV-III/LAV to T4+ T cells by a complex of the 110K viral protein and the T4 molecule. Science 231: 382-385.

6. Deng H, Liu R, Ellmeier W, Choe S, Unutmaz D, Burkhart M, Di Marzio P, Marmon S, Sutton RE, Hill CM, Davis CB, Peiper SC, Schall TJ, Littman DR, Landau NR (1996) Identification of a major co-receptor for primary isolates of HIV-1. Nature 381: 661-666.

7. Dragic T, Litwin V, Allaway GP, Martin SR, Huang Y, Nagashima KA, Cayanan C, Maddon PJ, Koup RA, Moore JP, Paxton WA (1996) HIV-1 entry into CD4+ cells is mediated by the chemokine receptor CC-CKR-5. Nature 381: 667-673.

8. Alkhatib G, Combadiere C, Broder CC, Feng Y, Kennedy PE, Murphy PM, Berger EA (1996) CC CKR5: a RANTES, MIP-1alpha, MIP-1beta receptor as a fusion cofactor for macrophage-tropic HIV-1. Science 272: 1955-1958.

9. Choe H, Farzan M, Sun Y, Sullivan N, Rollins B, Ponath PD, Wu L, Mackay CR, LaRosa G, Newman W, Gerard N, Gerard C, Sodroski J (1996) The beta-chemokine receptors CCR3 and CCR5 facilitate infection by primary HIV-1 isolates. Cell 85: 1135-1148.

10. Doranz BJ, Rucker J, Yi Y, Smyth RJ, Samson M, Peiper SC, Parmentier M, Collman RG, Doms RW (1996) A dual-tropic primary HIV-1 isolate that uses fusin and the beta-chemokine receptors CKR-5, CKR-3, and CKR-2b as fusion cofactors. Cell 85: 1149-1158.

11. Feng Y, Broder CC, Kennedy PE, Berger EA (1996) HIV-1 entry cofactor: functional cDNA cloning of a seven-transmembrane, G protein-coupled receptor. Science 272: 872-877.

12. Bleul CC, Farzan M, Choe H, Parolin C, Clark-Lewis I, Sodroski J, Springer TA (1996) The lymphocyte chemoattractant SDF-1 is a ligand for LESTR/fusin and blocks HIV-1 entry. Nature 382: 829-833.

13. Oberlin E, Amara A, Bachelerie F, Bessia C, Virelizier JL, Arenzana-Seisdedos F, Schwartz O, Heard JM, Clark-Lewis I, Legler DF, Loetscher M, Baggiolini M, Moser B (1996) The CXC chemokine SDF-1 is the ligand for LESTR/fusin and prevents infection by T-cell-line-adapted HIV-1. Nature 382: 833-835.

14. Hu WS, Hughes SH (2012) HIV-1 reverse transcription. Cold Spring Harbor perspectives in medicine 2.

15. Donehower LA, Varmus HE (1984) A mutant murine leukemia virus with a single missense codon in pol is defective in a function affecting integration. Proc Natl Acad Sci U S A 81: 6461-6465.

16. Panganiban AT, Temin HM (1984) The retrovirus pol gene encodes a product required for DNA integration: identification of a retrovirus int locus. Proc Natl Acad Sci U S A 81: 7885-7889.

17. Schwartzberg P, Colicelli J, Goff SP (1984) Construction and analysis of deletion mutations in the pol gene of Moloney murine leukemia virus: a new viral function required for productive infection. Cell 37: 1043-1052.

18. Feinberg MB, Jarrett RF, Aldovini A, Gallo RC, Wong-Staal F (1986) HTLV-III expression and production involve complex regulation at the levels of splicing and translation of viral RNA. Cell 46: 807-817.

19. Jouvenet N, Neil SJ, Bess C, Johnson MC, Virgen CA, Simon SM, Bieniasz PD (2006) Plasma membrane is the site of productive HIV-1 particle assembly. PLoS biology 4: e435.

20. von Schwedler UK, Stuchell M, Muller B, Ward DM, Chung HY, Morita E, Wang HE, Davis T, He GP, Cimbora DM, Scott A, Krausslich HG, Kaplan J, Morham SG, Sundquist WI (2003) The protein network of HIV budding. Cell 114: 701-713.

21. Roe T, Reynolds TC, Yu G, Brown PO (1993) Integration of murine leukemia virus DNA depends on mitosis. EMBO J 12: 2099-2108.

22. Gartner S, Markovits P, Markovitz DM, Kaplan MH, Gallo RC, Popovic M (1986) The role of mononuclear phagocytes in HTLV-III/LAV infection. Science 233: 215-219.

23. Rout MP, Aitchison JD, Suprapto A, Hjertaas K, Zhao Y, Chait BT (2000) The yeast nuclear pore complex: composition, architecture, and transport mechanism. J Cell Biol 148: 635-651.

24. Cronshaw JM, Krutchinsky AN, Zhang W, Chait BT, Matunis MJ (2002) Proteomic analysis of the mammalian nuclear pore complex. J Cell Biol 158: 915-927.

25. Reichelt R, Holzenburg A, Buhle EL, Jr., Jarnik M, Engel A, Aebi U (1990) Correlation between structure and mass distribution of the nuclear pore complex and of distinct pore complex components. J Cell Biol 110: 883-894.

26. Pante N, Kann M (2002) Nuclear pore complex is able to transport macromolecules with diameters of about 39 nm. Mol Biol Cell 13: 425-434.

27. Conti E, Muller CW, Stewart M (2006) Karyopherin flexibility in nucleocytoplasmic transport. Curr Opin Struct Biol 16: 237-244.

28. Brass AL, Dykxhoorn DM, Benita Y, Yan N, Engelman A, Xavier RJ, Lieberman J, Elledge SJ (2008) Identification of host proteins required for HIV infection through a functional genomic screen. Science 319: 921-926.

29. Konig R, Zhou Y, Elleder D, Diamond TL, Bonamy GM, Irelan JT, Chiang CY, Tu BP, De Jesus PD, Lilley CE, Seidel S, Opaluch AM, Caldwell JS, Weitzman MD, Kuhen KL, Bandyopadhyay S, Ideker T, Orth AP, Miraglia LJ, Bushman FD, Young JA, Chanda SK (2008) Global analysis of host-pathogen interactions that regulate early-stage HIV-1 replication. Cell 135: 49-60.

30. Zhou H, Xu M, Huang Q, Gates AT, Zhang XD, Castle JC, Stec E, Ferrer M, Strulovici B, Hazuda DJ, Espeseth AS (2008) Genome-scale RNAi screen for host factors required for HIV replication. Cell Host Microbe 4: 495-504.

31. Yeung ML, Houzet L, Yedavalli VS, Jeang KT (2009) A genome-wide short hairpin RNA screening of jurkat T-cells for human proteins contributing to productive HIV-1 replication. J Biol Chem 284: 19463-19473.

32. Terry LJ, Wente SR (2009) Flexible gates: dynamic topologies and functions for FG nucleoporins in nucleocytoplasmic transport. Eukaryotic cell 8: 1814-1827.

33. Nemergut ME, Mizzen CA, Stukenberg T, Allis CD, Macara IG (2001) Chromatin docking and exchange activity enhancement of RCC1 by histones H2A and H2B. Science 292: 1540-1543.

34. Saitoh H, Pu R, Cavenagh M, Dasso M (1997) RanBP2 associates with Ubc9p and a modified form of RanGAP1. Proc Natl Acad Sci U S A 94: 3736-3741.

35. Radu A, Moore MS, Blobel G (1995) The peptide repeat domain of nucleoporin Nup98 functions as a docking site in transport across the nuclear pore complex. Cell 81: 215-222.

36. Bischoff FR, Klebe C, Kretschmer J, Wittinghofer A, Ponstingl H (1994) RanGAP1 induces GTPase activity of nuclear Ras-related Ran. Proc Natl Acad Sci U S A 91: 2587-2591.

37. Kehlenbach RH, Dickmanns A, Kehlenbach A, Guan T, Gerace L (1999) A role for RanBP1 in the release of CRM1 from the nuclear pore complex in a terminal step of nuclear export. J Cell Biol 145: 645-657.

38. Koyama M, Matsuura Y (2010) An allosteric mechanism to displace nuclear export cargo from CRM1 and RanGTP by RanBP1. EMBO J 29: 2002-2013.

39. Berthet-Colominas C, Monaco S, Novelli A, Sibai G, Mallet F, Cusack S (1999) Head-to-tail dimers and interdomain flexibility revealed by the crystal structure of HIV-1 capsid protein (p24) complexed with a monoclonal antibody Fab. EMBO J 18: 1124-1136.

40. Ganser BK, Li S, Klishko VY, Finch JT, Sundquist WI (1999) Assembly and analysis of conical models for the HIV-1 core. Science 283: 80-83.

41. Pornillos O, Ganser-Pornillos BK, Kelly BN, Hua Y, Whitby FG, Stout CD, Sundquist WI, Hill CP, Yeager M (2009) X-ray structures of the hexameric building block of the HIV capsid. Cell 137: 1282-1292.

42. Pornillos O, Ganser-Pornillos BK, Yeager M (2011) Atomic-level modelling of the HIV capsid. Nature 469: 424-427.

43. Zhao G, Perilla JR, Yufenyuy EL, Meng X, Chen B, Ning J, Ahn J, Gronenborn AM, Schulten K, Aiken C, Zhang P (2013) Mature HIV-1 capsid structure by cryo-electron microscopy and all-atom molecular dynamics. Nature 497: 643-646.

44. Fassati A, Goff SP (2001) Characterization of intracellular reverse transcription complexes of human immunodeficiency virus type 1. J Virol 75: 3626-3635.

45. Hulme AE, Perez O, Hope TJ (2011) Complementary assays reveal a relationship between HIV-1 uncoating and reverse transcription. Proc Natl Acad Sci U S A 108: 9975-9980.

46. Yu Z, Dobro MJ, Woodward CL, Levandovsky A, Danielson CM, Sandrin V, Shi J, Aiken C, Zandi R, Hope TJ, Jensen GJ (2013) Unclosed HIV-1 capsids suggest a curled sheet model of assembly. J Mol Biol 425: 112-123.

47. Pereira CF, Rossy J, Owen DM, Mak J, Gaus K (2012) HIV taken by STORM: super-resolution fluorescence microscopy of a viral infection. Virol J 9: 84.

48. Lelek M, Di Nunzio F, Henriques R, Charneau P, Arhel N, Zimmer C (2012) Superresolution imaging of HIV in infected cells with FlAsH-PALM. Proc Natl Acad Sci U S A 109: 8564-8569.

49. McDonald D, Vodicka MA, Lucero G, Svitkina TM, Borisy GG, Emerman M, Hope TJ (2002) Visualization of the intracellular behavior of HIV in living cells. J Cell Biol 159: 441-452.

50. Zack JA, Arrigo SJ, Weitsman SR, Go AS, Haislip A, Chen IS (1990) HIV-1 entry into quiescent primary lymphocytes: molecular analysis reveals a labile, latent viral structure. Cell 61: 213-222.

51. Butler SL, Hansen MS, Bushman FD (2001) A quantitative assay for HIV DNA integration in vivo. Nature medicine 7: 631-634.

52. Sherman PA, Fyfe JA (1990) Human immunodeficiency virus integration protein expressed in Escherichia coli possesses selective DNA cleaving activity. Proc Natl Acad Sci U S A 87: 5119-5123.

53. Bushman FD, Craigie R (1991) Activities of human immunodeficiency virus (HIV) integration protein in vitro: specific cleavage and integration of HIV DNA. Proc Natl Acad Sci U S A 88: 1339-1343.

54. Engelman A, Mizuuchi K, Craigie R (1991) HIV-1 DNA integration: mechanism of viral DNA cleavage and DNA strand transfer. Cell 67: 1211-1221.

55. Thomas JA, Ott DE, Gorelick RJ (2007) Efficiency of human immunodeficiency virus type 1 postentry infection processes: evidence against disproportionate numbers of defective virions. J Virol 81: 4367-4370.

56. Iordanskiy S, Berro R, Altieri M, Kashanchi F, Bukrinsky M (2006) Intracytoplasmic maturation of the human immunodeficiency virus type 1 reverse transcription complexes determines their capacity to integrate into chromatin. Retrovirology 3: 4.

57. Yamashita M, Perez O, Hope TJ, Emerman M (2007) Evidence for direct involvement of the capsid protein in HIV infection of nondividing cells. PLoS Pathog 3: 1502-1510.

58. Thomas JA, Gagliardi TD, Alvord WG, Lubomirski M, Bosche WJ, Gorelick RJ (2006) Human immunodeficiency virus type 1 nucleocapsid zinc-finger mutations cause defects in reverse transcription and integration. Virology 353: 41-51.

59. Kilzer JM, Stracker T, Beitzel B, Meek K, Weitzman M, Bushman FD (2003) Roles of host cell factors in circularization of retroviral dna. Virology 314: 460-467.

60. Miller MD, Wang B, Bushman FD (1995) Human immunodeficiency virus type 1 preintegration complexes containing discontinuous plus strands are competent to integrate in vitro. J Virol 69: 3938-3944.

61. Munir S, Thierry S, Subra F, Deprez E, Delelis O (2013) Quantitative analysis of the time-course of viral DNA forms during the HIV-1 life cycle. Retrovirology 10: 87.

62. Li L, Olvera JM, Yoder KE, Mitchell RS, Butler SL, Lieber M, Martin SL, Bushman FD (2001) Role of the non-homologous DNA end joining pathway in the early steps of retroviral infection. EMBO J 20: 3272-3281.

63. Li Y, Kappes JC, Conway JA, Price RW, Shaw GM, Hahn BH (1991) Molecular characterization of human immunodeficiency virus type 1 cloned directly from uncultured human brain tissue: identification of replication-competent and -defective viral genomes. J Virol 65: 3973-3985.

64. Farnet CM, Haseltine WA (1991) Circularization of human immunodeficiency virus type 1 DNA in vitro. J Virol 65: 6942-6952.

65. Yan N, Cherepanov P, Daigle JE, Engelman A, Lieberman J (2009) The SET complex acts as a barrier to autointegration of HIV-1. PLoS Pathog 5: e1000327.

66. De Iaco A, Santoni F, Vannier A, Guipponi M, Antonarakis S, Luban J (2013) TNPO3 protects HIV-1 replication from CPSF6-mediated capsid stabilization in the host cell cytoplasm. Retrovirology 10: 20.

67. Brussel A, Sonigo P (2003) Analysis of early human immunodeficiency virus type 1 DNA synthesis by use of a new sensitive assay for quantifying integrated provirus. J Virol 77: 10119-10124.

68. Schroder AR, Shinn P, Chen H, Berry C, Ecker JR, Bushman F (2002) HIV-1 integration in the human genome favors active genes and local hotspots. Cell 110: 521-529.

69. Mitchell RS, Beitzel BF, Schroder AR, Shinn P, Chen H, Berry CC, Ecker JR, Bushman FD (2004) Retroviral DNA integration: ASLV, HIV, and MLV show distinct target site preferences. PLoS biology 2: E234.

70. Christ F, Thys W, De Rijck J, Gijsbers R, Albanese A, Arosio D, Emiliani S, Rain JC, Benarous R, Cereseto A, Debyser Z (2008) Transportin-SR2 imports HIV into the nucleus. Curr Biol 18: 1192-1202.

71. Di Primio C, Quercioli V, Allouch A, Gijsbers R, Christ F, Debyser Z, Arosio D, Cereseto A (2013) Single-cell imaging of HIV-1 provirus (SCIP). Proc Natl Acad Sci U S A 110: 5636-5641.

72. Li M, Mizuuchi M, Burke TR, Jr., Craigie R (2006) Retroviral DNA integration: reaction pathway and critical intermediates. EMBO J 25: 1295-1304.

73. Hare S, Gupta SS, Valkov E, Engelman A, Cherepanov P (2010) Retroviral intasome assembly and inhibition of DNA strand transfer. Nature 464: 232-236.

74. Bukrinsky MI, Sharova N, McDonald TL, Pushkarskaya T, Tarpley WG, Stevenson M (1993) Association of integrase, matrix, and reverse transcriptase antigens of human immunodeficiency virus type 1 with viral nucleic acids following acute infection. Proc Natl Acad Sci U S A 90: 6125-6129.

75. Gallay P, Swingler S, Song J, Bushman F, Trono D (1995) HIV nuclear import is governed by the phosphotyrosine-mediated binding of matrix to the core domain of integrase. Cell 83: 569-576.

76. Gallay P, Hope T, Chin D, Trono D (1997) HIV-1 infection of nondividing cells through the recognition of integrase by the importin/karyopherin pathway. Proc Natl Acad Sci U S A 94: 9825-9830.

77. Heinzinger NK, Bukinsky MI, Haggerty SA, Ragland AM, Kewalramani V, Lee MA, Gendelman HE, Ratner L, Stevenson M, Emerman M (1994) The Vpr protein of human immunodeficiency virus type 1 influences nuclear localization of viral nucleic acids in nondividing host cells. Proc Natl Acad Sci U S A 91: 7311-7315.

78. Karageorgos L, Li P, Burrell C (1993) Characterization of HIV replication complexes early after cell-to-cell infection. AIDS Res Hum Retrov 9: 817-823.

79. Miller MD, Farnet CM, Bushman FD (1997) Human immunodeficiency virus type 1 preintegration complexes: studies of organization and composition. J Virol 71: 5382-5390.

80. Arhel NJ, Souquere-Besse S, Munier S, Souque P, Guadagnini S, Rutherford S, Prevost MC, Allen TD, Charneau P (2007) HIV-1 DNA Flap formation promotes uncoating of the pre-integration complex at the nuclear pore. EMBO J 26: 3025-3037.

81. Zhou L, Sokolskaja E, Jolly C, James W, Cowley SA, Fassati A (2011) Transportin 3 promotes a nuclear maturation step required for efficient HIV-1 integration. PLoS Pathog 7: e1002194.

82. Di Nunzio F, Danckaert A, Fricke T, Perez P, Fernandez J, Perret E, Roux P, Shorte S, Charneau P, Diaz-Griffero F, Arhel NJ (2012) Human nucleoporins promote HIV-1 docking at the nuclear pore, nuclear import and integration. PLoS One 7: e46037.

83. Bukrinsky MI, Haggerty S, Dempsey MP, Sharova N, Adzhubel A, Spitz L, Lewis P, Goldfarb D, Emerman M, Stevenson M (1993) A nuclear localization signal within HIV-1 matrix protein that governs infection of non-dividing cells. Nature 365: 666-669.

84. Haffar OK, Popov S, Dubrovsky L, Agostini I, Tang H, Pushkarsky T, Nadler SG, Bukrinsky M (2000) Two nuclear localization signals in the HIV-1 matrix protein regulate nuclear import of the HIV-1 pre-integration complex. J Mol Biol 299: 359-368.

85. Bouyac-Bertoia M, Dvorin JD, Fouchier RA, Jenkins Y, Meyer BE, Wu LI, Emerman M, Malim MH (2001) HIV-1 infection requires a functional integrase NLS. Mol Cell 7: 1025-1035.

86. Fouchier RA, Meyer BE, Simon JH, Fischer U, Albright AV, Gonzalez-Scarano F, Malim MH (1998) Interaction of the human immunodeficiency virus type 1 Vpr protein with the nuclear pore complex. J Virol 72: 6004-6013.

87. Vodicka MA, Koepp DM, Silver PA, Emerman M (1998) HIV-1 Vpr interacts with the nuclear transport pathway to promote macrophage infection. Gene Dev 12: 175-185.

88. Popov S, Rexach M, Ratner L, Blobel G, Bukrinsky M (1998) Viral protein R regulates docking of the HIV-1 preintegration complex to the nuclear pore complex. J Biol Chem 273: 13347-13352.

89. Popov S, Rexach M, Zybarth G, Reiling N, Lee MA, Ratner L, Lane CM, Moore MS, Blobel G, Bukrinsky M (1998) Viral protein R regulates nuclear import of the HIV-1 pre-integration complex. EMBO J 17: 909-917.

90. Jenkins Y, McEntee M, Weis K, Greene WC (1998) Characterization of HIV-1 vpr nuclear import: analysis of signals and pathways. J Cell Biol 143: 875-885.

91. Ao Z, Danappa Jayappa K, Wang B, Zheng Y, Kung S, Rassart E, Depping R, Kohler M, Cohen EA, Yao X (2010) Importin alpha3 interacts with HIV-1 integrase and contributes to HIV-1 nuclear import and replication. J Virol 84: 8650-8663.

92. Fassati A, Gorlich D, Harrison I, Zaytseva L, Mingot JM (2003) Nuclear import of HIV-1 intracellular reverse transcription complexes is mediated by importin 7. EMBO J 22: 3675-3685.

93. Ao Z, Huang G, Yao H, Xu Z, Labine M, Cochrane AW, Yao X (2007) Interaction of human immunodeficiency virus type 1 integrase with cellular nuclear import receptor importin 7 and its impact on viral replication. J Biol Chem 282: 13456-13467.

94. Larue R, Gupta K, Wuensch C, Shkriabai N, Kessl JJ, Danhart E, Feng L, Taltynov O, Christ F, Van Duyne GD, Debyser Z, Foster MP, Kvaratskhelia M (2012) Interaction of the HIV-1 intasome with transportin 3 protein (TNPO3 or TRN-SR2). J Biol Chem 287: 34044-34058.

95. Zielske SP, Stevenson M (2005) Importin 7 may be dispensable for human immunodeficiency virus type 1 and simian immunodeficiency virus infection of primary macrophages. J Virol 79: 11541-11546.

96. Krishnan L, Matreyek KA, Oztop I, Lee K, Tipper CH, Li X, Dar MJ, Kewalramani VN, Engelman A (2010) The requirement for cellular transportin 3 (TNPO3 or TRN-SR2) during infection maps to human immunodeficiency virus type 1 capsid and not integrase. J Virol 84: 397-406.

97. Cribier A, Segeral E, Delelis O, Parissi V, Simon A, Ruff M, Benarous R, Emiliani S (2011) Mutations affecting interaction of integrase with TNPO3 do not prevent HIV-1 cDNA nuclear import. Retrovirology 8: 104.

98. Woodward CL, Prakobwanakit S, Mosessian S, Chow SA (2009) Integrase interacts with nucleoporin NUP153 to mediate the nuclear import of human immunodeficiency virus type 1. J Virol 83: 6522-6533.

99. Le Rouzic E, Mousnier A, Rustum C, Stutz F, Hallberg E, Dargemont C, Benichou S (2002) Docking of HIV-1 Vpr to the nuclear envelope is mediated by the interaction with the nucleoporin hCG1. J Biol Chem 277: 45091-45098.

100. Zennou V, Petit C, Guetard D, Nerhbass U, Montagnier L, Charneau P (2000) HIV-1 genome nuclear import is mediated by a central DNA flap. Cell 101: 173-185.

101. Follenzi A, Ailles LE, Bakovic S, Geuna M, Naldini L (2000) Gene transfer by lentiviral vectors is limited by nuclear translocation and rescued by HIV-1 pol sequences. Nature genetics 25: 217-222.

102. Limon A, Nakajima N, Lu R, Ghory HZ, Engelman A (2002) Wild-type levels of nuclear localization and human immunodeficiency virus type 1 replication in the absence of the central DNA flap. J Virol 76: 12078-12086.

103. Dvorin JD, Bell P, Maul GG, Yamashita M, Emerman M, Malim MH (2002) Reassessment of the roles of integrase and the central DNA flap in human immunodeficiency virus type 1 nuclear import. J Virol 76: 12087-12096.

104. Marsden MD, Zack JA (2007) Human immunodeficiency virus bearing a disrupted central DNA flap is pathogenic in vivo. J Virol 81: 6146-6150.

105. De Rijck J, Debyser Z (2006) The central DNA flap of the human immunodeficiency virus type 1 is important for viral replication. Biochemical and biophysical research communications 349: 1100-1110.

106. Riviere L, Darlix JL, Cimarelli A (2010) Analysis of the viral elements required in the nuclear import of HIV-1 DNA. J Virol 84: 729-739.

107. Ao Z, Yao X, Cohen EA (2004) Assessment of the role of the central DNA flap in human immunodeficiency virus type 1 replication by using a single-cycle replication system. J Virol 78: 3170-3177.

108. Skasko M, Kim B (2008) Compensatory role of human immunodeficiency virus central polypurine tract sequence in kinetically disrupted reverse transcription. J Virol 82: 7716-7720.

109. Hu C, Saenz DT, Fadel HJ, Walker W, Peretz M, Poeschla EM (2010) The HIV-1 central polypurine tract functions as a second line of defense against APOBEC3G/F. J Virol 84: 11981-11993.

110. Wurtzer S, Goubard A, Mammano F, Saragosti S, Lecossier D, Hance AJ, Clavel F (2006) Functional central polypurine tract provides downstream protection of the human immunodeficiency virus type 1 genome from editing by APOBEC3G and APOBEC3B. J Virol 80: 3679-3683.

111. Suspene R, Rusniok C, Vartanian JP, Wain-Hobson S (2006) Twin gradients in APOBEC3 edited HIV-1 DNA reflect the dynamics of lentiviral replication. Nucleic Acids Res 34: 4677-4684.

112. Limon A, Devroe E, Lu R, Ghory HZ, Silver PA, Engelman A (2002) Nuclear localization of human immunodeficiency virus type 1 preintegration complexes (PICs): V165A and R166A are pleiotropic integrase mutants primarily defective for integration, not PIC nuclear import. J Virol 76: 10598-10607.

113. Fouchier RA, Meyer BE, Simon JH, Fischer U, Malim MH (1997) HIV-1 infection of non-dividing cells: evidence that the amino-terminal basic region of the viral matrix protein is important for Gag processing but not for post-entry nuclear import. EMBO J 16: 4531-4539.

114. Freed EO, Englund G, Martin MA (1995) Role of the basic domain of human immunodeficiency virus type 1 matrix in macrophage infection. J Virol 69: 3949-3954.

115. Katz RA, Greger JG, Boimel P, Skalka AM (2003) Human immunodeficiency virus type 1 DNA nuclear import and integration are mitosis independent in cycling cells. J Virol 77: 13412-13417.

116. Yamashita M, Emerman M (2004) Capsid is a dominant determinant of retrovirus infectivity in nondividing cells. J Virol 78: 5670-5678.

117. Qi M, Yang R, Aiken C (2008) Cyclophilin A-dependent restriction of human immunodeficiency virus type 1 capsid mutants for infection of nondividing cells. J Virol 82: 12001-12008.

118. Ylinen LM, Schaller T, Price A, Fletcher AJ, Noursadeghi M, James LC, Towers GJ (2009) Cyclophilin A levels dictate infection efficiency of human

immunodeficiency virus type 1 capsid escape mutants A92E and G94D. J Virol 83: 2044-2047.

119. Dismuke DJ, Aiken C (2006) Evidence for a functional link between uncoating of the human immunodeficiency virus type 1 core and nuclear import of the viral preintegration complex. J Virol 80: 3712-3720.

120. Forshey BM, von Schwedler U, Sundquist WI, Aiken C (2002) Formation of a human immunodeficiency virus type 1 core of optimal stability is crucial for viral replication. J Virol 76: 5667-5677.

121. Stremlau M, Owens CM, Perron MJ, Kiessling M, Autissier P, Sodroski J (2004) The cytoplasmic body component TRIM5alpha restricts HIV-1 infection in Old World monkeys. Nature 427: 848-853.

122. Stremlau M, Perron M, Lee M, Li Y, Song B, Javanbakht H, Diaz-Griffero F, Anderson DJ, Sundquist WI, Sodroski J (2006) Specific recognition and accelerated uncoating of retroviral capsids by the TRIM5alpha restriction factor. Proc Natl Acad Sci U S A 103: 5514-5519.

123. Wu X, Anderson JL, Campbell EM, Joseph AM, Hope TJ (2006) Proteasome inhibitors uncouple rhesus TRIM5alpha restriction of HIV-1 reverse transcription and infection. Proc Natl Acad Sci U S A 103: 7465-7470.

124. Kutluay SB, Perez-Caballero D, Bieniasz PD (2013) Fates of retroviral core components during unrestricted and TRIM5-restricted infection. PLoS Pathog 9: e1003214.

125. Anderson JL, Campbell EM, Wu X, Vandegraaff N, Engelman A, Hope TJ (2006) Proteasome inhibition reveals that a functional preintegration complex intermediate can be generated during restriction by diverse TRIM5 proteins. J Virol 80: 9754-9760.

126. Danielson CM, Cianci GC, Hope TJ (2012) Recruitment and dynamics of proteasome association with rhTRIM5alpha cytoplasmic complexes during HIV-1 infection. Traffic 13: 1206-1217.

127. Yap MW, Dodding MP, Stoye JP (2006) Trim-cyclophilin A fusion proteins can restrict human immunodeficiency virus type 1 infection at two distinct phases in the viral life cycle. J Virol 80: 4061-4067.

128. Fassati A, Goff SP (1999) Characterization of intracellular reverse transcription complexes of Moloney murine leukemia virus. J Virol 73: 8919-8925.

129. Yuan B, Li X, Goff SP (1999) Mutations altering the moloney murine leukemia virus p12 Gag protein affect virion production and early events of the virus life cycle. EMBO J 18: 4700-4710.

130. Prizan-Ravid A, Elis E, Laham-Karam N, Selig S, Ehrlich M, Bacharach E (2010) The Gag cleavage product, p12, is a functional constituent of the murine leukemia virus pre-integration complex. PLoS Pathog 6: e1001183.

131. Schneider WM, Brzezinski JD, Aiyer S, Malani N, Gyuricza M, Bushman FD, Roth MJ (2013) Viral DNA tethering domains complement replication-defective mutations in the p12 protein of MuLV Gag. Proc Natl Acad Sci U S A 110: 9487-9492.

132. Elis E, Ehrlich M, Prizan-Ravid A, Laham-Karam N, Bacharach E (2012) p12 tethers the murine leukemia virus pre-integration complex to mitotic chromosomes. PLoS Pathog 8: e1003103.

133. Best S, Le Tissier P, Towers G, Stoye JP (1996) Positional cloning of the mouse retrovirus restriction gene Fv1. Nature 382: 826-829.

134. Hopkins N, Schindler J, Hynes R (1977) Six-NB-tropic murine leukemia viruses derived from a B-tropic virus of BALB/c have altered p30. J Virol 21: 309-318.

135. Rommelaere J, Donis-Keller H, Hopkins N (1979) RNA sequencing provides evidence for allelism of determinants of the N-, B- or NB-tropism of murine leukemia viruses. Cell 16: 43-50.

136. Hilditch L, Matadeen R, Goldstone DC, Rosenthal PB, Taylor IA, Stoye JP (2011) Ordered assembly of murine leukemia virus capsid protein on lipid nanotubes directs specific binding by the restriction factor, Fv1. Proc Natl Acad Sci U S A 108: 5771-5776.

137. Pryciak PM, Varmus HE (1992) Fv-1 restriction and its effects on murine leukemia virus integration in vivo and in vitro. J Virol 66: 5959-5966.

138. Yang WK, Kiggans JO, Yang DM, Ou CY, Tennant RW, Brown A, Bassin RH (1980) Synthesis and circularization of N- and B-tropic retroviral DNA Fv-1 permissive and restrictive mouse cells. Proc Natl Acad Sci U S A 77: 2994-2998.

139. Jolicoeur P, Rassart E (1980) Effect of Fv-1 gene product on synthesis of linear and supercoiled viral DNA in cells infected with murine leukemia virus. J Virol 33: 183-195.

140. Schaller T, Ylinen LM, Webb BL, Singh S, Towers GJ (2007) Fusion of cyclophilin A to Fv1 enables cyclosporine-sensitive restriction of human and feline immunodeficiency viruses. J Virol 81: 10055-10063.

141. Bushman FD, Malani N, Fernandes J, D'Orso I, Cagney G, Diamond TL, Zhou H, Hazuda DJ, Espeseth AS, Konig R, Bandyopadhyay S, Ideker T, Goff SP, Krogan NJ, Frankel AD, Young JA, Chanda SK (2009) Host cell factors in HIV replication: meta-analysis of genome-wide studies. PLoS Pathog 5: e1000437.

142. Lai MC, Lin RI, Tarn WY (2001) Transportin-SR2 mediates nuclear import of phosphorylated SR proteins. Proc Natl Acad Sci U S A 98: 10154-10159.

143. Yokoyama N, Hayashi N, Seki T, Pante N, Ohba T, Nishii K, Kuma K, Hayashida T, Miyata T, Aebi U, et al. (1995) A giant nucleopore protein that binds Ran/TC4. Nature 376: 184-188.

144. Wu J, Matunis MJ, Kraemer D, Blobel G, Coutavas E (1995) Nup358, a cytoplasmically exposed nucleoporin with peptide repeats, Ran-GTP binding sites, zinc fingers, a cyclophilin A homologous domain, and a leucine-rich region. J Biol Chem 270: 14209-14213.

145. Wilken N, Senecal JL, Scheer U, Dabauvalle MC (1995) Localization of the Ran-GTP binding protein RanBP2 at the cytoplasmic side of the nuclear pore complex. European journal of cell biology 68: 211-219.

146. Melchior F, Guan T, Yokoyama N, Nishimoto T, Gerace L (1995) GTP hydrolysis by Ran occurs at the nuclear pore complex in an early step of protein import. J Cell Biol 131: 571-581.

147. Prunuske AJ, Liu J, Elgort S, Joseph J, Dasso M, Ullman KS (2006) Nuclear envelope breakdown is coordinated by both Nup358/RanBP2 and Nup153, two nucleoporins with zinc finger modules. Mol Biol Cell 17: 760-769.

148. Pichler A, Gast A, Seeler JS, Dejean A, Melchior F (2002) The nucleoporin RanBP2 has SUMO1 E3 ligase activity. Cell 108: 109-120.

149. Cho KI, Cai Y, Yi H, Yeh A, Aslanukov A, Ferreira PA (2007) Association of the kinesin-binding domain of RanBP2 to KIF5B and KIF5C determines mitochondria localization and function. Traffic 8: 1722-1735.

150. Joseph J, Dasso M (2008) The nucleoporin Nup358 associates with and regulates interphase microtubules. FEBS Lett 582: 190-196.

151. Ferreira PA, Nakayama TA, Pak WL, Travis GH (1996) Cyclophilin-related protein RanBP2 acts as chaperone for red/green opsin. Nature 383: 637-640.

152. Lin DH, Zimmermann S, Stuwe T, Stuwe E, Hoelz A (2013) Structural and functional analysis of the C-terminal domain of Nup358/RanBP2. J Mol Biol 425: 1318-1329.

153. Bichel K, Price AJ, Schaller T, Towers GJ, Freund SM, James LC (2013) HIV-1 capsid undergoes coupled binding and isomerization by the nuclear pore protein NUP358. Retrovirology 10: 81.

154. Sukegawa J, Blobel G (1993) A nuclear pore complex protein that contains zinc finger motifs, binds DNA, and faces the nucleoplasm. Cell 72: 29-38.

155. Nakielny S, Shaikh S, Burke B, Dreyfuss G (1999) Nup153 is an M9-containing mobile nucleoporin with a novel Ran-binding domain. EMBO J 18: 1982-1995.

156. Enarson P, Enarson M, Bastos R, Burke B (1998) Amino-terminal sequences that direct nucleoporin nup153 to the inner surface of the nuclear envelope. Chromosoma 107: 228-236.

157. Vasu S, Shah S, Orjalo A, Park M, Fischer WH, Forbes DJ (2001) Novel vertebrate nucleoporins Nup133 and Nup160 play a role in mRNA export. J Cell Biol 155: 339-354.

158. Smitherman M, Lee K, Swanger J, Kapur R, Clurman BE (2000) Characterization and targeted disruption of murine Nup50, a p27(Kip1)-interacting component of the nuclear pore complex. Mol Cell Biol 20: 5631-5642.

159. Hase ME, Cordes VC (2003) Direct interaction with nup153 mediates binding of Tpr to the periphery of the nuclear pore complex. Mol Biol Cell 14: 1923-1940.

160. Higa MM, Alam SL, Sundquist WI, Ullman KS (2007) Molecular characterization of the Ran-binding zinc finger domain of Nup153. J Biol Chem 282: 17090-17100.

161. Liu J, Prunuske AJ, Fager AM, Ullman KS (2003) The COPI complex functions in nuclear envelope breakdown and is recruited by the nucleoporin Nup153. Dev Cell 5: 487-498.

162. Lim RY, Huang NP, Koser J, Deng J, Lau KH, Schwarz-Herion K, Fahrenkrog B, Aebi U (2006) Flexible phenylalanine-glycine nucleoporins as entropic barriers to nucleocytoplasmic transport. Proc Natl Acad Sci U S A 103: 9512-9517.

163. Cardarelli F, Lanzano L, Gratton E (2012) Capturing directed molecular motion in the nuclear pore complex of live cells. Proc Natl Acad Sci U S A 109: 9863-9868.

164. Fahrenkrog B, Maco B, Fager AM, Koser J, Sauder U, Ullman KS, Aebi U (2002) Domain-specific antibodies reveal multiple-site topology of Nup153 within the nuclear pore complex. J Struct Biol 140: 254-267.

165. Paulillo SM, Phillips EM, Koser J, Sauder U, Ullman KS, Powers MA, Fahrenkrog B (2005) Nucleoporin domain topology is linked to the transport status of the nuclear pore complex. J Mol Biol 351: 784-798.

166. Shah S, Forbes DJ (1998) Separate nuclear import pathways converge on the nucleoporin Nup153 and can be dissected with dominant-negative inhibitors. Curr Biol 8: 1376-1386.

167. Ullman KS, Shah S, Powers MA, Forbes DJ (1999) The nucleoporin nup153 plays a critical role in multiple types of nuclear export. Mol Biol Cell 10: 649-664.

168. Brown PO, Bowerman B, Varmus HE, Bishop JM (1989) Retroviral integration: structure of the initial covalent product and its precursor, and a role for the viral IN protein. Proc Natl Acad Sci U S A 86: 2525-2529.

169. Fujiwara T, Mizuuchi K (1988) Retroviral DNA integration: structure of an integration intermediate. Cell 54: 497-504.

170. Suzuki Y, Craigie R (2007) The road to chromatin - nuclear entry of retroviruses. Nat Rev Microbiol 5: 187-196.

171. Lewis PF, Emerman M (1994) Passage through mitosis is required for oncoretroviruses but not for the human immunodeficiency virus. J Virol 68: 510-516.

172. Mattaj IW, Englmeier L (1998) Nucleocytoplasmic transport: the soluble phase. Annual review of biochemistry 67: 265-306.

173. Yamashita M, Emerman M (2005) The cell cycle independence of HIV infections is not determined by known karyophilic viral elements. PLoS Pathog 1: e18.

174. Yamashita M, Emerman M (2006) Retroviral infection of non-dividing cells: old and new perspectives. Virology 344: 88-93.

175. Ebina H, Aoki J, Hatta S, Yoshida T, Koyanagi Y (2004) Role of Nup98 in nuclear entry of human immunodeficiency virus type 1 cDNA. Microbes Infect 6: 715-724.

176. Zaitseva L, Cherepanov P, Leyens L, Wilson SJ, Rasaiyaah J, Fassati A (2009) HIV-1 exploits importin 7 to maximize nuclear import of its DNA genome. Retrovirology 6: 11.

177. Lee K, Ambrose Z, Martin TD, Oztop I, Mulky A, Julias JG, Vandegraaff N, Baumann JG, Wang R, Yuen W, Takemura T, Shelton K, Taniuchi I, Li Y, Sodroski J, Littman DR, Coffin JM, Hughes SH, Unutmaz D, Engelman A, KewalRamani VN (2010) Flexible use of nuclear import pathways by HIV-1. Cell Host Microbe 7: 221-233.

178. Thys W, De Houwer S, Demeulemeester J, Taltynov O, Vancraenenbroeck R, Gerard M, De Rijck J, Gijsbers R, Christ F, Debyser Z (2011) Interplay between HIV entry and transportin-SR2 dependency. Retrovirology 8: 7.

179. Zhang R, Mehla R, Chauhan A (2010) Perturbation of host nuclear membrane component RanBP2 impairs the nuclear import of human immunodeficiency virus -1 preintegration complex (DNA). PLoS One 5: e15620.

180. Walther TC, Fornerod M, Pickersgill H, Goldberg M, Allen TD, Mattaj IW (2001) The nucleoporin Nup153 is required for nuclear pore basket formation, nuclear pore complex anchoring and import of a subset of nuclear proteins. EMBO J 20: 5703-5714.

181. Rabut G, Doye V, Ellenberg J (2004) Mapping the dynamic organization of the nuclear pore complex inside single living cells. Nat Cell Biol 6: 1114-1121.

182. Varadarajan P, Mahalingam S, Liu P, Ng SB, Gandotra S, Dorairajoo DS, Balasundaram D (2005) The functionally conserved nucleoporins Nup124p from fission yeast and the human Nup153 mediate nuclear import and activity of the Tf1 retrotransposon and HIV-1 Vpr. Mol Biol Cell 16: 1823-1838.

183. Harborth J, Elbashir SM, Bechert K, Tuschl T, Weber K (2001) Identification of essential genes in cultured mammalian cells using small interfering RNAs. J Cell Sci 114: 4557-4565.

184. Mackay DR, Elgort SW, Ullman KS (2009) The nucleoporin Nup153 has separable roles in both early mitotic progression and the resolution of mitosis. Mol Biol Cell 20: 1652-1660.

185. Bastos R, Lin A, Enarson M, Burke B (1996) Targeting and function in mRNA export of nuclear pore complex protein Nup153. J Cell Biol 134: 1141-1156.

186. Limon A, Nakajima N, Lu R, Ghory HZ, Engelman A (2002) Wild-type levels of nuclear localization and human immunodeficiency virus type 1 replication in the absence of the central DNA flap. Journal of virology 76: 12078-12086.

187. Yoo S, Myszka DG, Yeh C, McMurray M, Hill CP, Sundquist WI (1997) Molecular recognition in the HIV-1 capsid/cyclophilin A complex. J Mol Biol 269: 780-795.

188. Hatziioannou T, Perez-Caballero D, Cowan S, Bieniasz PD (2005) Cyclophilin interactions with incoming human immunodeficiency virus type 1 capsids with opposing effects on infectivity in human cells. J Virol 79: 176-183.

189. Song C, Aiken C (2007) Analysis of human cell heterokaryons demonstrates that target cell restriction of cyclosporine-resistant human immunodeficiency virus type 1 mutants is genetically dominant. J Virol 81: 11946-11956.

190. Ganser-Pornillos BK, von Schwedler UK, Stray KM, Aiken C, Sundquist WI (2004) Assembly properties of the human immunodeficiency virus type 1 CA protein. J Virol 78: 2545-2552.

191. Li Y, Kar AK, Sodroski J (2009) Target cell type-dependent modulation of human immunodeficiency virus type 1 capsid disassembly by cyclophilin A. J Virol 83: 10951-10962.

192. Sokolskaja E, Sayah DM, Luban J (2004) Target cell cyclophilin A modulates human immunodeficiency virus type 1 infectivity. J Virol 78: 12800-12808.

193. Koh Y, Haim H, Engelman A (2011) Identification and characterization of persistent intracellular human immunodeficiency virus type 1 integrase strand transfer inhibitor activity. Antimicrob Agents Chemother 55: 42-49.

194. Hazuda DJ, Felock P, Witmer M, Wolfe A, Stillmock K, Grobler JA, Espeseth A, Gabryelski L, Schleif W, Blau C, Miller MD (2000) Inhibitors of strand transfer that prevent integration and inhibit HIV-1 replication in cells. Science 287: 646-650.

195. Guntaka RV, Richards OC, Shank PR, Kung HJ, Davidson N (1976) Covalently closed circular DNA of avian sarcoma virus: purification from nuclei of infected quail tumor cells and measurement by electron microscopy and gel electrophoresis. J Mol Biol 106: 337-357.

196. Braaten D, Franke EK, Luban J (1996) Cyclophilin A is required for the replication of group M human immunodeficiency virus type 1 (HIV-1) and simian immunodeficiency virus SIV(CPZ)GAB but not group O HIV-1 or other primate immunodeficiency viruses. J Virol 70: 4220-4227.

197. Balasundaram D, Benedik MJ, Morphew M, Dang VD, Levin HL (1999) Nup124p is a nuclear pore factor of Schizosaccharomyces pombe that is important for nuclear import and activity of retrotransposon Tf1. Mol Cell Biol 19: 5768-5784.

198. Dang VD, Levin HL (2000) Nuclear import of the retrotransposon Tf1 is governed by a nuclear localization signal that possesses a unique requirement for the FXFG nuclear pore factor Nup124p. Mol Cell Biol 20: 7798-7812.

199. Kim MK, Claiborn KC, Levin HL (2005) The long terminal repeat-containing retrotransposon Tf1 possesses amino acids in gag that regulate nuclear localization and particle formation. J Virol 79: 9540-9555.

200. Schmitz A, Schwarz A, Foss M, Zhou L, Rabe B, Hoellenriegel J, Stoeber M, Pante N, Kann M (2010) Nucleoporin 153 arrests the nuclear import of hepatitis B virus capsids in the nuclear basket. PLoS Pathog 6: e1000741.

201. Ball JR, Ullman KS (2005) Versatility at the nuclear pore complex: lessons learned from the nucleoporin Nup153. Chromosoma 114: 319-330.

202. Sabri N, Roth P, Xylourgidis N, Sadeghifar F, Adler J, Samakovlis C (2007) Distinct functions of the Drosophila Nup153 and Nup214 FG domains in nuclear protein transport. J Cell Biol 178: 557-565.

203. Zhou L, Pante N (2010) The nucleoporin Nup153 maintains nuclear envelope architecture and is required for cell migration in tumor cells. FEBS Lett 584: 3013-3020.

204. Mackay DR, Makise M, Ullman KS (2010) Defects in nuclear pore assembly lead to activation of an Aurora B-mediated abscission checkpoint. J Cell Biol 191: 923-931.

205. Vaquerizas JM, Suyama R, Kind J, Miura K, Luscombe NM, Akhtar A (2010) Nuclear pore proteins nup153 and megator define transcriptionally active regions in the Drosophila genome. PLoS genetics 6: e1000846.

206. Olsen JC (1998) Gene transfer vectors derived from equine infectious anemia virus. Gene Ther 5: 1481-1487.

207. O'Rourke JP, Newbound GC, Kohn DB, Olsen JC, Bunnell BA (2002) Comparison of gene transfer efficiencies and gene expression levels achieved with equine infectious anemia virus- and human immunodeficiency virus type 1-derived lentivirus vectors. J Virol 76: 1510-1515.

208. He J, Chen Y, Farzan M, Choe H, Ohagen A, Gartner S, Busciglio J, Yang X, Hofmann W, Newman W, Mackay CR, Sodroski J, Gabuzda D (1997) CCR3 and CCR5 are co-receptors for HIV-1 infection of microglia. Nature 385: 645-649.

209. Chen CM, Smith DM, Peters MA, Samson ME, Zitz J, Tabin CJ, Cepko CL (1999) Production and design of more effective avian replication-incompetent retroviral vectors. Dev Biol 214: 370-384.

210. Khare PD, Loewen N, Teo W, Barraza RA, Saenz DT, Johnson DH, Poeschla EM (2008) Durable, safe, multi-gene lentiviral vector expression in feline trabecular meshwork. Mol Ther 16: 97-106.

211. Loewen N, Barraza R, Whitwam T, Saenz DT, Kemler I, Poeschla EM (2003) FIV Vectors. Methods Mol Biol 229: 251-271.

212. Perron MJ, Stremlau M, Song B, Ulm W, Mulligan RC, Sodroski J (2004) TRIM5alpha mediates the postentry block to N-tropic murine leukemia viruses in human cells. Proc Natl Acad Sci U S A 101: 11827-11832.

213. Ulm JW, Perron M, Sodroski J, R CM (2007) Complex determinants within the Moloney murine leukemia virus capsid modulate susceptibility of the virus to Fv1 and Ref1-mediated restriction. Virology 363: 245-255.

214. Newman RM, Hall L, Connole M, Chen GL, Sato S, Yuste E, Diehl W, Hunter E, Kaur A, Miller GM, Johnson WE (2006) Balancing selection and the evolution of functional polymorphism in Old World monkey TRIM5alpha. Proc Natl Acad Sci U S A 103: 19134-19139.

215. Zhang F, Hatziioannou T, Perez-Caballero D, Derse D, Bieniasz PD (2006) Antiretroviral potential of human tripartite motif-5 and related proteins. Virology 353: 396-409.

216. Lu R, Limon A, Devroe E, Silver PA, Cherepanov P, Engelman A (2004) Class II integrase mutants with changes in putative nuclear localization signals are primarily blocked at a postnuclear entry step of human immunodeficiency virus type 1 replication. J Virol 78: 12735-12746.

217. Chang LJ, Urlacher V, Iwakuma T, Cui Y, Zucali J (1999) Efficacy and safety analyses of a recombinant human immunodeficiency virus type 1 derived vector system. Gene Ther 6: 715-728.

218. Hofmann W, Schubert D, LaBonte J, Munson L, Gibson S, Scammell J, Ferrigno P, Sodroski J (1999) Species-specific, postentry barriers to primate immunodeficiency virus infection. J Virol 73: 10020-10028.

219. Nakajima N, Lu R, Engelman A (2001) Human immunodeficiency virus type 1 replication in the absence of integrase-mediated dna recombination: definition of permissive and nonpermissive T-cell lines. J Virol 75: 7944-7955.

220. Morner A, Bjorndal A, Albert J, Kewalramani VN, Littman DR, Inoue R, Thorstensson R, Fenyo EM, Bjorling E (1999) Primary human immunodeficiency virus type 2 (HIV-2) isolates, like HIV-1 isolates, frequently use CCR5 but show promiscuity in coreceptor usage. J Virol 73: 2343-2349.

221. Chatterji U, Bobardt M, Selvarajah S, Yang F, Tang H, Sakamoto N, Vuagniaux G, Parkinson T, Gallay P (2009) The isomerase active site of cyclophilin A is critical for hepatitis C virus replication. J Biol Chem 284: 16998-17005.

222. Willey RL, Smith DH, Lasky LA, Theodore TS, Earl PL, Moss B, Capon DJ, Martin MA (1988) In vitro mutagenesis identifies a region within the envelope gene of the human immunodeficiency virus that is critical for infectivity. J Virol 62: 139-147.

223. Engelman A, Oztop I, Vandegraaff N, Raghavendra NK (2009) Quantitative analysis of HIV-1 preintegration complexes. Methods 47: 283-290.

224. Julias JG, Ferris AL, Boyer PL, Hughes SH (2001) Replication of phenotypically mixed human immunodeficiency virus type 1 virions containing catalytically active and catalytically inactive reverse transcriptase. J Virol 75: 6537-6546.

225. Dar MJ, Monel B, Krishnan L, Shun MC, Di Nunzio F, Helland DE, Engelman A (2009) Biochemical and virological analysis of the 18-residue C-terminal tail of HIV-1 integrase. Retrovirology 6: 94.

226. Lewis P, Hensel M, Emerman M (1992) Human immunodeficiency virus infection of cells arrested in the cell cycle. EMBO J 11: 3053-3058.

227. Brohawn SG, Partridge JR, Whittle JR, Schwartz TU (2009) The nuclear pore complex has entered the atomic age. Structure 17: 1156-1168.

228. Strambio-De-Castillia C, Niepel M, Rout MP (2010) The nuclear pore complex: bridging nuclear transport and gene regulation. Nature reviews Molecular cell biology 11: 490-501.

229. Peleg O, Lim RY (2010) Converging on the function of intrinsically disordered nucleoporins in the nuclear pore complex. Biological chemistry 391: 719-730.

230. Radu A, Blobel G, Moore MS (1995) Identification of a protein complex that is required for nuclear protein import and mediates docking of import substrate to distinct nucleoporins. Proc Natl Acad Sci U S A 92: 1769-1773.

231. Matreyek KA, Engelman A (2011) The requirement for nucleoporin NUP153 during human immunodeficiency virus type 1 infection is determined by the viral capsid. J Virol 85: 7818-7827.

232. Gamble TR, Vajdos FF, Yoo S, Worthylake DK, Houseweart M, Sundquist WI, Hill CP (1996) Crystal structure of human cyclophilin A bound to the amino-terminal domain of HIV-1 capsid. Cell 87: 1285-1294.

233. Schaller T, Ocwieja KE, Rasaiyaah J, Price AJ, Brady TL, Roth SL, Hue S, Fletcher AJ, Lee K, KewalRamani VN, Noursadeghi M, Jenner RG, James LC, Bushman FD, Towers GJ (2011) HIV-1 capsid-cyclophilin interactions determine nuclear import pathway, integration targeting and replication efficiency. PLoS Pathog 7: e1002439.

234. Price AJ, Fletcher AJ, Schaller T, Elliott T, Lee K, KewalRamani VN, Chin JW, Towers GJ, James LC (2012) CPSF6 defines a conserved capsid interface that modulates HIV-1 replication. PLoS Pathog 8: e1002896.

235. Blair WS, Pickford C, Irving SL, Brown DG, Anderson M, Bazin R, Cao J, Ciaramella G, Isaacson J, Jackson L, Hunt R, Kjerrstrom A, Nieman JA, Patick AK, Perros M, Scott AD, Whitby K, Wu H, Butler SL (2010) HIV capsid is a tractable target for small molecule therapeutic intervention. PLoS Pathog 6: e1001220.

236. Gamble TR, Yoo S, Vajdos FF, von Schwedler UK, Worthylake DK, Wang H, McCutcheon JP, Sundquist WI, Hill CP (1997) Structure of the carboxyl-terminal dimerization domain of the HIV-1 capsid protein. Science 278: 849-853.

237. Ohkura S, Goldstone DC, Yap MW, Holden-Dye K, Taylor IA, Stoye JP (2011) Novel escape mutants suggest an extensive TRIM5alpha binding site spanning the entire outer surface of the murine leukemia virus capsid protein. PLoS Pathog 7: e1002011.

238. McCarthy KR, Schmidt AG, Kirmaier A, Wyand AL, Newman RM, Johnson WE (2013) Gain-of-Sensitivity Mutations in a Trim5-Resistant Primary Isolate of Pathogenic SIV Identify Two Independent Conserved Determinants of Trim5alpha Specificity. PLoS Pathog 9: e1003352.

239. Pertel T, Hausmann S, Morger D, Zuger S, Guerra J, Lascano J, Reinhard C, Santoni FA, Uchil PD, Chatel L, Bisiaux A, Albert ML, Strambio-De-Castillia C, Mothes W, Pizzato M, Grutter MG, Luban J (2011) TRIM5 is an innate immune sensor for the retrovirus capsid lattice. Nature 472: 361-365.

240. Lee K, Mulky A, Yuen W, Martin TD, Meyerson NR, Choi L, Yu H, Sawyer SL, Kewalramani VN (2012) HIV-1 capsid-targeting domain of cleavage and polyadenylation specificity factor 6. J Virol 86: 3851-3860.

241. Sayah DM, Sokolskaja E, Berthoux L, Luban J (2004) Cyclophilin A retrotransposition into TRIM5 explains owl monkey resistance to HIV-1. Nature 430: 569-573.

242. De Iaco A, Luban J (2011) Inhibition of HIV-1 infection by TNPO3 depletion is determined by capsid and detectable after viral cDNA enters the nucleus. Retrovirology 8: 98.

243. Yang R, Aiken C (2007) A mutation in alpha helix 3 of CA renders human immunodeficiency virus type 1 cyclosporin A resistant and dependent: rescue by a second-site substitution in a distal region of CA. J Virol 81: 3749-3756.

244. Li X, Koh Y, Engelman A (2012) Correlation of recombinant integrase activity and functional preintegration complex formation during acute infection by replication-defective integrase mutant human immunodeficiency virus. J Virol 86: 3861-3879.

245. Shi J, Zhou J, Shah VB, Aiken C, Whitby K (2011) Small-molecule inhibition of human immunodeficiency virus type 1 infection by virus capsid destabilization. J Virol 85: 542-549.

246. Jin Z, Jin L, Peterson DL, Lawson CL (1999) Model for lentivirus capsid core assembly based on crystal dimers of EIAV p26. J Mol Biol 286: 83-93.

247. Mortuza GB, Haire LF, Stevens A, Smerdon SJ, Stoye JP, Taylor IA (2004) High-resolution structure of a retroviral capsid hexameric amino-terminal domain. Nature 431: 481-485.

248. Di Nunzio F, Fricke T, Miccio A, Valle-Casuso JC, Perez P, Souque P, Rizzi E, Severgnini M, Mavilio F, Charneau P, Diaz-Griffero F (2013) Nup153 and Nup98 bind the HIV-1 core and contribute to the early steps of HIV-1 replication. Virology 440: 8-18.

249. Jun S, Ke D, Debiec K, Zhao G, Meng X, Ambrose Z, Gibson GA, Watkins SC, Zhang P (2011) Direct visualization of HIV-1 with correlative live-cell microscopy and cryo-electron tomography. Structure 19: 1573-1581.

250. Fricke T, Valle-Casuso JC, White TE, Brandariz-Nunez A, Bosche WJ, Reszka N, Gorelick R, Diaz-Griffero F (2013) The ability of TNPO3-depleted cells to inhibit HIV-1 infection requires CPSF6. Retrovirology 10: 46.

251. Hori T, Takeuchi H, Saito H, Sakuma R, Inagaki Y, Yamaoka S (2013) A carboxy-terminally truncated human CPSF6 lacking residues encoded by exon 6 inhibits HIV-1 cDNA synthesis and promotes capsid disassembly. J Virol.

252. Lamorte L, Titolo S, Lemke CT, Goudreau N, Mercier JF, Wardrop E, Shah VB, von Schwedler UK, Langelier C, Banik SS, Aiken C, Sundquist WI, Mason SW (2013) Discovery of novel small molecule HIV-1 replication inhibitors that stabilize capsid complexes. Antimicrob Agents Chemother, in press.

253. Shah VB, Shi J, Hout DR, Oztop I, Krishnan L, Ahn J, Shotwell MS, Engelman A, Aiken C (2013) The host proteins transportin SR2/TNPO3 and cyclophilin A exert opposing effects on HIV-1 uncoating. J Virol 87: 422-432.

254. Loewen N, Barraza R, Whitwam T, Saenz DT, Kemler I, Poeschla EM (2003) FIV Vectors. Method Mol Biol 229: 251-271.

255. Shun MC, Raghavendra NK, Vandegraaff N, Daigle JE, Hughes S, Kellam P, Cherepanov P, Engelman A (2007) LEDGF/p75 functions downstream from preintegration complex formation to effect gene-specific HIV-1 integration. Gene Dev 21: 1767-1778.

256. Cherepanov P, Devroe E, Silver PA, Engelman A (2004) Identification of an evolutionarily conserved domain in human lens epithelium-derived growth

factor/transcriptional co-activator p75 (LEDGF/p75) that binds HIV-1 integrase. J Biol Chem 279: 48883-48892.

257. Ambrose Z, Lee K, Ndjomou J, Xu H, Oztop I, Matous J, Takemura T, Unutmaz D, Engelman A, Hughes SH, KewalRamani VN (2012) Human immunodeficiency virus type 1 capsid mutation N74D alters cyclophilin A dependence and impairs macrophage infection. J Virol 86: 4708-4714.

258. Koh Y, Wu X, Ferris AL, Matreyek KA, Smith SJ, Lee K, KewalRamani VN, Hughes SH, Engelman A (2013) Differential effects of human immunodeficiency virus type 1 capsid and cellular factors nucleoporin 153 and LEDGF/p75 on the efficiency and specificity of viral DNA integration. J Virol 87: 648-658.

259. Sistla S, Pang JV, Wang CX, Balasundaram D (2007) Multiple conserved domains of the nucleoporin Nup124p and its orthologs Nup1p and Nup153 are critical for nuclear import and activity of the fission yeast Tf1 retrotransposon. Mol Biol Cell 18: 3692-3708.

260. Beliakova-Bethell N, Terry LJ, Bilanchone V, DaSilva R, Nagashima K, Wente SR, Sandmeyer S (2009) Ty3 nuclear entry is initiated by viruslike particle docking on GLFG nucleoporins. J Virol 83: 11914-11925.

261. Mamede JI, Sitbon M, Battini JL, Courgnaud V (2013) Heterogeneous susceptibility of circulating SIV isolate capsids to HIV-interacting factors. Retrovirology 10: 77.

262. Holman AG, Coffin JM (2005) Symmetrical base preferences surrounding HIV-1, avian sarcoma/leukosis virus, and murine leukemia virus integration sites. Proc Natl Acad Sci U S A 102: 6103-6107.

263. Wu X, Li Y, Crise B, Burgess SM, Munroe DJ (2005) Weak palindromic consensus sequences are a common feature found at the integration target sites of many retroviruses. J Virol 79: 5211-5214.

264. Pryciak PM, Varmus HE (1992) Nucleosomes, DNA-binding proteins, and DNA sequence modulate retroviral integration target site selection. Cell 69: 769-780.

265. Wang GP, Ciuffi A, Leipzig J, Berry CC, Bushman FD (2007) HIV integration site selection: analysis by massively parallel pyrosequencing reveals association with epigenetic modifications. Genome research 17: 1186-1194.

266. Ciuffi A, Llano M, Poeschla E, Hoffmann C, Leipzig J, Shinn P, Ecker JR, Bushman F (2005) A role for LEDGF/p75 in targeting HIV DNA integration. Nature medicine 11: 1287-1289.

267. Marshall HM, Ronen K, Berry C, Llano M, Sutherland H, Saenz D, Bickmore W, Poeschla E, Bushman FD (2007) Role of PSIP1/LEDGF/p75 in lentiviral infectivity and integration targeting. PLoS One 2: e1340.

268. Ocwieja KE, Brady TL, Ronen K, Huegel A, Roth SL, Schaller T, James LC, Towers GJ, Young JA, Chanda SK, Konig R, Malani N, Berry CC, Bushman FD (2011) HIV integration targeting: a pathway involving Transportin-3 and the nuclear pore protein RanBP2. PLoS Pathog 7: e1001313.

Appendix 1: Contributions to additional authored publications

1) Krishnan L*, **Matreyek KA***, Oztop I*, Lee K, Tipper CH, Li X, Dar MJ, Kewalramani VN, Engelman A. The requirement for cellular transportin 3 (TNPO3 or TRN-SR2) during infection maps to human immunodeficiency virus type 1 capsid and not integrase. J Virol. 2010 Jan;84(1):397-406. *** contributed equally**

Contibution: Generated and analyzed data for Figure 2: induced and quantitated levels of TNPO3 knockdown, and quantitated resulting retroviral infectivities in TNPO3 depleted cells. Wrote the associated text in the publication.

2) Koh Y, **Matreyek KA**, Engelman A. Differential sensitivities of retroviruses to integrase strand transfer inhibitors. J Virol. 2011 Apr;85(7):3677-82.

Contribution: Aided in the generation and analysis of data in Table 2

3) **Matreyek KA***, Oztop I*, Freed EO, Engelman A. Viral latency and potential eradication of HIV-1. Expert Rev Anti Infect Ther. 2012 Aug;10(8):855-7. *** contributed equally**

Contribution: Meeting review for Keystone Symposium: Frontiers in HIV pathogenesis, Therapy and Eradication, March 2012 in Whistler, British Columbia, Canada. Contributed writing for the publication

4) Koh Y, Wu X, Ferris AL, **Matreyek KA**, Smith SJ, Lee K, KewalRamani VN, Hughes SH, Engelman A. Differential effects of human immunodeficiency virus type 1 capsid and cellular factors nucleoporin 153 and LEDGF/p75 on the efficiency and specificity of viral DNA integration. J Virol. 2013 Jan;87(1):648-58

Contribution: Generated NUP153 knockdown and control infection samples for integration site sequencing performed by a collaborating lab, and collected associated infectivity measurements Figure 4A. Generated CA mutant viruses for Figure 2.